SOLAR POWERED MULTISTAGE DIRECT CONTACT MEMBRANE DISTILLATION SYSTEM

BY

AHMED ABDALMONEM ABDALGHANY ABDALMONEM

A Thesis Presented to the

DEANSHIP OF GRADUATE STUDIES

KING FAHD UNIVERSITY OF PETROLEUM & MINERALS

DHAHRAN, SAUDI ARABIA

In Partial Fulfillment of the
Requirements for the Degree of

MASTER OF SCIENCE

In

MECHANICAL ENGINEERING

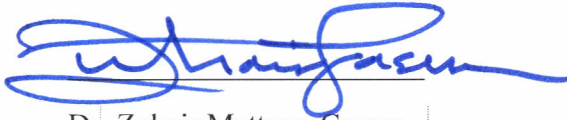MAY 2017

KING FAHD UNIVERSITY OF PETROLEUM & MINERALS

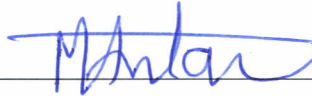DHAHRAN- 31261, SAUDI ARABIA

DEANSHIP OF GRADUATE STUDIES

This thesis, written by **AHMED ABDALMONEM ABDALGHANY ABDALMONEM**
under the direction of his thesis advisor and approved by his thesis committee, has been
presented and accepted by the Dean of Graduate Studies, in partial fulfillment of the
requirements for the degree of **MASTER OF SCIENCE IN MECHANICAL
ENGINEERING.**

Dr. Atia E. Khalifa
(Advisor)

Dr. Zuhair Mattoug Gasem
Department Chairman

Dr. Mohammed A. Antar
(Member)

Dr. Salam A. Zummo
Dean of Graduate Studies

Dr. Fahad A. Al-Sulaiman
(Member)

24/8/17

Date

ii

This work is dedicated to my family

ACKNOWLEDGMENTS

TABLE OF CONTENTS

LIST OF TABLES

LIST OF FIGURES

LIST OF ABBREVIATIONS

MD	Membrane Distillation
ETSC	Evacuated Tube Solar Collector
DCMD	Direct Contact Membrane Distillation
MS-DCMD	Multistage Direct Contact Membrane Distillation
DCMA	Direct Contact Module Arrangement
AGMD	Air Gap Membrane Distillation
VMD	Vacuum Membrane Distillation
SGMD	Sweeping Gas Membrane Distillation
TDS	Total Dissolved Solids [mg/L or ppm]
GOR	Gain output ratio
MSF	Multi-stage flash distillation system
MED	Multi-effect distillation system
MVC	Mechanical vapor compression system
TVC	Thermal vapor compression system
HDH	Humidification-dehumidification system
SRF	Salt rejection factor

LIST OF NOMENCLATURES

V	wind speed [m/s]
A$_{s-g}$	surface area of glass [m^2]
A$_{s-p}$	surface area of copper pipe [m^2]
G	solar radiation [W/m^2]
α$_g$	absorptivity of the glass [-]
C$_{pg}$	specific heat at constant pressure for the glass [j/kg.K]
m$_g$	mass of the glass [kg]
C$_{pw}$	specific heat at constant pressure for the water [j/kg.K]
T$_g$	the temperature of the outer glass tube [K]
t	time [sec]
ε	the emissivity of the outer glass [-]
σ	the Stefan –Boltzmann Constant (5.6697×10^{-8}) [W/m^2.K^4]
m$_w$	the mass of water in the tank [kg]
h$_g$	Convective heat transfer coefficient [W/m^{2}K]
Q$_{tank}$	Rate of heat transfer to the water inside the tank [j]
Q$_{conv,fluid}$	heat transfer from the pipe to the fluid inside the pipe [j]
q$_{g-air}$	losses from glass to air due to radiation and convection [j/kg K]
T$_{initial}$	Initial temperature of water inside the tank [K]
T$_{final}$	Final temperature of water inside the tank [K]
Q$_{conv\_g\_air}$	Convection heat transfer between the glass and the air [W]
Q$_{rad\_g\_sky}$	Radiation heat transfer between the glass and the sky [W]

Q_{abd_g}	The amount of heat absorbed by the glass [W]
Q_{abd_p}	The amount of heat absorbed by the copper pipe [W]
$Q_{radp\text{-}g}$	Radiation heat transfer between the pipe and the glass [W]
$Q_{convp\text{-}g}$	Convective heat transfer between the pipe and the glass [W]
Q_{conv}	Convective heat between the pipe and the working fluid [W]
q_f	Feed flow rate [L/min]
q_p	Permeate flow rate [L/min]
T_f	Feed temperature [°C]
T_p	Permeate temperature [°C]
θ	Temperature polarization
ρ	Density [kg/m³]
δ	Membrane thickness; film thickness [m]
μ	Viscosity [N.s/m²]

ABSTRACT

Full Name : Ahmed Abdalmonem Abdalghany Abdalmonem
Thesis Title : Solar Powered Direct Contact Membrane Distillation System
Major Field : Mechanical Engineering
Date of Degree : May 2017

One of the most promising thermal-membrane technologies for water desalination is Membrane Distillation (MD). It's considered as a low energy consumption desalination technique with good productivity as it operates at low feed temperatures (40 to 90°C) such that solar collection systems and industrial waste energy can be used directly to produce distillate. A micro-porous hydrophobic membrane is used to separate the vapor from the hot feed water driven by the vapor pressure difference across the membrane.

In this study, the performance of a Multi-Stage Direct Contact Membrane Distillation System (MS-DCMD) is investigated using two different energy sources. A laboratory scaled MS-DCMD system powered by an electric heater used as a heating source supply to feed water and a solar powered MS-DCMD system with an evacuated tube solar collector (ETSC) used to heat the feed water. A mathematical model is developed and validated to predict the performance of the evacuated tube solar collector in the city of Dhahran, KSA. Three flow arrangements (parallel, series, and mixed) for feed and permeate streams in the MS-DCMD are experimentally studied under different operating conditions.

The theoretical model results showed that the evacuated tube solar collector is a suitable heating source for MD systems. It can provide feed water for different MD systems at 90°C during the summer months. Moreover, the experimental investigations of different flow arrangements for the laboratory scaled MS-DCMD system showed that the productivity of

the parallel flow arrangement is much higher than the mixed and series flow arrangements. Furthermore, the experimental study on the solar MS-DCMD system showed the difficulty of maintaining the feed and permeate temperatures at the required values due to the high conduction heat transfer between feed and permeate sides across the membrane; which is a design characteristic of the DCMD modules. A very high salt rejection factor (SRF) had been achieved around 99.9%.

ملخص الرسالة

الاسم الكامل: أحمد عبد المنعم عبد الغني عبد المنعم

عنوان الرسالة: استخدام الطاقة الشمسية لتحلية المياه باستخدام التقطير بالغشاء متعدد المراحل

التخصص: الهندسة الميكانيكية

تاريخ الدرجة العلمية: مايو2017

أحد أكثر الطرق الواعد لتحلية المياه عن طريق المعالجة الحرارية هي التحلية عن طريق التقطير بالغشاء. هذه الطريقة تعتبر كأحد الطرق الموفرة للطاقة لكونها تستطيع ان تعمل من 40 وحتى 90 درجة مئوية ويمكن الحصول على هذه الطاقة عن طريق الطاقة الشمسية كمثال او عن طريق النفايات الصناعية. وتتم من خلال فصل بخار الماء عن المحلول الملحي الساخن عن طريق غشاء فاصل بين اثنين من السوائل أحدهما ساخن والاخر بارد. هذا الغشاء يسمح بمرور البخار من الجانب الساخن ولا يسمح بمرور الماء ليتكثف مع الماء البارد في الجانب الاخر. وتتم هذه المعالجة استنادا الى مبدأ اختلاف ضغوط البخار على جانبي الغشاء.

في هذه الدراسة سيتم اختبار منظومة التقطير بالغشاء متعدد المراحل ذو نوع التلامس المباشر [MS-DCMD] باستخدام مصدرين للطاقة هما مسخن الماء الكهربائي ومجمع الطاقة الشمسية. تم عمل نموذج رياضي للتنبؤ بأداء مجمع الطاقة الشمسية كمسخن للماء في أنظمة التقطير بالغشاء وتمت مقارنته بالتجارب العملية. وتم الاختبار العملي لمنظومة التقطير بالغشاء متعدد المراحل ذو نوع التلامس المباشر (على التوالي، على التوازي، وعلى التوالي والتوازي معا) تحت مختلف ظروف التشغيل. النموذج الرياضي تنبأ بأن مجمع الطاقة الشمسية قادر على تسخين درجة حرارة الماء الى درجات الحرارة التي تحتاجها منظومات التقطير بالغشاء فقد أوصل درجة حرارة الماء بداخله الى 90 درجة مئوية خلال شهور الصيف. اما التجارب العملية على منظومة التقطير بالغشاء متعدد المراحل ذو نوع التلامس المباشر أثبتت أن توصيل المنظومة على التوازي تحقق اعلى كمية لمعدل التدفق مقارنة بتوصيلات التوالي والتوصيلات المشتركة (على التوازي وعلى التوالي معا). استهلاك الطاقة للسخان الكهربائي كان كبيرا مقارنة باستهلاك المبرد الكهربائي نظرا لفرق درجات الحرارة العالي في دائرة الماء الساخن بين بداية الدائرة ونهايتها. التجارب العملية على منظومة التقطير عند توصيلها بمجمع الطاقة الشمسية أثبتت صعوبة المحافظة على درجات الحرارة ماء التغذية وسوائل التبريد في حدود الدرجات المطلوبة بسبب المعدل العالي لانتقال الحرارة بينهما. معدل طرد الملوحة وصل ل99.9%.

CHAPTER 1

INTRODUCTION & LITERATURE REVIEW

1.1 INTRODUCTION

1.1.1 Water Scarcity & Demand

Water is the most important substance on earth. Due to the limitation of potable water resources and with the increase of the population in rural, remote areas such as Africa, Southeast Asia and Middle East, applying cost effective and energy efficient desalination technologies became a necessity to combat the water scarcity[1,2,3]. Water desalination processes have high importance for human beings as they help to secure the potable water needed for drinking and also for industrial, agricultural and domestic purposes[4,5,6]. Water covers about 71% of the earth's surface where 2.5% of this percentage is fresh water while 96.5% is oceans and 0.9% is other saline water. Out of the 2.5% there is only 1.2% is surface water, which serves most of life's needs[7]. The majority of this surface water is locked up in ice and about 20.9% is found in lakes and about 0.49% in rivers which is represented in the following Figure 1.1[8].
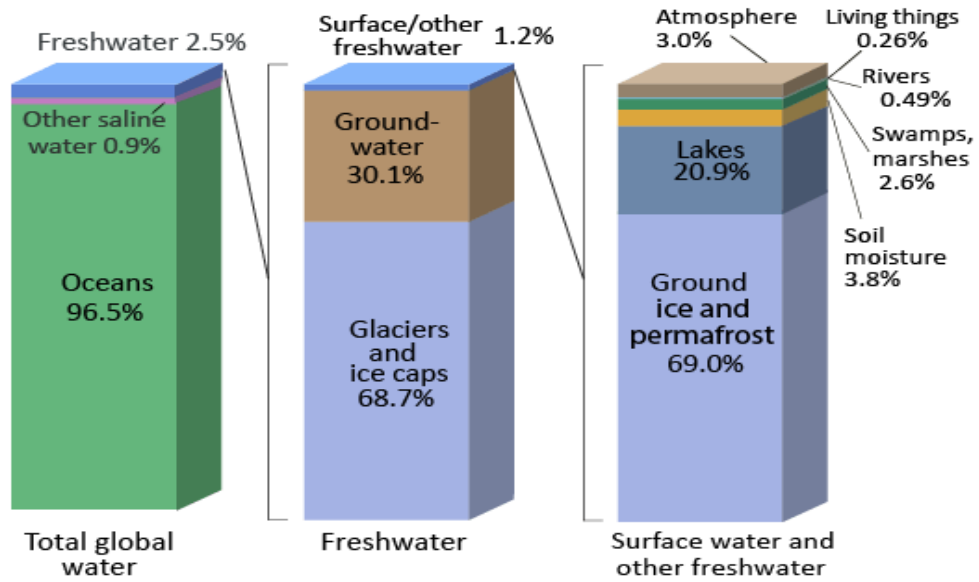
Figure 1.1: Distribution of Earth's Water [8]

Kingdom of Saudi Arabia is the largest producer of desalinated water in the world. With the increase in its population and industrial growth, the water demands increase rapidly in the past few years.

The World Resources Institute in 2013 [9] studied the water demand around the world, as shown in Figure 1.2, and stated that Saudi Arabia faces the danger of withdrawn of more than 80% of its annual renewable water resources that is usable for daily consumption, agriculture and industry.
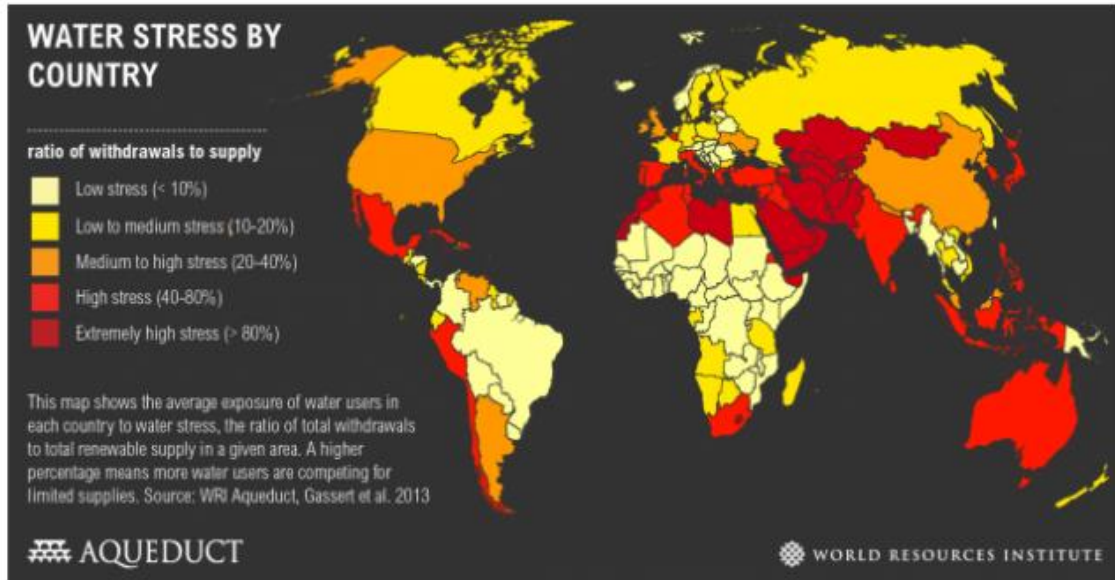
Figure 1.2: Water Stress by Country in 2013 [9]

In 2006, Al-Saadi [10] predicted in his study an estimation for the water requirements for the Kingdom of Saudi Arabia in the next twenty years considering 2005 as the base year. He divided the water requirements into three main sectors: agricultural requirements, urban water need and the industrial requirements. The total future water requirements given in million cubic meter (MCM) is the summation of the three main sectors, and is given in Table 1.1, with an annual increase of 5%. The agricultural requirements based on the strategy of the Ministry of Agricultural in KSA and the major crops irrigation requirements while the urban water needs were estimated based on the country population and its growth rates.

Table 1.1: Total Future Water Requirements (MCM) [10]

Year	2005	2010	2015	2020	2025
Agriculture(MCM)	17373	16099	14823	13546	**13546**
Urban (MCM)	2191	2307	2425	2534	**2630**
Industrial (MCM)	640	800	960	1120	**1280**
Total (MCM)	**20204**	**19206**	**18208**	**17200**	**17456**

1.1.2 Water Desalination Role

Water Desalination plays an important role in supplying fresh water in both developing and developed nations. Desalination is the process of removing salt and other dissolved solids from water in order to produce water suitable either for human consumption or agricultural purposes and industrial processes. Desalination does not only pertain sea and ocean water but also brackish water such as agricultural and industrial waters.

At the end of 2015, desalination of seawater accounts for a worldwide water production of 86.55 million m^3/year (0.6% of global water supply). The Middle East and North Africa (MENA) account for 38% of global desalination efforts, but other regional centers of activity are becoming more prominent, such as the Mediterranean Sea and the Red Sea, or the coastal waters of California, China and Australia [4,5]. Desalination is more practical in these seas because they have lower water salinity than the ocean which significantly lowers energy consumption.

Countries in The Arabian Gulf region face the largest per capita water scarcity in MENA, with an average water availability of less than 300 m^3 per capita per year [13]. Water desalination researchers nowadays focus on using solar energy as it is free and does not negatively affect the environment. Kingdom of Saudi Arabia is considered one of the most promising potentials countries in producing solar energy worldwide due to its location in the sun belt. In addition, the solar intensity increases significantly in summer with the increasing of demand on electricity and water.

1.1.3 Water Desalination Technologies

Desalination technologies for large operations have significant capital cost and energy requirement. The European Union (EU) funded a project assessing the best available technologies for desalination in local areas [11]. This project assessed the current state of 11 different desalination technologies. The EU report mentioned the Membrane Distillation (MD) technology as low cost and effective desalination techniques if it is integrated with a renewable energy source as the solar or waste energy. In Table 1.2, a comparison is made between those 11 desalination technologies including their pros & cons, operating skills required on a defined scale, energy type required, energy consumption, capital and operating cost. We can classify these technologies based on the type of energy used [14] as shown in Figure 1.3.
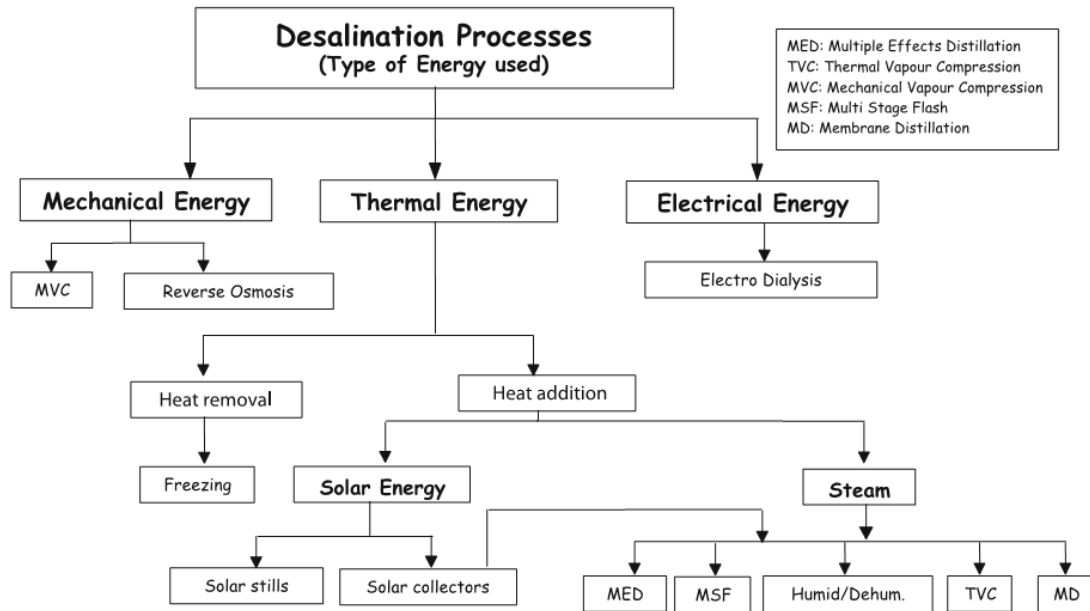
Figure 1.3: Desalination technologies classification based on the type of energy used

Table 1.2: Comparison of desalination technologies [11]

Desalination Process	Cost	Energy consumption	Other O&M cost	Advantages	Disadvantages	O&M Skill required (scale 1-5)	Energy Type required
MSF[15,16,17]	High	High	Low	- Suitable for high TDS feed technology - Less pre-treatment required. - Robust and reliable - Mature and proven	- More brine to be disposed. - High Feed water Requirement. - High specific energy consumption	2	Heat + power
MED & TVC[18,19,20]	Medium	High	Low	- Mature and proven technology - Suitable for high TDS feed - Robust and reliable - Less pre-treatment required. - can use low-grade heat	- Low recovery ratio, when cooling water is accounted for. - High specific heat consumption	2	Heat + power
MVC[21,22,23]	Medium to high	High	Low	- Suitable for high TDS feed - Compact - Robust - Mature and proven technology	- Mechanical compressor requires skilled O&M - High scaling potential under variable conditions.	4	Power
Reverse Osmosis [24,25,26]	Medium	Low	Medium	- Suitable for high TDS feed - Compact - Reliable - Less start-up and shutdown time - Mature and proven technology - High recovery ratio	- Variability in operating conditions and/or frequent start-up/shutdown cycles shorten membrane life - Susceptible to various types membrane fouling. - Pre-treatment requires careful design.	3	Power
Electro-dialysis (ED & EDR) [27,28,29]	Low	Low	Low	- Less pre-treatment required - Reliable -High recovery ratio - Compact - Less start-up and shutdown time - Proven technology.	- Suitable for TDS up to 3000 mg/l.	3	Power
Membrane distillation (MD) [30,31,32]	High/ medium	High	Low	- Suitable for very high TDS feed - Low pressure operation - Compact - needs less feed water for a given output. - Less pre-treatment required - Low grade heat usage	- High specific heat consumption - Technology is still under development.	2	Heat + minor power req.

6

Electro Dialysis Metathesis (EDM) [33,34,34]	High	High	NA	- Less pre-treatment required - Compact - Recovery more than RO possible and can be used for zero discharge -Improved version of ED.	- Emerging technology.	4	Power
Thermo-Ionic™ Desalination	High	High	NA	- Needs less feed water for a given output and has high recovery rate - Less pre-treatment required - Compact - Low grade heat usage	- Proprietary design and information kept confidential - Promising technology. - High specific heat consumption.	4	Power + Heat
Forward Osmosis [35,36,37]	NA	Low (prospective)	NA	- Less pre-treatment required. - Low pressure operation and hence consumes less power.	- Emerging technology. Process optimisation is going on	4	Power (+heat in some cases)
Solar Stills[38], [39]	V. low	High	V. low	- Simple and easy to operate - Uses solar energy	- Not practical for large capacity - Large area required.	1	Solar (Heat)
Humidification/ Dehumidification (HDH) [40]–[42]	Medium	High	Low	- Simple design using cheap material - Can use low grade thermal energy.	- Requires large area - Suitable only for small capacities.	3	Heat + power

1.1.4   Membrane Distillation for Desalination

Membrane Distillation (MD) is a thermally driven membrane separation technique. MD technique is emerging as an attractive alternative low energy desalination process. It's an efficient and cost-effective technology which can be operated utilizing low grade waste heat from industrial processes or renewable energy sources such as geothermal and solar energies.

In MD, a micro-porous hydrophobic membrane separates the hot feed solution and the cold side/permeate. Using the vapor pressure difference developed across the membrane due to the temperature difference, a driving force is generated to transfer the vapor across the membrane from the hot feed solution to the cold side/permeate; where it condensate [43]. We can summarize the water desalination process through the MD into three main steps:

(1) Evaporation in the hot feed side of membrane

(2) Transport of water vapor from the hot side to the cold permeate side through the membrane

(3) Vapor condensation in the cold permeate side of the membrane

There are four main configurations for the MD are shown in Figure 1.4:

    1-   Direct contact membrane distillation (DCMD);

    2-   Air gap membrane distillation (AGMD);

    3-   Sweeping gas membrane distillation (SGMD);

    4-   Vacuum membrane distillation (VMD).
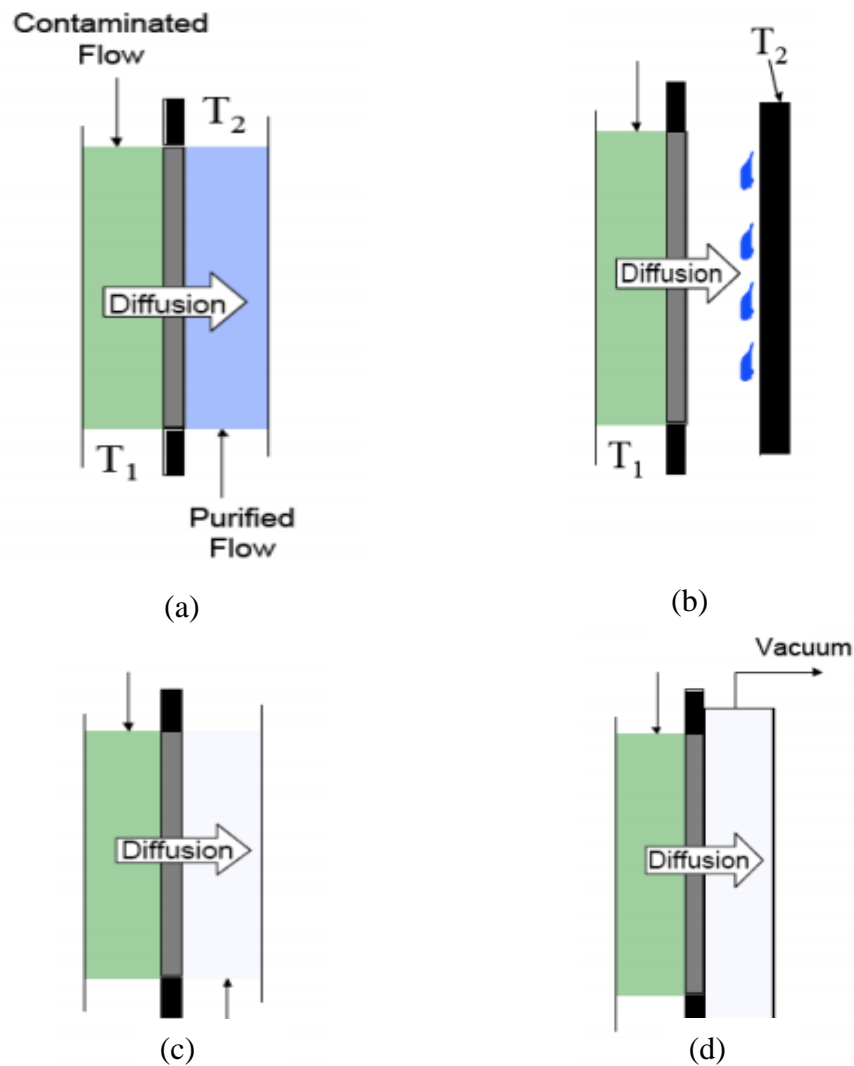
Figure 1.4: MD configurations [13]

a-Direct Contact Membrane Distillation

b-Air Gap Membrane Distillation

c- Sweeping Gas Membrane Distillation

d- Vacuum Membrane Distillation

In direct contact membrane distillation, the permeate is in direct contact with the cold

membrane side surface. Evaporation takes place at the feed-membrane interface. The vapor

is moved by the vapor pressure difference across the membrane to the permeate side and

condenses in the cold permeate stream inside the membrane module. In air gap membrane distillation, stagnant air is introduced between the membrane and a condensation surface. The vapor crosses the air gap to condense over the cold surface inside the membrane cell. In VMD on the other hand, a pump is used to create a vacuum in the permeate membrane side. Condensation takes place outside the membrane module. In SGMD, inert gas is used to sweep the vapor at the permeate membrane side to condense outside the membrane module.

Main advantages of MD:

- Water can be distilled at relatively low temperatures (40 to 90 °C).

- Low-grade energy (solar, industrial waste heat or desalination waste heat) may be used.

- It produces high-quality distillate (almost 100% salt rejection).

- Good productivity (flux) due to advances in membrane manufacturing and module designs.

- Cost effective, less expensive material can be used such as plastics.

- Less/No corrosion problems (since plastic can be used).

- Compact design.

Limitations and challenges facing MD technology

- Permeate flux is still lower than well-established industrial techniques (MSF-MED-RO).

- Membrane wetting is possible.

- Energy recovery.

- Multistage design.

1.2 LITURATURE REVIEW

At the beginning of the fourth century, various techniques started to develop for getting fresh water to cover the shortage in natural water resources. The technique of using solar energy to evaporate, condense the water and then collect it within the same closed system is known as solar distillation. Talbert et al. [44] wrote a great review paper on solar distillation. Delyannis [45] made an overview of the recent solar distillation plants in the world. The following Figure 1.5 represents the classification of the solar desalination technologies based on the way of utilizing solar energy.
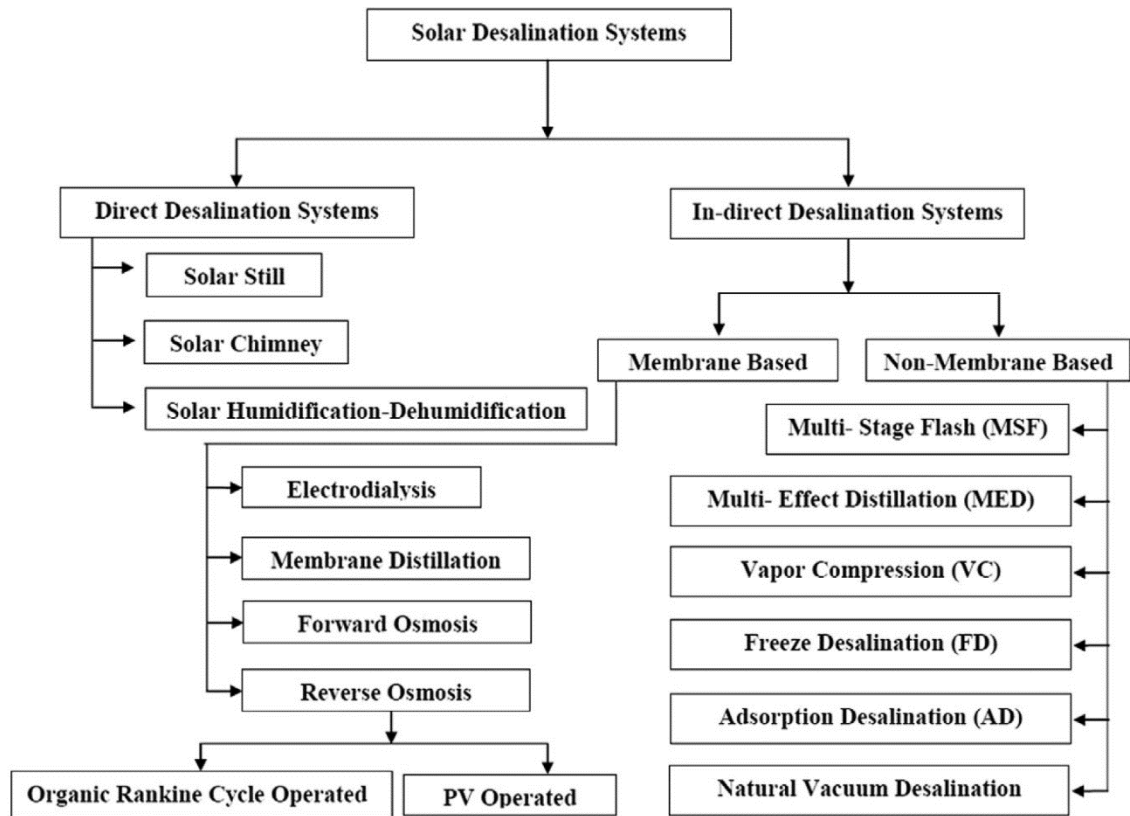
Figure 1.5: Solar Desalination Technologies [46]

1.2.1 Desalination using Direct Contact Membrane Distillation

In the 1960's, Findley was the first to contribute with his work in the DCMD research area [47]. His experiments results were based on different membrane materials and he also contributed to the basic theory of the MD technique. By the mid of the 90's, the number of publications that deals with the MD was doubled including a review by Sirkar published in 1992 [48]. Also a large number of review papers wrote to evaluate the performance of the DCMD such as Lloyd and Lawson [49], Vahdati and Burgoyne [50]. Martinez & Diaz [51] studied the MD process from a theoretical point of view. An evaluation for a model based on gas transfer in the porous media showed an agreement with experimental results. A DCMD experiment conducted using two different membrane materials HVHP45 & GVHP22. The same model can predict also of salt solutions desalination.

Jian-Mei Li et al. [52] conducted experiments on vacuum membrane distillation and direct contact membrane distillation systems using two different microporous hollow-fiber membranes polyethylene (PE) and polypropylene (PP). The experiments showed that with the increase in the feed flow and the temperature, the flux can increase significantly. The polyethylene membranes can permeate more distillate water than the polypropylene due to the advantage of the large pore size and the high porosity for the former.

Lawal & Khalifa [53], [54] predicted the output flux in DCMD using a theoretical model based on the analysis of the heat and mass transfer through the membrane and then the authors created a statistical model using the analysis of variance (ANOVA) technique to determine the significant effect of each operating parameter in the DCMD system performance which are the coolant inlet temperature, feed inlet temperature, coolant flow

12

rate and feed flow rate. Using the taguchi technique and applied regression, they determined the maximum positive effect for the DCMD system input variables was for the feed water temperature and the highest negative effect was for the coolant water temperature. Both the feed and coolant flow rates showed a small difference on the performance of the DCMD system.

Khalifa et al. [55] studied experimentally and analytically the performance of a DCMD system. Based on the equations of mass and heat transfer, an analytical model was developed. This model proved its ability to predict the effect of different operating parameters inlet feed temperature, cold permeate temperature, feed flow rate, permeate flow rate, feed salinity concertation and membrane pore size. The model was validated with the experimental results and showed an error percentage less than 10%. The model showed that the permeate flux increases as the inlet feed temperature increases and as the permeate temperature decreases. Comparing the two operating parameters on permeate flux, the author mentioned that the feed inlet temperature has a higher effect than the permeate temperature. It's important to mention that the DCMD system has an ability to handle high salt concentration feeds (100 g/L) with a high salt rejection factor. Khalifa et al. [56] mentioned in his experimental work on DCMD system that the salt rejection factor reached almost 100% after continues operation of the system for 48 hours while the gain output ratio (GOR) was between 0.8 and 1.2 for different values of feed inlet temperatures. Cath et al. [57] investigated experimentally a DCMD module to improve the water desalination process. With a turbulence flow regime, three microporous hydrophobic membranes evaluated with a feed water temperature around 40 °C. The results showed that the careful design of the membrane module may result a reduction in the temperature

polarization and the permeability obstructions. Based on the author results, the flux can be doubled compared to the usual mode of DCMD operation at low temperatures

Summers et al. [58] investigated the energy efficiency for different MD systems. The author compared the (GOR) value which is the ratio of the latent heat of vaporization for a one kilogram of the distillate water to the amount of energy used by the distillation systems. Increasing of the feed temperature and the membrane length led to a tremendous increase in the GOR value for the DCMD and the AGMD. The GOR for the VMD was much lower than the other configurations.

1.2.2 Multi-stage Membrane Distillation Systems for Water Desalination

Lee et al. [59] assessed theoretically a hybrid multi-stage VMD and a pressure-retarded osmosis (PRO) system to produce fresh water and power. They implemented a recycling flow scheme in the MS-VMD to produce both fresh water and highly concentrated brine. The concentrated brine is then provided to the PRO system as a draw solution for producing power. The authors found that the permeate flux increases when the recycling flow decrease at constant feed flow rate. Also, using the river water as feed water at constant hydraulic pressure difference the maximum power density of 9.7 W/m^2 is achieved with 0.5 kg/min feed flow rate. Pangarkar et al. [60] studied experimentally and theoretically the performance of a multi-effect AGMD system. A mathematical model was developed based on the equations of mass and heat transfer for a single AGMD stage and then applied on four stages multi-effect-AGMD and then compared the results with the experimental data. The validation results showed a percentage error of 9%. At the feed temperature of 80°C, feed flow rate of 1.5 L/min and coolant temperature of 20°C, the maximum flux of

the system achieved was 166.38 L/m²h, which is 3.2-3.6 times larger than the single stage

AGMD process.

Gilron et al. [61] designed a cascade of crossflow multi-stage DCMD system as shown in

Figure 1.6 to maximize the energy recovery. The GOR reached 20 in the system but with

low terminal temperature differences (TTD) for the DCMD and the heat exchangers. Then

the authors improved the system to maintain a good energy recovery rate [62]. They

connected the feed side of the multi-stage DCMD modules in a countercurrent series

cascades and concluded that in the former cascade it's preferable to use inter-stage heating

of brine between each cascade.
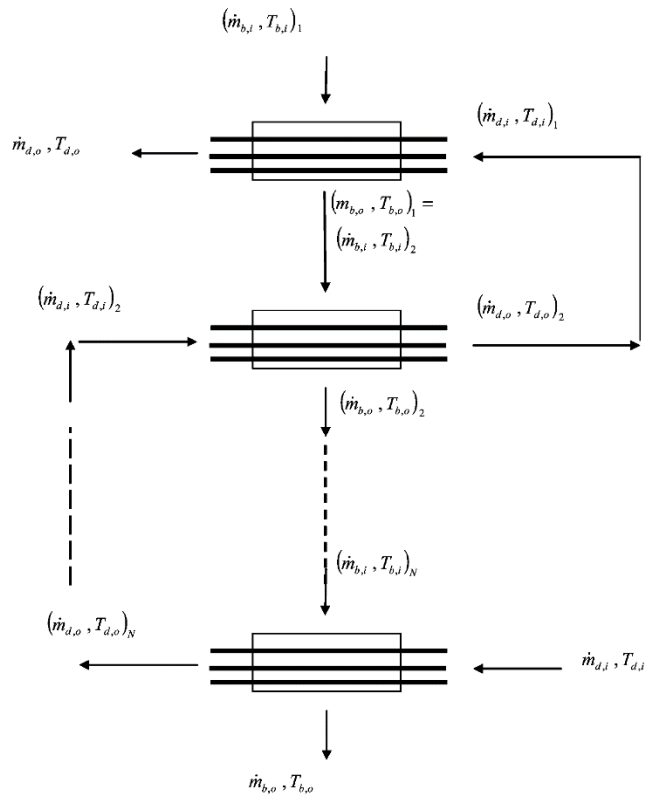
Figure 1.6: Scheme for using crossflow DCMD modules to obtain a countercurrent [61]

Lee et al. [63] made a comprehensive numerical analysis of productivity, the water product cost, and the membrane wetting problem to find the best arrangement for the system. He found that the mixed MVMD system with 20 stages, as shown in Figure 1.8, the highest productivity (3.79 m^3/day), lowest water product cost ($1.16/$m^3$), and lowest maximum trans-membrane pressure difference (93.8 kPa) in the studied arrangement. The results showed that when the inlet feed temperature is fixed, the higher feed velocity at module inlet is good at the productivity and the water product cost.

(a)   (b)
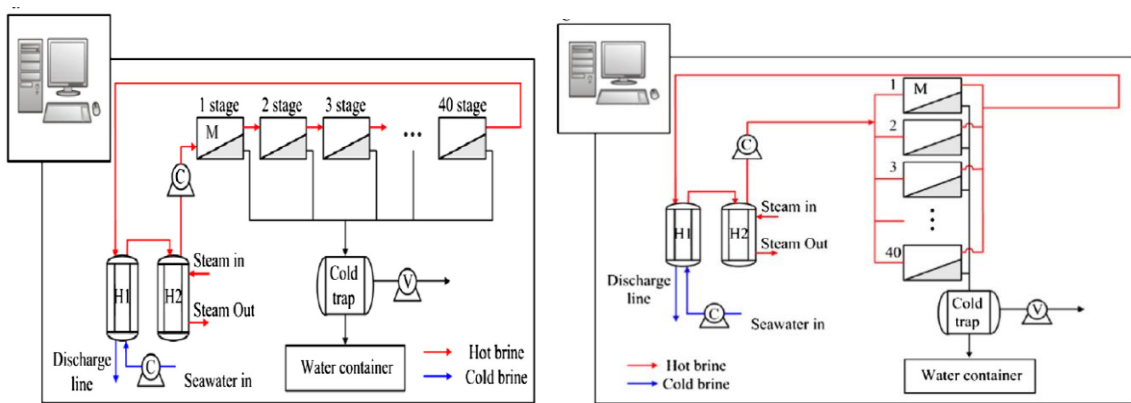
1.7: Schematics of Multistage MD systems [63]

a- Series arrangement, b- Parallel arrangement
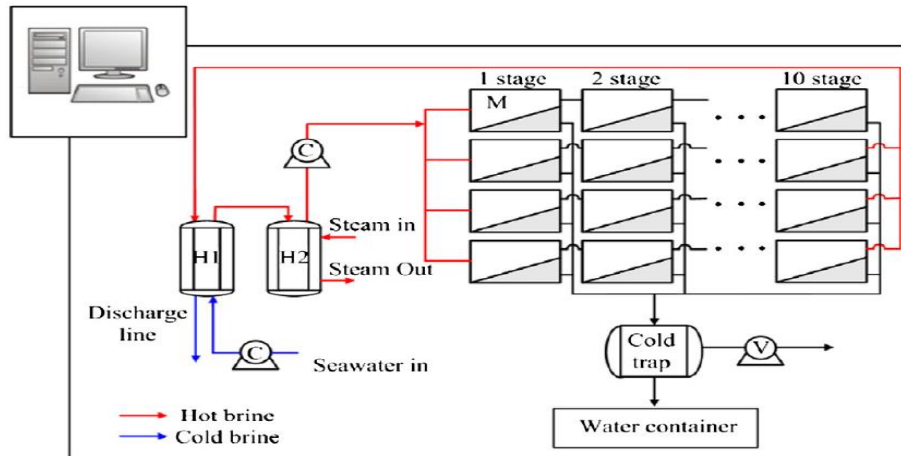
Figure 1.8: Mixed arrangement [63]

16

Geng et al. [64] investigated a multi-stage AGMD process for further concentrating RO brine and obtaining a high water recovery. Experiments conducted on an AGMD module with a series of hollow fiber membrane distributors to keep the distribution of membranes and hollow fibers uniform and stable. In one stage AGMD process the maximum value of the flux and GOR reached 6.8 kg/m^{2}h and 7.1 respectively. The water recovery of one stage varied between 5-8%. In the 14 AGMD process the maximum value of the recovery and the minimum value of the flux were 82.2% and 3.9 kg/m^{2}h respectively.

1.2.3   Solar Powered Membrane Distillation Systems

In 2014, Priya. D et al. [65], reported that integrating the solar energy collectors with the desalination systems offers a promising prospect in covering water and power needs in places that suffer in those two aspects. They divided the solar desalination processes into two categories: Direct processes where distillate water is produced directly in the solar collector. Indirect processes use sub-systems of solar energy collection and desalination. The direct methods are associated with low water demands due to a variety of simple stills used in that area. The indirect processes use thermal or electric energy, most commonly distillation and membrane methods using solar collectors and power generation or photovoltaic.

 Chafidz et al.[66] made an experimental study on an integrated solar Vacuum Multi-Effect MD (V-MEMD) desalination system. Tests were conducted to evaluate the performance of the system. Under the following conditions a higher thermal-tank temperature, low feed flow rate, high solar radiation and heat pump utilization, the largest amount of water

produced was 99.6L. The optimum feed flow rate was 69 L/h. The use a heat pump gave the biggest contribution to increase the distillate output.
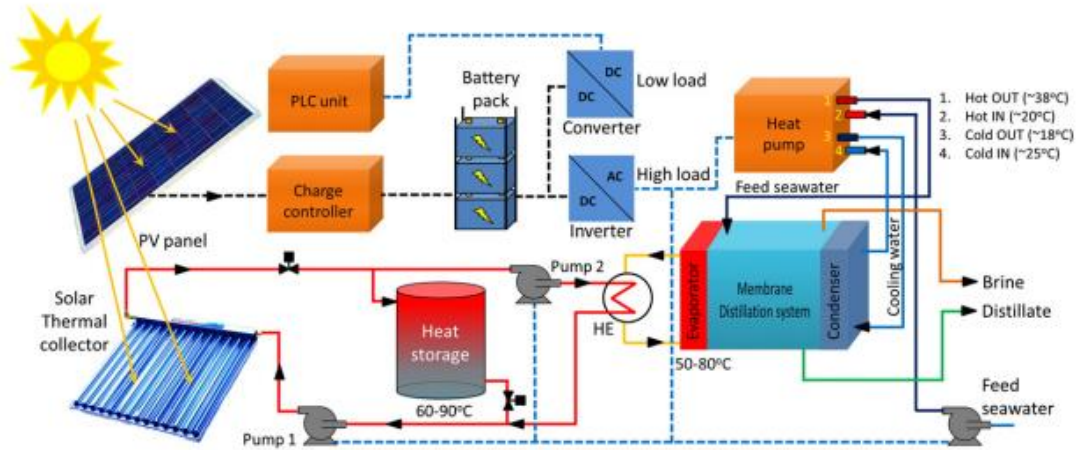
Figure 1.9:Simplified block diagram of the integrated solar-driven desalination system [66]

Meanwhile Zhao et al. [67] studied experimentally the performance of the memsys vacuum-multi-effect-membrane-distillation (V-MEMD) module. Solar and diesel heater were used as heating sources to drive the memsys V-MEMD module. The flow rate and temperature of cooling, heating and feed are the main parameters affecting the module performance and energy efficiency. The factors used to optimize module design and system scaling-up are the number of stages and the size of each stage. The GOR reached 1.52-1.66 and the flux varied from 3.9-8.7 (l/m^2 h) with different numbers of membrane frames.
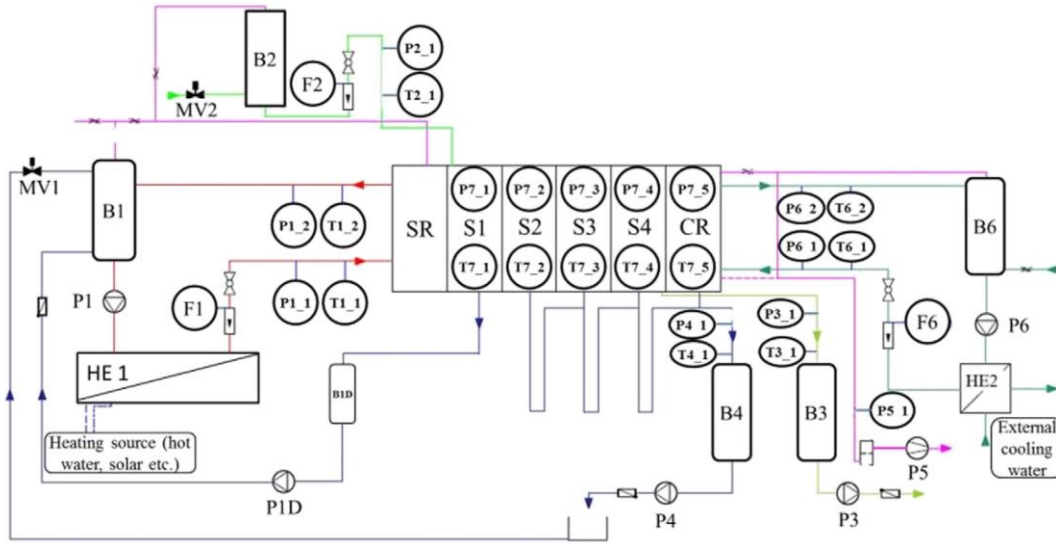
Figure 1.10: Diagram of standard memsys testing system [67]

Hogan et al.[68] studied experimentally and theoretically the performance of a solar powered distillation system. The authors used FORTRAN and TRNSYS to code the mass and energy balance equations. They investigated the effect of increasing the surface area of the membrane at constant feed water temperature and flow rate. The results showed that with as the surface area increase, the distillate flux rate increase too and the experimental results validated the simulation model.

Suarez et al.[69] investigated experimentally the performance of a DCMD driven by a salt-gradient solar pond (SGSP). From the experiments results the author found that the coupled DCMD/SGSP system can threats approximately six times the water flow treated by AGMD/SGSP system. The average fresh water flux reached 1 L h^{-1} per m^2 of membrane. This water production achieved with a temperature difference of 10°C between the feed and the distillate.
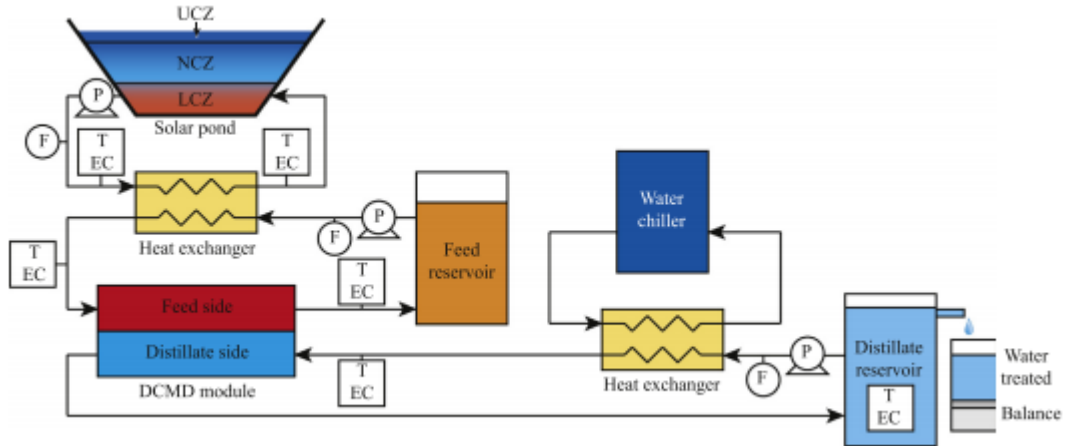
Figure 1.11: Diagram of the experimental setup. The symbols P, EC, F, and T represent pumps, electrical conductivity probes, flow meters, and temperature sensors, respectively; [69]

Zwijnenberg et al. [70] made an experimental analysis on the performance of a solar powered desalination system using membrane pervaporation. The author used synthesized seawater, Oman de-oiled formation water mad sea water from the North Sea. The fouling and feed concentration didn't affect the distillate flux.

Merciq et al. [71] did a study on a four different MD cases integrated with

    a- Solar pond that feed water to MD unit.

    b- MD unit immersed in SP.

    c- Solar collector heats the feed water for a MD unit.

    d- Solar collector integrated with MD unit that heats the feed water for the other MD unit.

The design of the solar collector MD systems was simple compared with SP-MD systems. The output flux from the solar MD systems was higher too.

Guillen-Burrieza et al. [72] conducted experiments on a two types of AGMD (module A and module B). The feed flow occurs through 6 parallel channels in module A while in

module B feed flow occurs through 2 parallel channels. Module A was having a better performance over module B with the increase in the feed flow rate. On the other hand, increasing the feed inlet water temperature has a positive effect on the distillate coming out from both modules

From the previous literature review, we can conclude that what has not been done in the literature is designing and experimental investigations on a solar powered multistage DCMD system.

1.3 THESIS OBJECTIVES

Designing a multi-stage MD system can be a prominent way to increase the amount of the distillate flux output from the system and the feed water energy can be saved using a suitable connection between the modules. The proposed system works close to the atmospheric pressure and hence the construction is simpler. The proposed system offers a sustainable environmental friendly desalination technology which can cover the need of potable water in rural, remote areas with a good solar energy potential.

The objectives of this work are to investigate experimentally the performance of the solar powered multistage membrane distillation system for water desalination and to model the solar system to predict the collector tank temperature and its general performance & efficiency.

The specific objectives are as follows:

- Investigate the performance of a laboratory-scaled Multistage Direct Contact Membrane Distillation (MS-DCMD) system.

- Study the effect of the main operating conditions such as feed temperature, coolant temperature, feed flow rate, coolant flow rate and feed concentration on the permeate flux of the MS-DCMD system.

- Develop mathematical models for predicting the performance of the Evacuated Tube Solar Collector (ETSC)

- Construction and testing of an outdoor solar system, with evacuated tube solar collector, for heating the feed water of the developed MS-DCMD system.

1.4 RESEARCH METHADOLOGY

The proposed work is to be accomplished as per the following stages:

1. Background work and literature review:

    - Build a background about water scarcity problem worldwide, human consumption and needs for fresh water, desalination role, desalination technologies, etc.

    - Conduct a comprehensive literature review on multi-stage membrane distillation and solar desalination systems.

    - Critical review on the direct contact multi-stage membrane distillation system.

22

2. Theoretical work:

A mathematical modeling will be undertaken to perform a parametric study on the energy balance equation of the evacuated tube solar collector to predict the water tank temperature, which is the feed water to the MD desalination system.

3. Experimental work:

The experimental work is divided into two main parts:

1- Multistage DCMD system to be tested inside the lab with a heater as a heating source for the feed water and a chiller to cool up the permeate water stream.

2- Multistage DCMD system to be integrated with the solar collector to heat up the feed water using the solar energy.

The performance of the evacuated tube solar collector with the multistage membrane distillation system to be evaluated. The solar MD system was instrumented with different sensors for monitoring and measuring different variables such as the salinity, pressure, hot and cold water flow rates and temperatures.

CHAPTER 2

EXPERIMENTAL SETUP & PROCEDURES

2.1   Introduction

In this chapter, the description of the indoor multistage direct contact membrane distillation (DCMD) and the outdoor integrated solar DCMD systems setup is presented. Details of the membrane material, the instrumentation used in the experiments, module design and components, and the assembling process of the multistage DMCD system is elaborated. Furthermore, the illustration of the multistage system with different flow arrangement (parallel, series and mixed) is introduced. Additionally, the experimental work objectives, plan and methodology will be summarized as well.

2.2   Description of the laboratory setup

The layout of the multi-stage DCMD system is presented in Figure 2.1. The multi-stage system consists of two water closed cycles, hot and cold, connected to the MD modules. The main components of the experimental setup are: A water chiller which can supply cold water flow at constant temperature and constant flow rate (Figure 2.3), an electric heater to feed the hot side of the system with water stream at constant temperature and constant flow rate (Figure 2.2), Chlorinated Poly-Vinyl Chloride (CPVC) pipes used to connect the system components which can withstand high water temperature (more than 90ºC), and the

three DCMD modules where the water vapor separation and condensation process takes place.
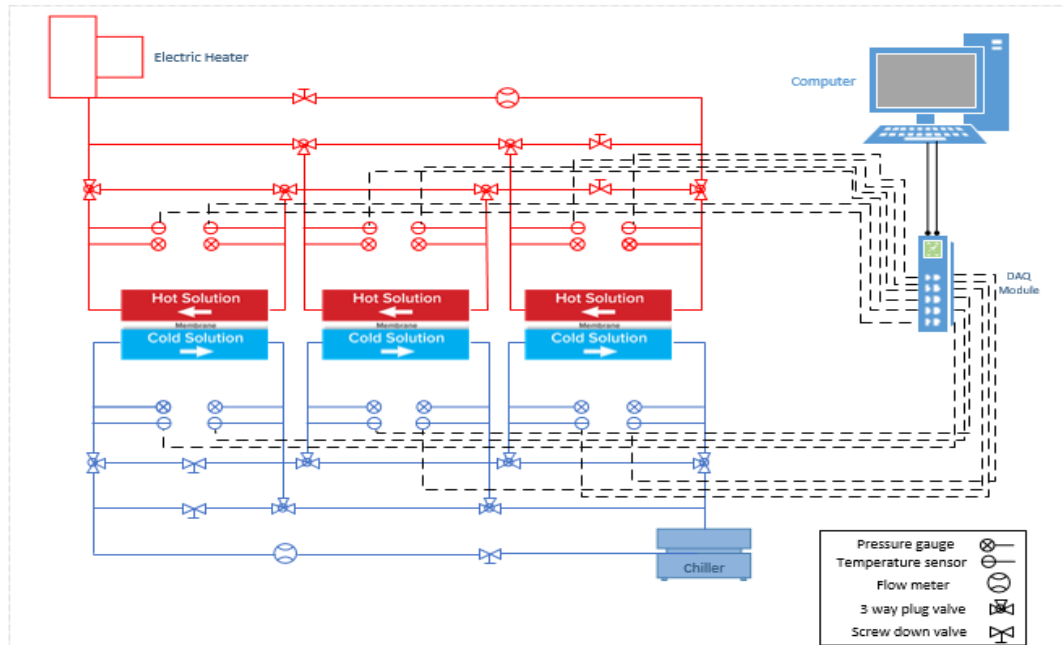
Figure 2.1: The layout of the indoor laboratory system

Figure 2.2: The electric heater

Figure 2.3: The electric chiller

The two cycles are manually controllable by some valves to change between different flow arrangement (parallel, series and mixed) and to change the water flow rate. The system setup is shown in the following Figure 2.4.
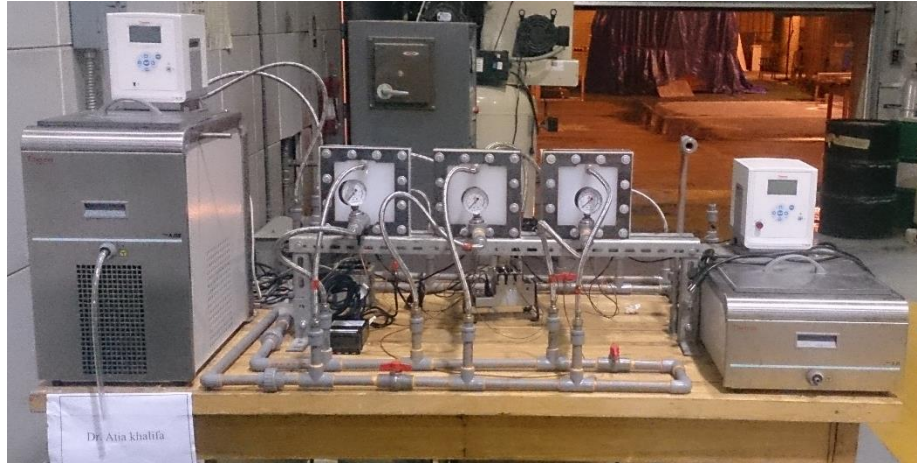
Figure 2.4: The actual experimental system

2.3 Description of the solar multistage DCMD system

The same multi-stage DCMD system with its two-closed water closed cycles, hot and cold, are connected to an evacuated tube solar collector tank with 150 L water capacity and a water chiller, respectively. The main components of the experimental setup are: A water chiller which can supply cold water stream at constant temperature and constant flow rate (Figure 2.3), an evacuated tube solar collector system to heat up the feed water to the required temperature (Figure 2.5), two 0.5 hp centrifugal pumps responsible for pumping the hot and cold water stream to the DCMD modules at selected flow rates (Figure 2.6), Chlorinated Poly-Vinyl Chloride (CPVC) pipes to connect the system components, and the three DCMD modules where water vapor separation and condensation process takes place. The layout of the solar multi-stage DCMD system is shown in Figure 2.7.

Figure 2.5: The evacuated tube solar collector

Figure 2.6: The electric water pump
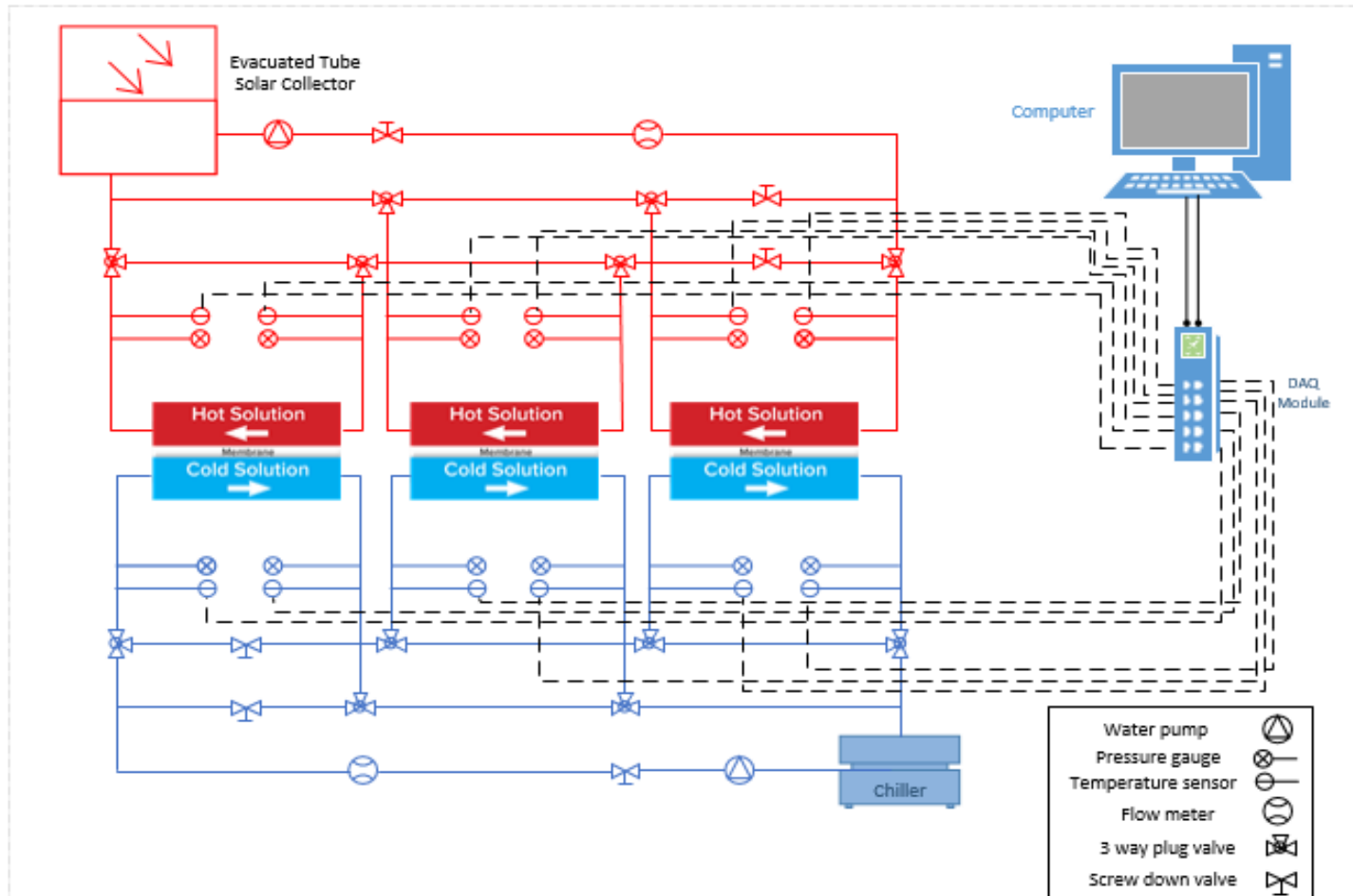
Figure 2.7: The layout of the multistage solar DCMD system

2.4 Module design

The multistage DCMD system contains three separated MD modules. High-Density-Poly-ethylene (HDPE) material is used to fabricate two chambers in each cell with total dimensions of 210 mm width, 210 mm length, and 40 mm thickness. The MD module chambers are feed chamber and cooling chamber, with two flow channels in each chamber. In-between every component within the module is a rubber gasket with 1.5 mm thickness to prevent internal and external leakage. The module flow channels were machined using CNC machine located at the main ME workshop. The module detail design and its dimensions are presented in Figure 2.8.
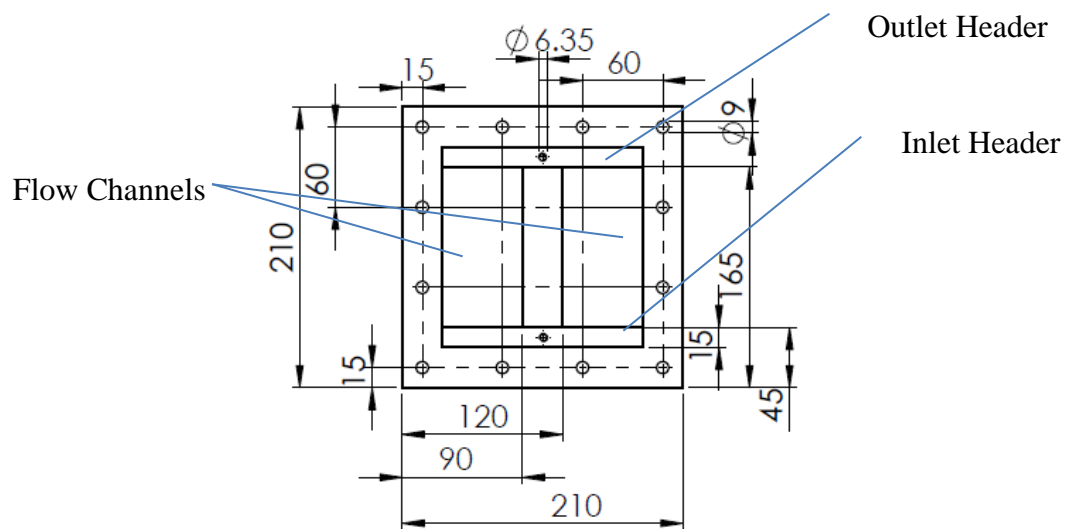
Figure 2.8: A detailed solidworks sketch for the module with its dimensions in mm

Figure 2.9 shows the detailed description of the parts used in designing the DCMD module which are two steel frame sheets, two plastic compartments for the module (HDPE) with two channels, three rubber gaskets, membrane, and one brass supportive perforated plate
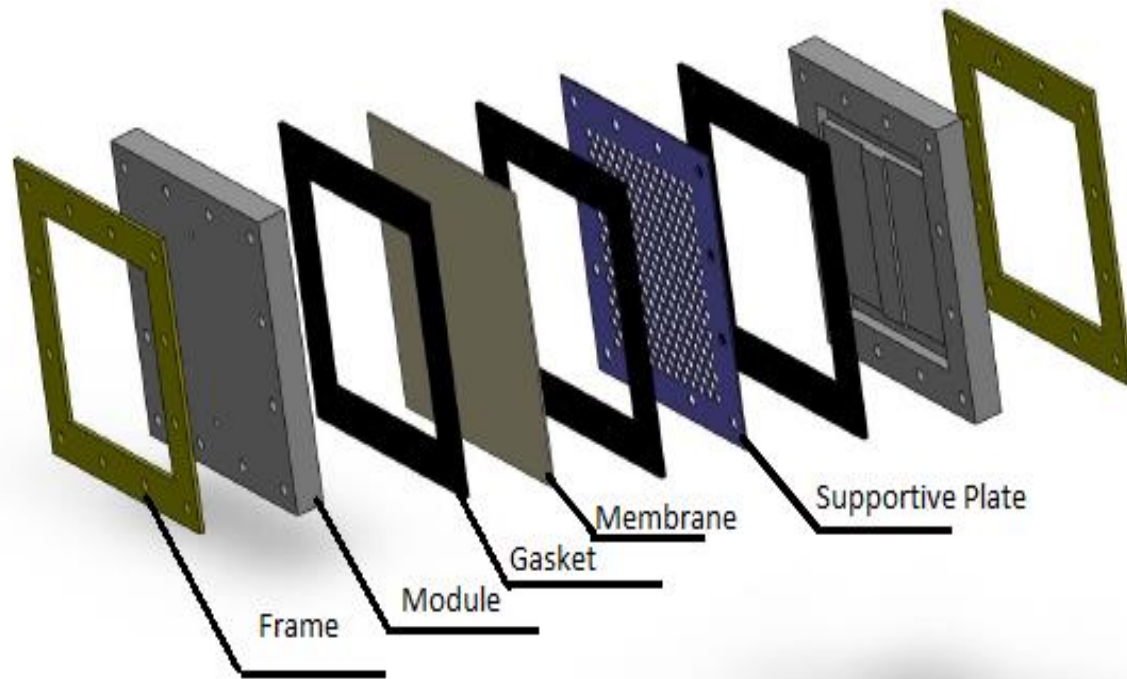
Figure 2.9: The detailed description of the module.
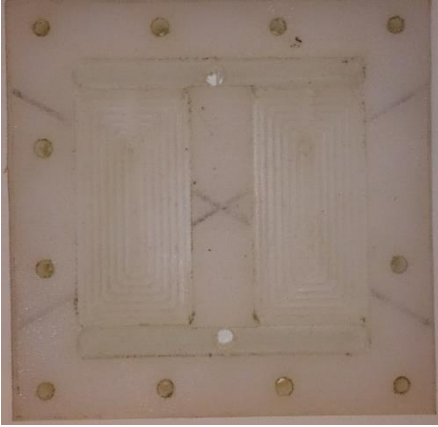
a- HDPE Module Chamber   b- Gasket   c- Membrane   brass support
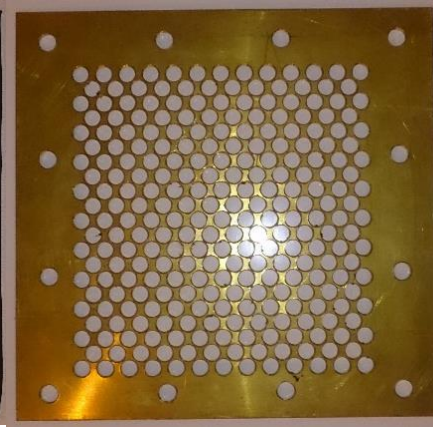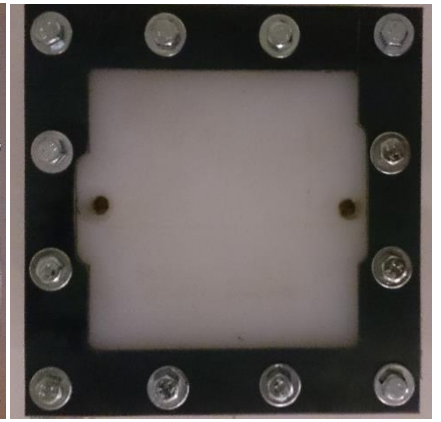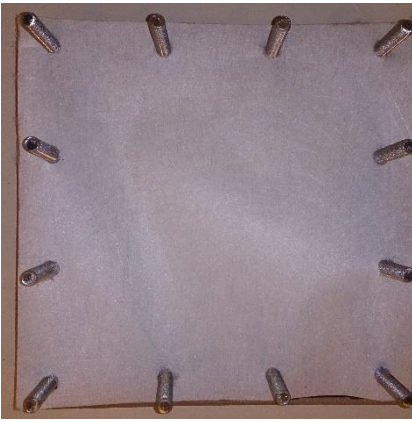
d- Membrane

Figure 2.10: Module parts used and the steps of the assembly process

2.5   Membrane characterization

The membrane material used in this study is polytetrafluoroethylene (PTFE) of 0.22 µm

pore size acquired from TISH SCIENTIFIC. It is a composite membrane that is composed

of an active layer and support layer. The properties of the membrane material are measured

in Universidad Complutense de Madrid (UCM), Spain and are tabulated in Table 2.1.

Table 2.1: Membrane properties

Properties	PTFE 0.22 µm
δfull membrane (µm)	159.5 ± 18.0
δteflon (µm)	7.9 ± 1.8
δsupport (µm)	143.3 ± 15.6
d_p (nm)	236 ± 6
porosity (%)	75.9 ± 5.4
θ (°) active layer	138.3 ± 2.4
θ (°) support layer	121.4 ± 3.4

2.6   Instrumentations and measuring devices

The main instrumentations used for the measurements are feed flow meter (OMEGA FL

50000), coolant flow meter (OMEGA FPR310) and a conductivity meter (DELTA-OHM

HD 3406.2) to measure the salinity of the water in the two cycles. Also, thermocouples and

pressure gauges have been installed at the inlet and exit of each MD module to measure

the temperatures and the pressures respectively. Using the LABVIEW software, a code

was created to transfer the thermocouple signals to a data acquisition system for recording

the temperature readings at the inlet and exit of each module and analyze it along with the

power consumption signals for both the chiller and the heater. The permeate flux can be calculated for the membrane effective area by collecting the product volume from the three MD modules which appear as an increase in the water level inside the electric chiller at a certain period. Additionally, by measuring the feed and permeate salinity (salt concentration), the salt rejection factor can be calculated.

Figure 2.11: Conductivity meter

Figure 2.12: Coolant flow meter

Figure 2.13: DAQ modules

Figure 2.14: Feed flow meter

Figure 2.15: Power transducer

2.7 Calibration of the coolant flow meter

To calibrate the coolant flow meter, manual measurements have been undertaken for the water volumetric flow rate leaving the chiller using a stop watch. Table 2.2 represents the difference between the manual measurements and the flow meter readings.

Table 2.2: Calibration of the flow meter

Chiller Pump Adjustments	Flow meter Reading (L/min)	Manual Measurements (L/min)	Error (%)
Low	6.53	6.52	0.15314
Medium	9.32	9.3	0.21459
High	12.52	12.5	0.15974

2.8   System operation

The system main components are the chiller, the heater in the indoor case (ETSC in the outdoor case), and the DCMD module stack. The feed water is pumped from the heater (ETSC) to the module stack after getting heated to the required temperature where it enters the modules from the inlet header, then it continues to flow over the channels where vapor transfers across the hydrophobic membrane to the permeate cycle. After that, it leaves the module through an opening in the outlet header. While the cold water in the permeate cycle is pumped from the chiller to the cold module chamber through the inlet header. Then it continues to flow over the permeate cold channels where vapor condensation occurs. After collecting the condensed vapor, cold water flows out of the MD module through the outlet header to the permeate cold bath in the chiller.

During this process, thermocouples installed at the inlet and exit of each module chamber measure the temperature of the feed and permeate streams. Furthermore, the flow rate of the feed and permeate streams is measured and manually controlled using flow meters and valves.

For measuring the increase in the permeate volume in the cold cycle at a specified time period from the three MD modules, a small pipe is settled at a certain level in the chiller. As the vapor condensation process occurs in the three modules, the permeate volume level increases in the chiller bath. Which appears as water droplets that fall from the small pipe as shown in the following Figure 2.16.
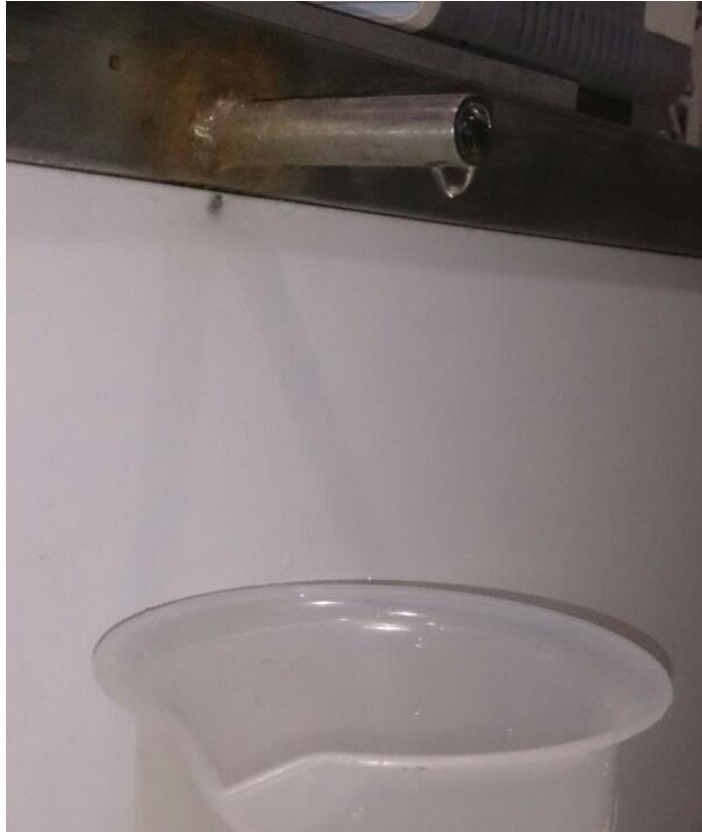
Figure 2.16: The permeate volume level increase pipe

2.9 System flow Arrangements

In this section, the different flow arrangements which will be experimentally investigated will be explained and summarized.

2.9.1 Parallel flow arrangement

The parallel flow arrangement is based on the idea of pumping feed and cold water in parallel lines where the inlet temperature to the MD modules is equal in both cycles. The feed water leaves the MD modules to the heater bath while the cold water in the permeate

side exits the MD modules to the chiller cold bath for cooling and recirculation. Figure 2.17 presents the parallel flow arrangement.
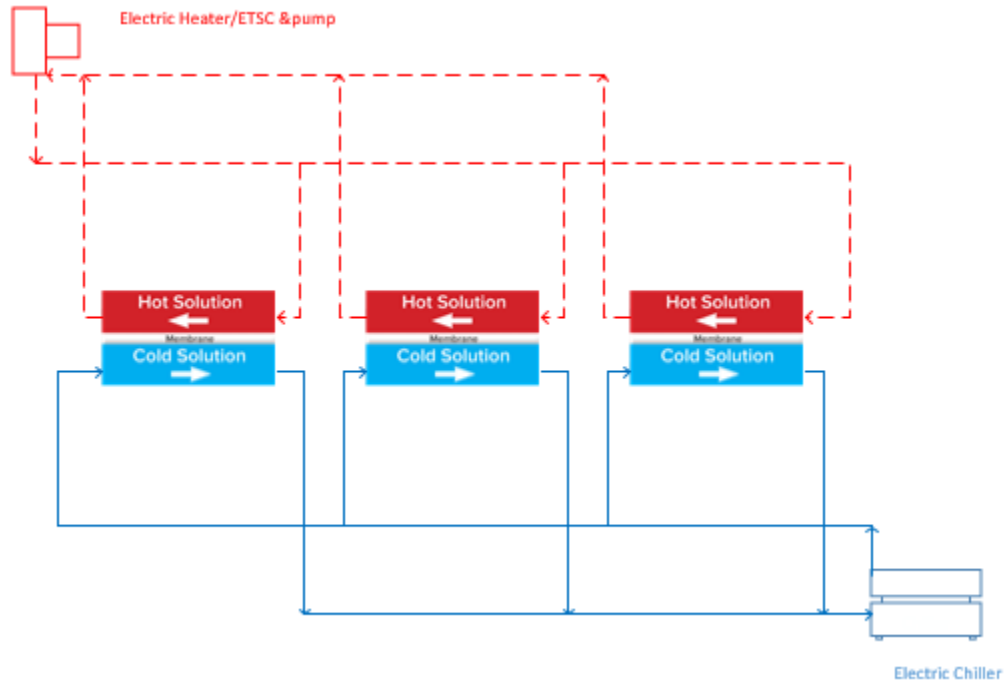
Figure 2.17: Parallel flow arrangement

2.9.2 Series flow arrangement

In the series flow arrangement, the feed and cold flow streams in both cycles are pumped to the first module chamber in each side. Then the flow goes from the first module to the next one until it reaches the heater bath in the hot side and the chiller cold bath in the permeate side. Figure 2.18 shows the layout of the series flow arrangement.
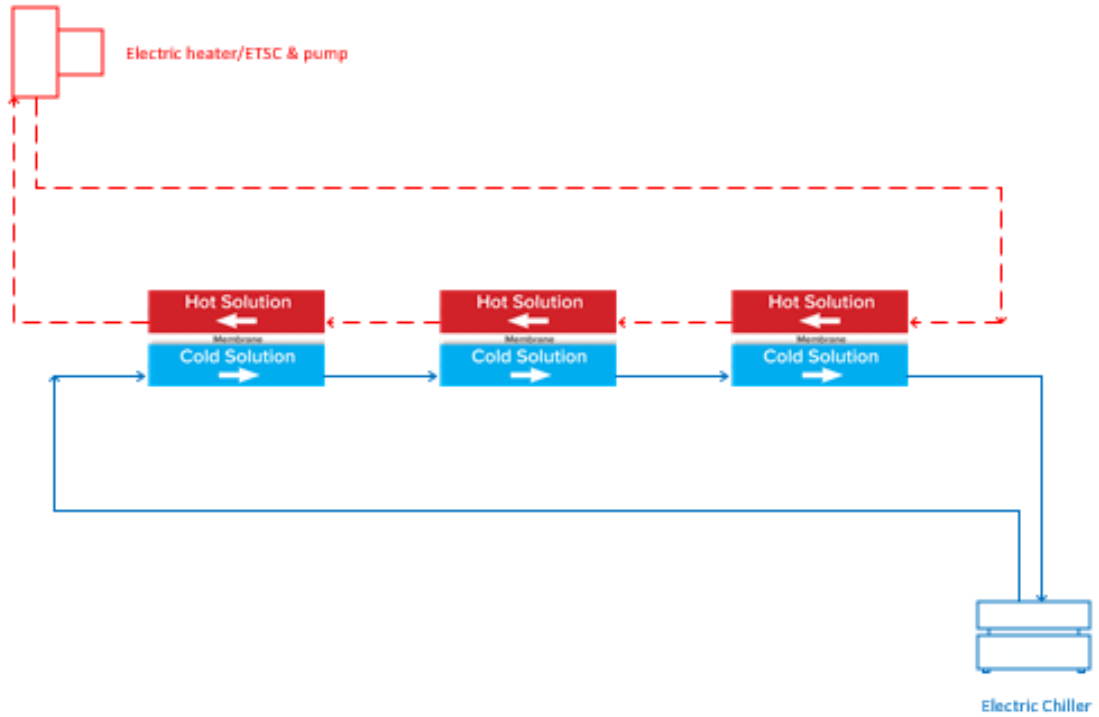
Figure 2.18: Series flow arrangement

2.9.3 Mixed flow arrangement (Series feed – Parallel permeate)

In the mixed flow arrangement, the feed cycle side is connected in series with the MD modules. The feed water is pumped from the heater to the first MD module chamber then it flows to the next one until it reaches the hot bath in the heater. While in the permeate cycle, the cold water is pumped at the same temperature to the three modules at the same time in parallel then the three outlet lines from the MD modules gathered together to the chiller bath.
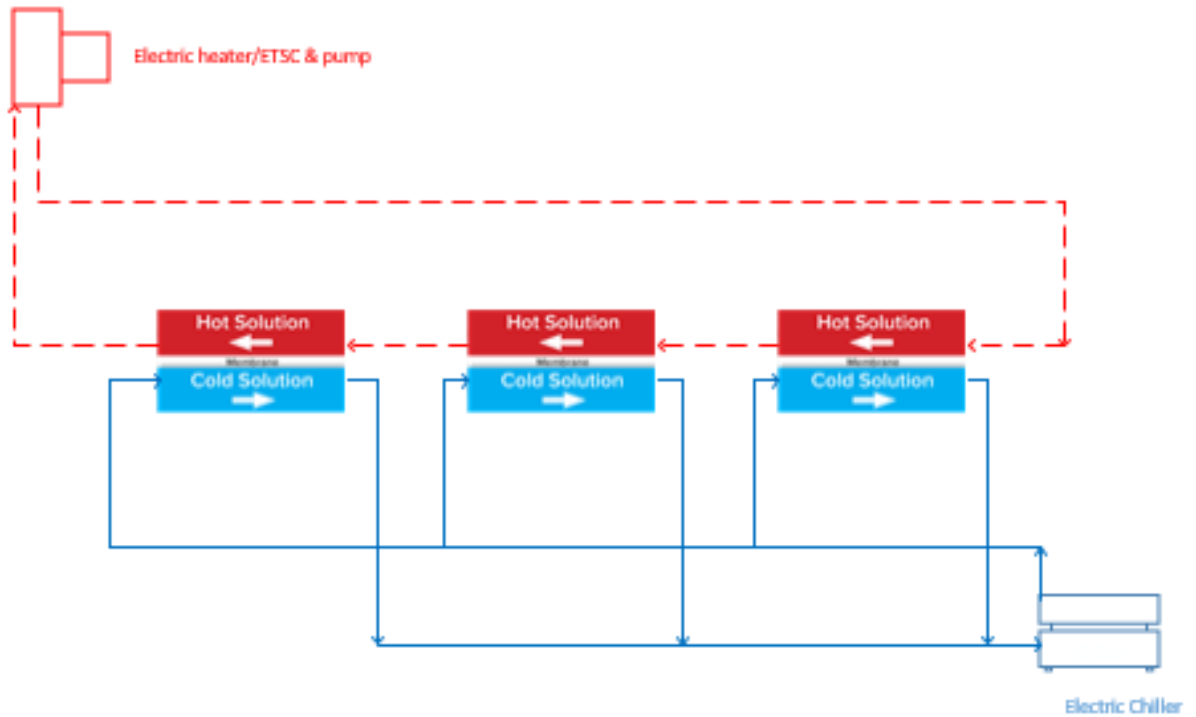
Figure 2.19: Mixed arrangement (Series feed- Parallel permeate)

2.10 Experimental plan

The operating parameters that are investigated are the feed temperature, feed flow rate, permeate temperature, permeate flow rate and feed concentration. The experiments are conducted by studying the effect of changing one of these variables with different flow arrangement. The experimental plan is presented in Table 2.3.

Table 2.3: Experimental plan

No	Variable	Range
1	Feed Temperature	40 ºC – 90 ºC
2	Coolant Temperature	15 ºC - 25 ºC
3	Flow Rate of Feed (Parallel)	4 L/min - 7 L/min
4	Flow Rate of Feed (Series)	1 L/min – 3 L/min
5	Flow Rate of Coolant (Parallel)	4 L/min – 6 L/min
6	Flow Rate of Coolant (Series)	1 L/min – 3 L/min
7	Feed Concentration	0.15 g/L, 3 g/L, and 35 g/L

CHAPTER 3

PERFORMANCE OF THE LABORATRY MS-DCMD

SYSTEM

In this chapter, the effect of different operating parameters on the permeate flux output from the laboratory MS-DCMD system are studied. The operating variables are the feed temperature, permeate temperature, feed flow rate, and permeate flow rate. The power consumption of both the electric heater and the chiller is measured. Furthermore, the output permeate flux studied at different feed concertation. The mentioned operating variables are changed for different flow arrangements.

3.1   Effect of feed temperature at different feed flow rates

The effect of feed water temperature at different feed flow rates is studied for the multistage direct contact membrane distillation system (MS-DCMD). Figure 3.1 shows the effect of varying feed temperature at different feed flow rates on the permeate flux for the three modules in the MS-DCMD system in case of the parallel flow arrangement. The feed temperature is changed from 40°C to 90°C with 10°C increment and the feed flow rate entering the three modules is changed from 5 to 7 L/min with 1 L/min increment. The measurement of the permeate flux (for the three modules) started from the steady state at permeate temperature 25°C, 3500 mg/L feed concentration, and permeate flow rate =6 L/min (the total flow rate for the three modules is 6 L/min such that 2 L/min for each module).

41

The permeate flux increases with the increase in feed temperature and feed flow rate since increasing the feed temperature increases the vaporization rate in the feed side and consequently the vapor pressure difference across the membrane.

With the increase in the feed flow rate, the permeate flux increases due to the enhancement in the turbulence level which leads to better mixing in the boundary layer and higher values of the heat and mass transfer coefficients through the membrane.

The maximum value of the system permeate flux (flux is based on the total area of membrane in the three modules) is reached at 90°C, and it is about:

- 87.84 kg/m^2.hr for the MS-DCMD system in the parallel flow arrangement at total feed flow rate= 7 L/min

- 79.88 kg/m^2.hr for the MS-DCMD system in the parallel flow arrangement at total feed flow rate= 6 L/min

- 67.03 kg/m^2.hr for the MS-DCMD system in the parallel flow arrangement at total feed flow rate= 5 L/min

The percentage increase in the permeate flux due to change the feed temperature from 40°C to 90°C at total feed flow rate 7 L /min is 374.34% while the percentage increase in the permeate flux due to change the feed flow rate from 5 L/min to 7 L/min at 90°C feed temperature is 31.04%.

Figure 3.1: The effect of varying feed temperature and feed flow rate on the permeate flux for the parallel flow arrangement

Conditions: membrane PTFE 0.22 μm, permeate temperature 25ºC, feed salinity 3500 mg/L, permeate flow rate of 2 L/min for each module.

In the series flow arrangement, the feed temperature is changed from 40ºC to 90ºC with 10ºC increment and the feed flow rate entering modules in series is changed from 2 to 3 L/min with 0.5 increment. The measurement of the permeate flux (for the three modules) started from the thermal steady state for the modules at permeate temperature 25ºC, 3500 mg/L feed concentration, and the total permeate flow rate passing the modules in series is 2 L/min.

Figure 3.2 presents the effect of varying the feed temperature and feed flow rate on the permeate flux for the three modules in the MS-DCMD system in case of the series flow arrangement.

The maximum value of the system permeate flux (the total permeate flux from the three modules) is reached at 90°C, and it is about:

- 73.46 kg/m^2.hr for the MS-DCMD system in the series flow arrangement at feed flow rate= 3 L/min

- 59.68 kg/m^2.hr for the MS-DCMD system in the series flow arrangement at feed flow rate= 2.5 L/min

- 54.17 kg/m^2.hr for the MS-DCMD system in the series flow arrangement at feed flow rate= 2 L/min.

The percentage increase in the permeate flux due to change the feed temperature from 40°C to 90°C at feed flow rate passing the modules in series 3 L /min is 336.4% while the percentage increase in the permeate flux due to change the feed flow rate that passes the modules in series from 2 L/min to 3 L/min at 90°C feed temperature is 35.59%

Figure 3.2: The effect of varying feed temperature and feed flow rate on the permeate flux for the series flow arrangement

Conditions: membrane PTFE 0.22 μm, permeate temperature 25°C, feed salinity 3500 mg/L, permeate flow rate of 2 L/min for each module.

3.2 Effect of feed temperature with changing the permeate flow rate

Figure 3.3 shows the variation of the permeate flux with the feed temperature at different permeate flow rates in the parallel flow arrangement. The feed temperature is changed from 40°C to 90°C with 10°C step increase and the permeate flow rate entering the three modules changed from 4 to 6 L/min with 1 increment in case of parallel flow arrangement.

From Figure 3.3, the permeate flux increase with the increase in the permeate flow rate and with the increase in the feed temperature. Increasing the permeate flow rate for the MS-

45

DCMD enhances the turbulence level in the permeate channels, which leads to higher values of the mass and heat transfer coefficients in the permeate side of the module and that will enhances the condensation rate of the vapor. It is noted that the effect of changing the permeate flow rate is much less than the effect of varying feed flow rate. The percentage increase in the permeate flux due to change the feed temperature from 40°C to 90°C at total permeate flow rate 6 L /min is 521.9% while the percentage increase in the permeate flux due to change the permeate flow rate from 4 L/min to 6 L/min at 90°C feed temperature is 4.1%.

Figure 3.3: The effect of varying feed temperature and permeate flow rate on the permeate flux for the parallel flow arrangement

Conditions: membrane PTFE 0.22 μm, permeate temperature 25°C, feed salinity 3500 mg/L, feed flow rate of 2 L/min for each module.

Figure 3.4 shows the variation of the permeate flux with the feed temperature and permeate flow rate for the series flow arrangement. The feed temperature is changed from 40°C to 90°C with 10°C step increase and the permeate flow rate is changed from 2 to 3 L/min with 0.5 increment in case of series flow arrangement. The percentage increase in the permeate flux due to change the feed temperature from 40°C to 90°C at permeate flow rate passing the modules in series 3 L /min is 470.2% while the percentage increase in the permeate flux due to change the permeate flow rate that passes the modules in series from 2 L/min to 3 L/min at 90°C feed temperature is 8.2%.

Figure 3.4: The effect of varying feed temperature and permeate flow rate on the permeate flux for the series flow arrangement

Conditions: membrane PTFE 0.22 µm, permeate temperature 25°C, feed salinity 3500 mg/L, feed flow rate of 2 L/min for each module.

3.3 Effect of feed flow rate with changing the permeate flow rate

In this section, the effect of varying the feed flow rate with the permeate flow rate on the permeate flux will be investigated. In the parallel flow arrangement, the total feed flow rate values used for the three modules are 5 L/min, 6 L/min, and 7 L/min while the total permeate flow rate are 4 L/min, 5 L/min, and 6 L/min for the three modules. The permeate flux variation is recorded at constant feed temperature 50°C, permeate temperature of 25°C, and 3500 mg/L feed concentration.

Figure 3.5 presents the variation of feed flow rate with permeate flow rate in the parallel flow arrangement. The permeate flux increases with the increase in the feed flow rate and permeate flow rate due to the increase in the turbulence levels in both the feed and permeate sides which increase the heat and mas transfer coefficients and also the rate of condensation of the vapor. The effect of changing the permeate flow rate is much less than the effect of varying the feed flow rate. The percentage increase in the permeate flux due to change the total feed flow rate from 5 L/min to 7 L/min at total permeate flow rate 6 L /min is 164.3% while the percentage increase in the permeate flux due to change the total permeate flow rate from 4 L/min to 6 L/min at total feed temperature 7 L/min is 7%.
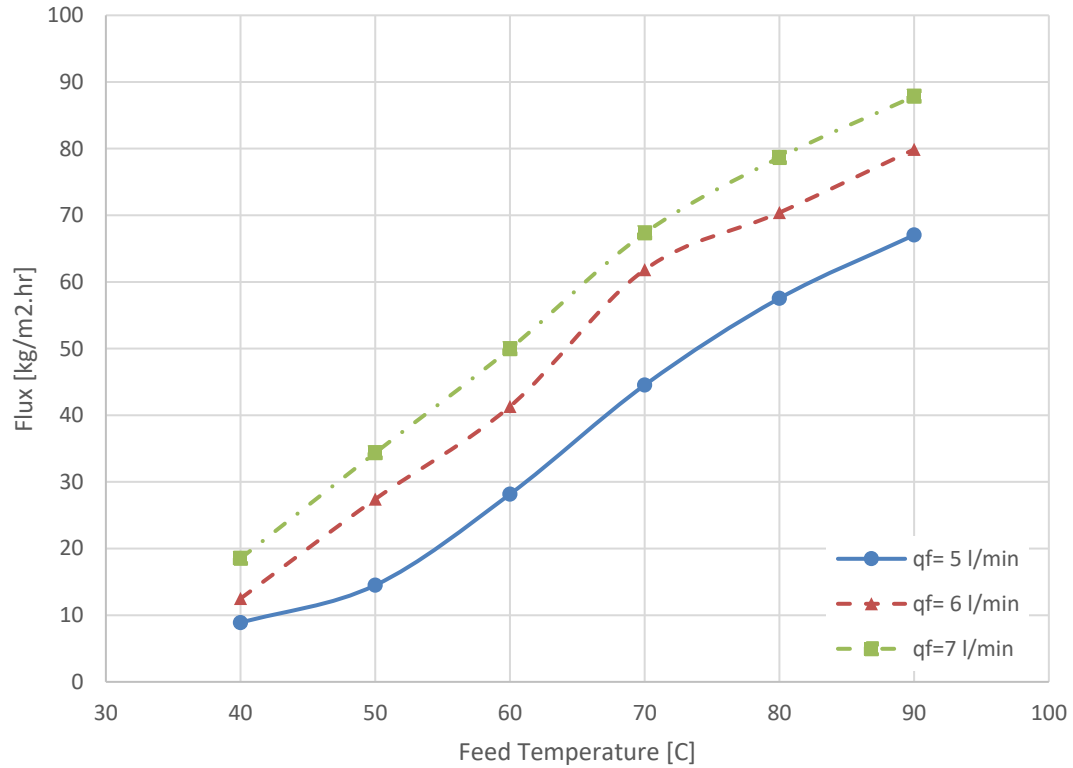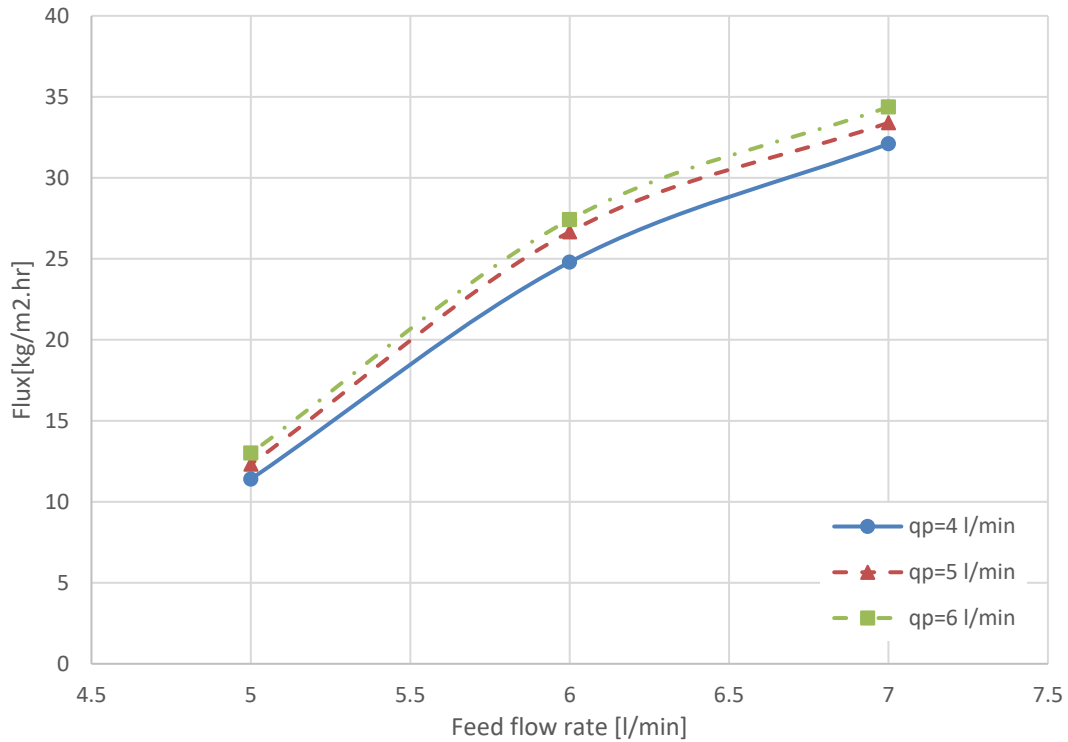
Figure 3.5: The effect of varying feed flow rate and permeate flow rate on the permeate flux for the parallel flow arrangement

Conditions: membrane PTFE 0.22 μm, permeate temperature 25°C, feed salinity 3500 mg/L, feed temperature 50°C.

Figure 3.6 shows the effect of changing the feed flow rate and the permeate flow rate on the permeate flux for the series arrangement. The feed flow rate varied for three different values passing each module are 2 L/min, 2.5 L/min, and 3 L/min and the permeate flow rate values 2 L/min, 2.5 L/min, and 3 L/min (for each module). The percentage increase in the permeate flux due to change the feed flow rate passing the modules in series from 2 L/min to 3 L/min at permeate flow rate passing the modules in series 3 L /min is 224.2% while the percentage increase in the permeate flux due to change the permeate flow rate that passes the modules in series from 2 L/min to 3 L/min at feed flow rate passing the modules in series 3 L /min is 7.4%.
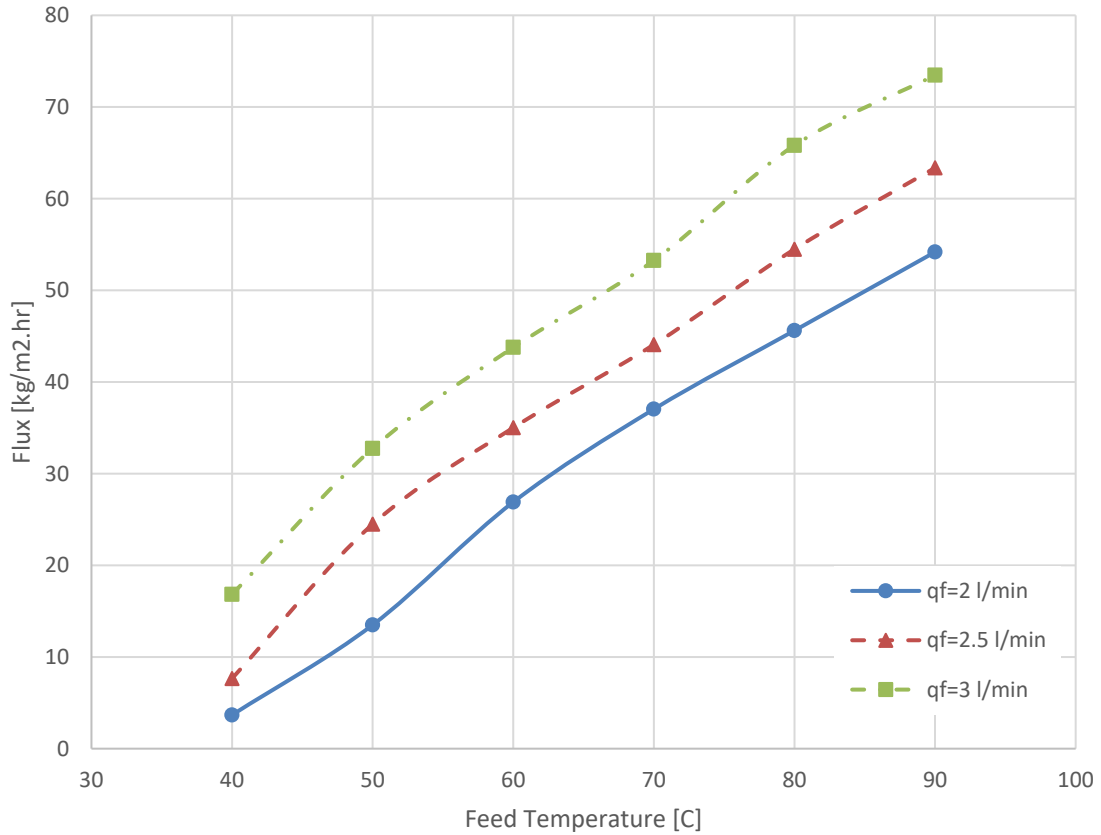
49
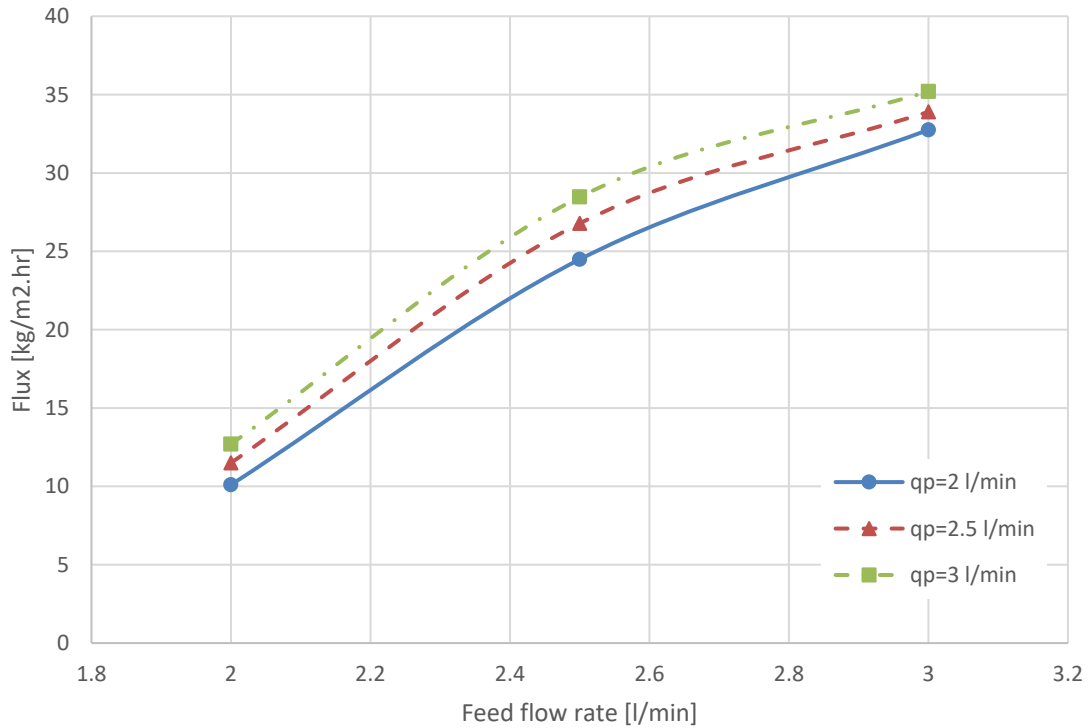
Figure 3.6: The effect of varying feed flow rate and permeate flow rate on the permeate flux for the series flow arrangement

Conditions: membrane PTFE 0.22 μm, permeate temperature 25ºC, feed salinity 3500 mg/L, feed temperature 50ºC.

3.4 Effect of feed temperature at different permeate temperature

The effect of varying feed temperature and permeate temperature on permeate flux will be studied. The permeate temperature is varied from 15ºC to 25ºC with 5ºC step increase. The change in the permeate temperature is observed and recorded at different feed temperature varied from 50ºC to 70ºC with 10ºC step increase. The feed salinity concentration is 3500 mg/L. In the parallel flow arrangement, the total inlet feed and permeate flow rates are 6 L/min (the flow rate for the three modules) while 2 L/min for the series flow arrangement.

Figure 3.7 shows the effect of permeate temperature with changing the feed temperature on the permeate flux in the parallel flow arrangement. The increase in the permeate temperature decreases both the temperature and pressure difference between feed and permeate sides across the membrane resulting a decrease in the permeate flux. The percentage increase in the permeate flux due to change the feed temperature from 50°C to 70°C at 15°C permeate temperature is 101.1% while the percentage increase in the permeate flux due to change the permeate temperature from 25°C to 15°C at 70°C feed temperature is 35.43%.
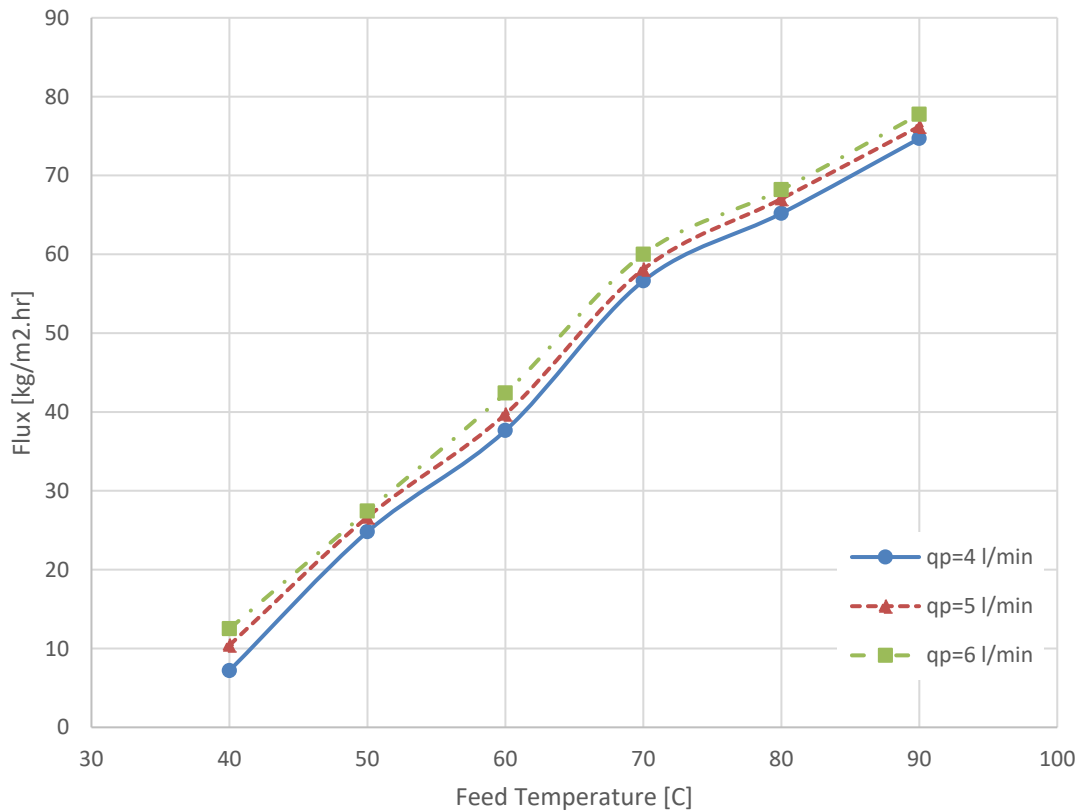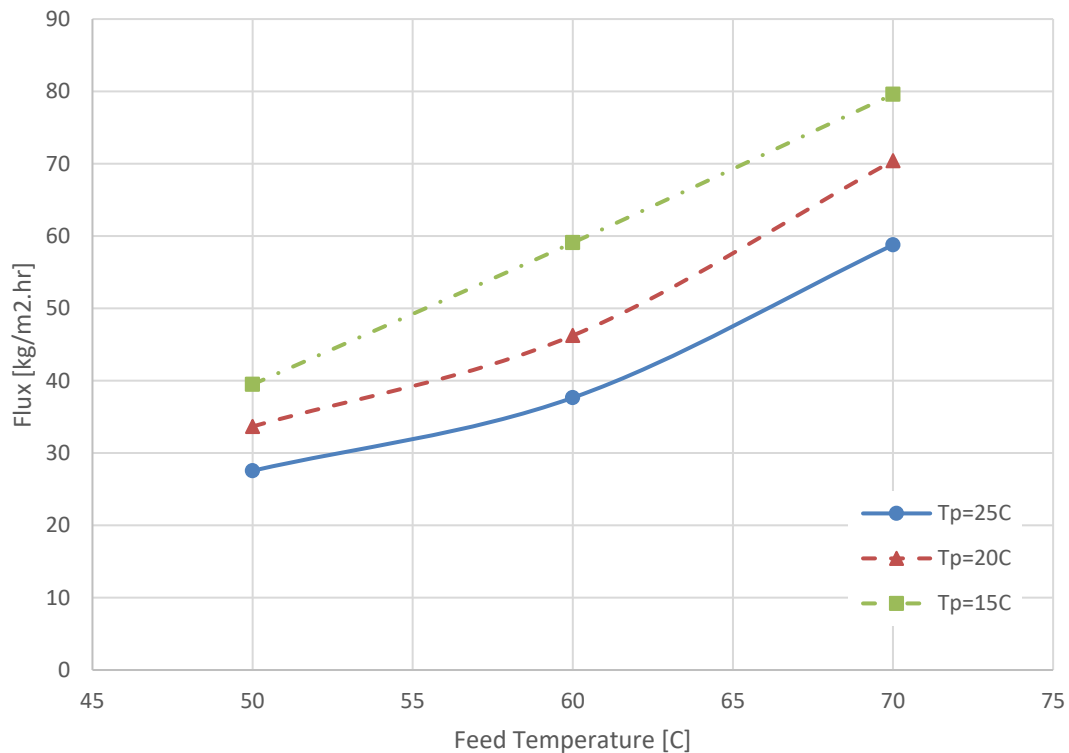

Figure 3.7: The effect of varying feed temperature and permeate temperature on the permeate flux for the parallel flow arrangement

Conditions: membrane PTFE 0.22 μm, total permeate flow rate 6 L/min, feed salinity 3500 mg/L, total feed flow rate 6 L/min.

51

For the series flow arrangement in the MS-DCMD system, the effect of permeate temperature on the permeate flux studied at feed flow rate 2 L/min and permeate flow rate 2 L/min as shown in Figure 3.8. The percentage increase in the permeate flux due to change the feed temperature from 50°C to 70°C at 15°C permeate temperature is 85.22% while the percentage increase in the permeate flux due to change the permeate temperature from 25°C to 15°C at 70°C feed temperature is 34.71%.
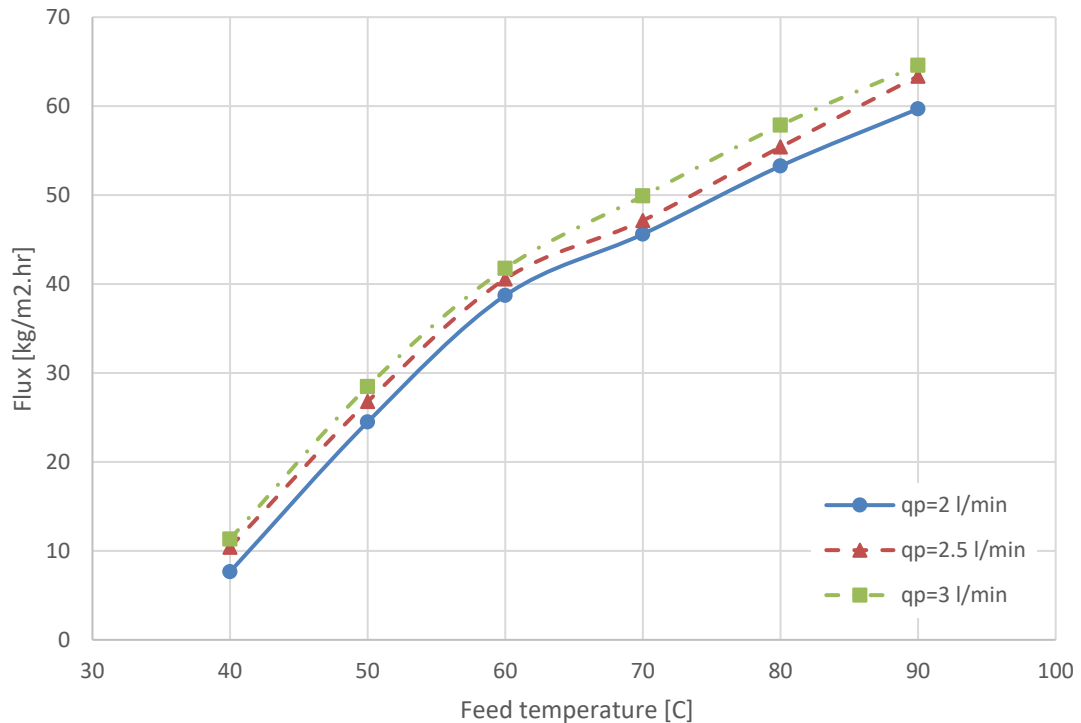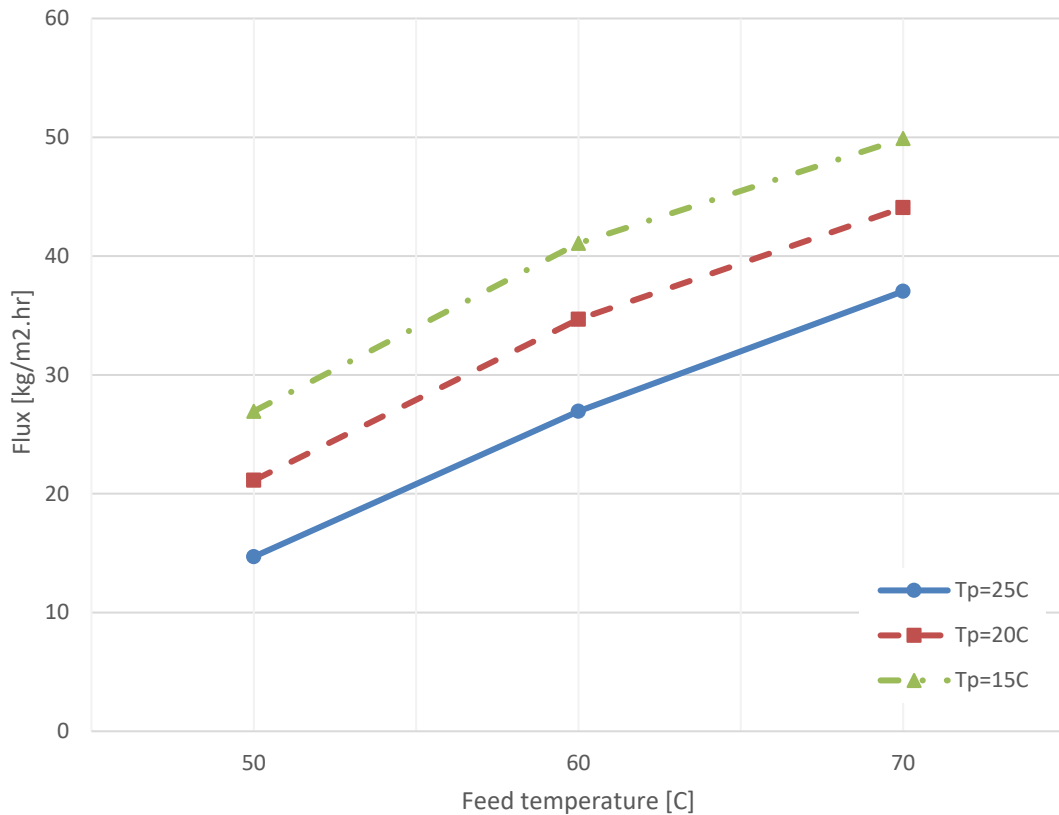

Figure 3.8: The effect of varying feed temperature and permeate temperature on the permeate flux for the series flow arrangement

Conditions: membrane PTFE 0.22 μm, permeate flow rate 2 L/min, feed salinity 3500 mg/L, feed flow rate 2 L/min.

3.5 Effect of flow arrangement

The mixed flow arrangement (series feed – parallel permeate) for the MS-DCMD system has been compared to both the parallel and series flow arrangements at feed temperature changed between 40°C to 90°C. These three flow arrangements were tested at permeate temperature 25°C, 3500 mg/L feed concentration, and permeate flow rate =6 L/min (the total flow rate for the three modules such that 2 L/min passing each module in the series case).

Figure 3.9 shows the comparison between the three-different flow arrangements at different feed temperatures.
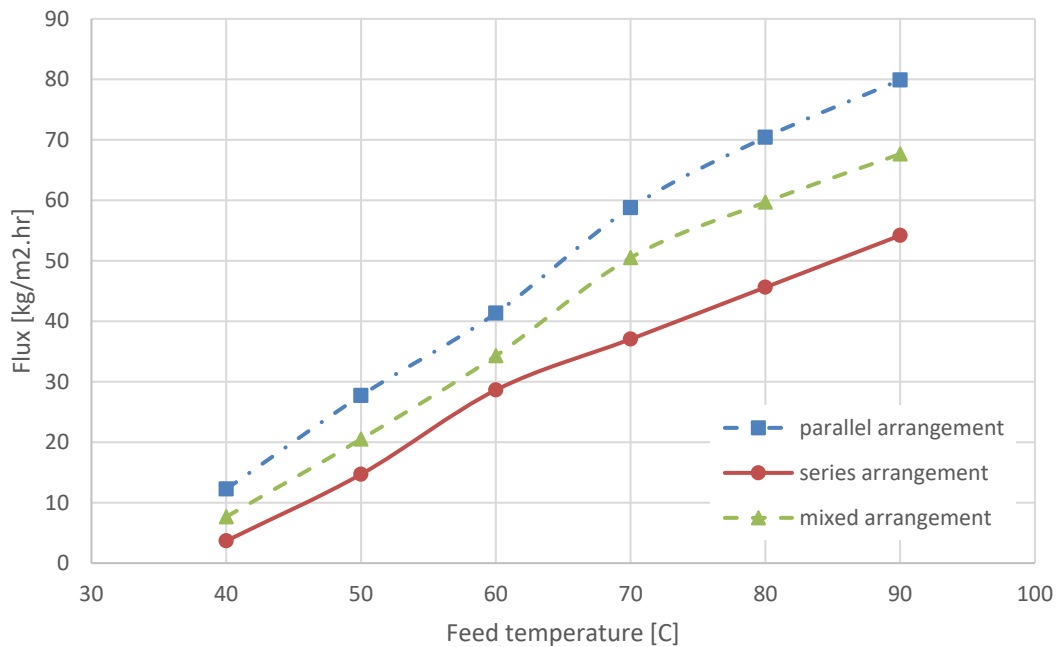
Figure 3.9: The comparison between the three-flow arrangements at different feed temperatures

Conditions: membrane PTFE 0.22 μm, permeate temperature 25°C, feed salinity 3500 mg/L, feed and permeate flow rates of 2 L/min for each module.

From Figure 3.9 it can be clearly seen that; the output permeate flux for the MS-DCMD system in the parallel flow arrangement is much higher than both the mixed and series flow

arrangements. This is due to the high temperature difference across the membrane for the three modules in the parallel flow arrangement case compared to the other cases.

Figure 3.10 presents the percentage increase in the permeate flux due to change the flow arrangement from series to mixed flow arrangement and from series to parallel flow arrangement at feed temperature 90°C, permeate temperature 25°C, feed salinity 3500 mg/L, and feed and permeate flow rate of 2 L/min for each module.
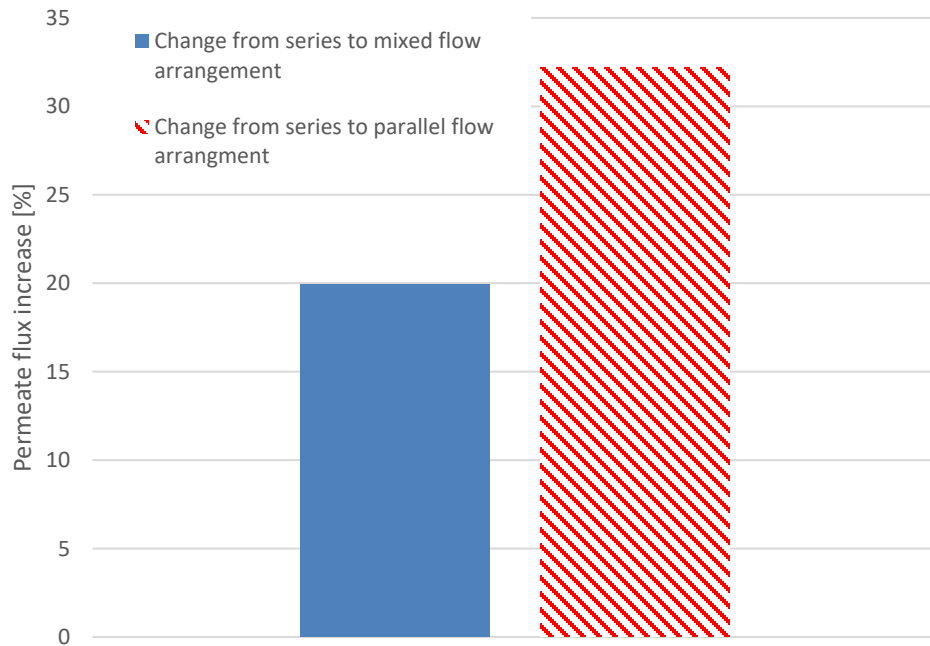
Figure 3.10: Percentage increase in the output flux due to change from series to mixed and parallel flow arrangement at feed temperature 90°C

Conditions: membrane PTFE 0.22 μm, feed temperature 90°C, permeate temperature 25°C, feed salinity 3500 mg/L, feed and permeate flow rate of 2 L/min for each module.

Figure 3.11 presents the comparison between the three-flow arrangements at different feed flow rates. These three flow arrangements tested at feed temperature 50°C, permeate temperature 25°C, 3500 mg/L feed concentration, and permeate flow rate =6 L/min (the

total flow rate for the three modules such that 2 L/min passing each module in the series case).
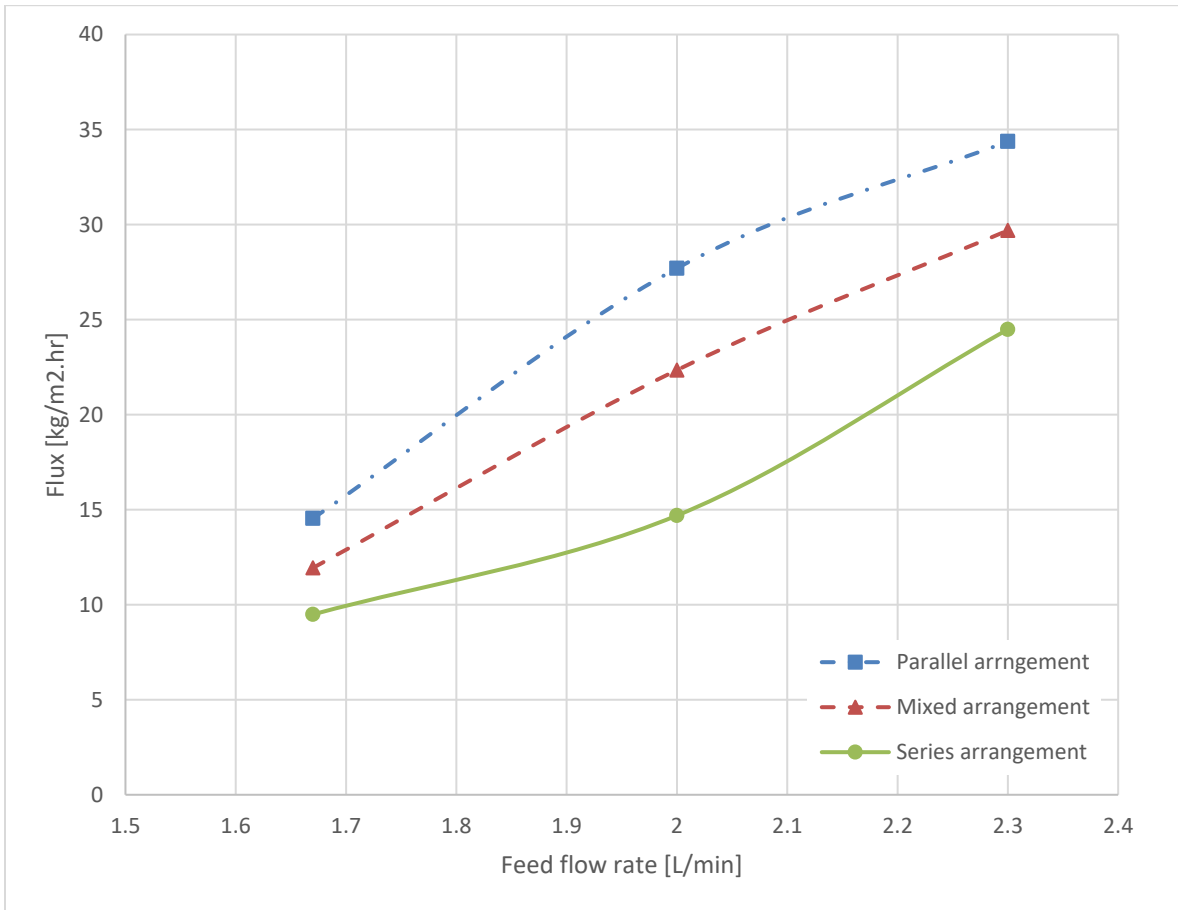
Figure 3.11: The comparison between the three-flow arrangements at the different feed flow rates

Conditions: membrane PTFE 0.22 μm, feed temperature 50°C, permeate temperature 25°C, feed salinity 3500 mg/L, permeate flow rate of 2 L/min for each module.

Figure 3.12 shows the percentage increase in the permeate flux due to change the flow arrangement from series to mixed flow arrangement and from series to parallel flow arrangement at feed flow rate 2.3 L/min, feed temperature 50°C, permeate temperature 25°C, feed salinity 3500 mg/L, and permeate flow rate of 2 L/min for each module.
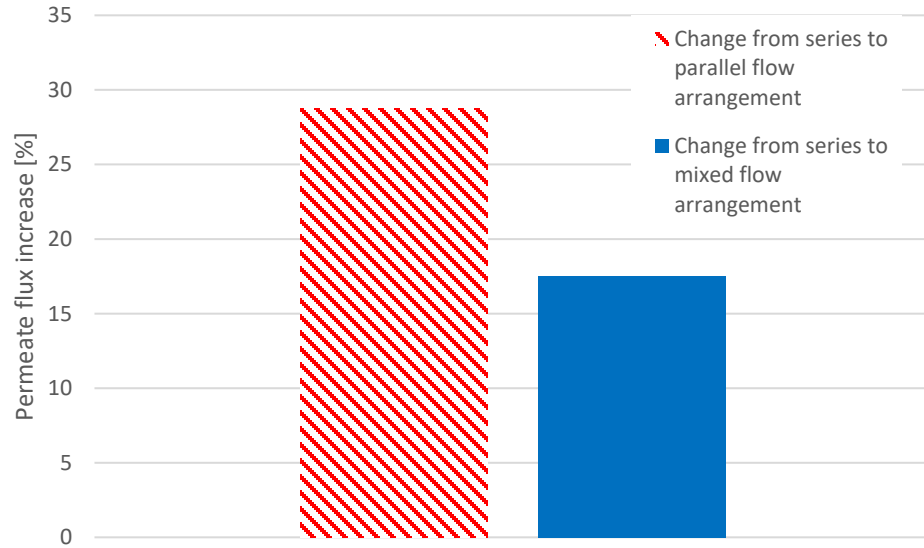
Figure 3.12: Percentage increase in the output flux due to change from series to mixed and parallel flow

arrangement at feed flow rate 2.3 L/min

Conditions: membrane PTFE 0.22 μm, feed temperature 50℃, permeate temperature 25℃, feed salinity 3500 mg/L, permeate flow rate of 2 L/min for each module

3.6 Effect of feed concentration

The effect of feed salinity concentration on the permeate flux is shown in Figure 3.13. The three-different arrangements have been tested at three feed concentrations (0.15 g/L, 3.55 g/L, and 35 g/L) to study the effect of feed salinity on permeate flux of the MS-DCMD system. The system operating condition was 50℃, permeate temperature 25℃, the total feed flow rate for the three modules is 6 L/min for the parallel flow arrangement (2 L/min passing each module in the series arrangement), and the total permeate flow rate for the three modules is 6 L/min for the parallel flow arrangement (2 L/min passing each module in the series arrangement). We can observe from Figure 3.13 that with the increase in feed salinity concentration, the permeate flux decrease for the three flow arrangements, because

of the increase of salt precipitation on the membrane feed surface due to adding a resistance layer on the membrane surface and that prevents the passage of vapor through the membrane.
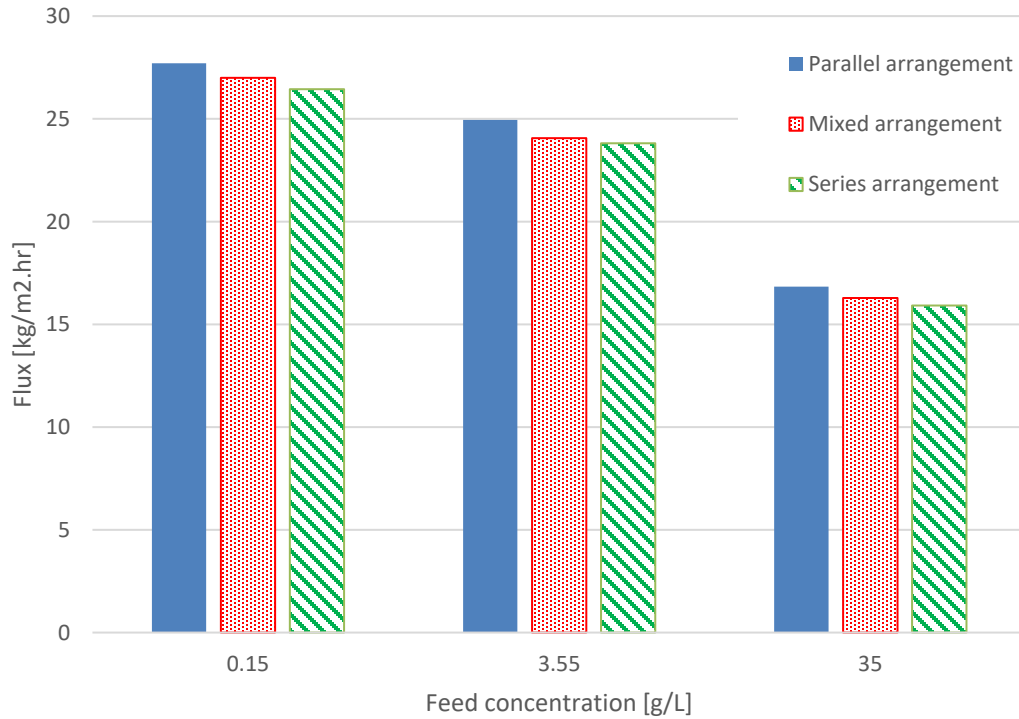
Figure 3.13: Effect of feed salinity concentration on the permeate flux

Conditions: membrane PTFE 0.22 μm, feed temperature 50ºC, coolant temperature 25ºC, feed and permeate flow rates of 2 L/min for each module.

3.6.1 Permeate concentration

Figure 3.14 presents the effect of feed concentration on the permeate salts concentration for the three-different arrangement. It can be seen that the permeate salts concentration increase with the increase in the feed concentration. The three different flow arrangements show almost the same results on the permeate concentration as the feed salts concentration increase.

57
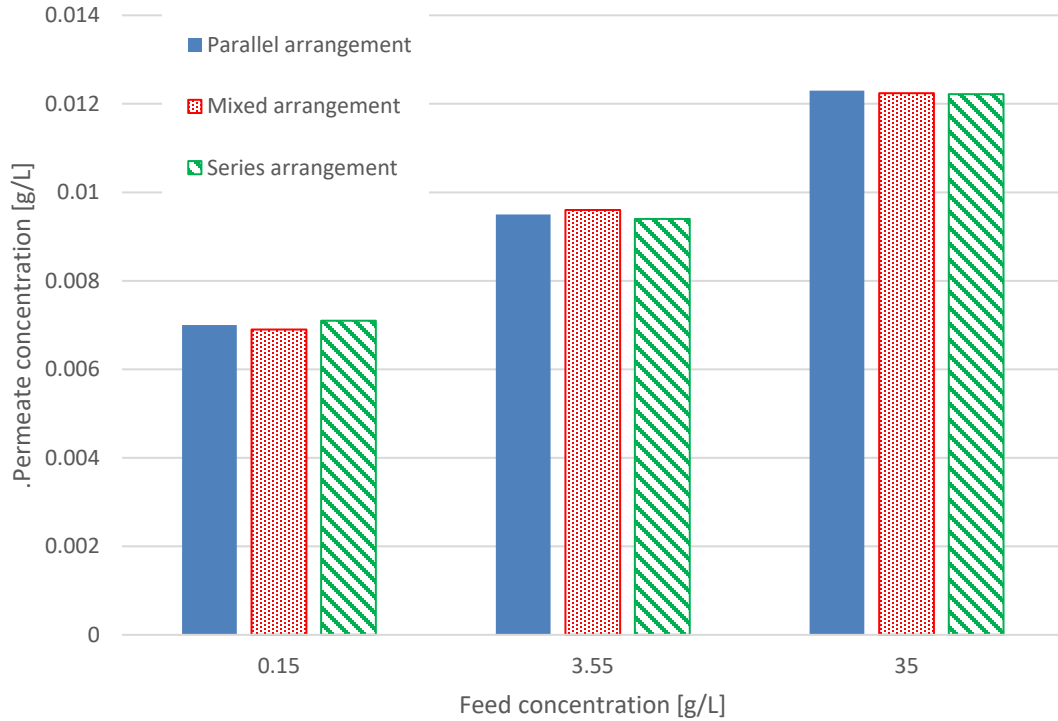
Figure 3.14: The effect of feed concentration on the permeate salts concentration

Conditions: membrane PTFE 0.22 μm, feed temperature 50°C, coolant temperature 25°C, feed and permeate flow rates of 2 L/min for each module.

3.6.2 Salt rejection factor

The salt rejection factor is a parameter used to verify the quantity of salt removed from the feedwater stream as a percentage.

The salt rejection factor defined as

$$SRF = \frac{\text{Feed Concentration} - \text{Permeate Concentration}}{\text{Feed Concentration}} * 100$$

Figure 3.15 presents the effect of feed concentration on the salt rejection factor for the three different flow arrangements. With the increase in the feed concentration between the values 0.15 g/L, 3.55 g/L, and 35 g/L, the salt rejection also increase to reach 99.99% In case of 35 g/L feed concentration.

58
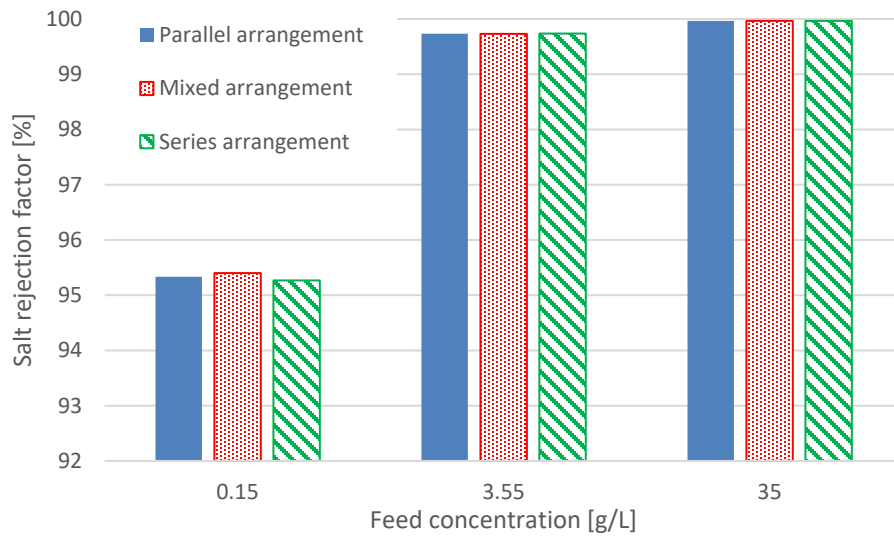
Figure 3.15: The effect of feed concentration on the salt rejection factor

Conditions: membrane PTFE 0.22 μm, feed temperature 50ºC, coolant temperature 25ºC, feed and permeate flow rates of 2 L/min for each module.

3.7 Power consumption

To measure the power consumed by the electric heater and the water chiller, power transducers were connected to the data acquisition system to record the electrical power consumption for the two-main flow arrangements (Parallel & Series flow arrangements) in the MS-DCMD system. The change in feed temperature, permeate temperature, feed flow rate, and permeate flow rate will be studied in the following subsections.

3.7.1 Effect of temperature on the power consumption

The power consumption for the MS-DCMD system in the parallel flow arrangement was measured at total feed and permeate flow rates 6 L/min while the system in the series flow arrangement was measured at feed and permeate flow rates 2 L/min. The electric heater power consumption was measured at different feed temperature changed from 40ºC to

59

90°C and the water chiller power consumption was measured at different permeate temperature varied from 15°C to 25°C.

Figure 3.16 presents the electric heater power consumption at different feed temperature. The maximum power consumed by the electric heater was 1.92 KW in case of parallel flow arrangement and 2.02 KW in case of series flow arrangement at feed temperature 90°C and permeate temperature 25°C.

Figure 3.17 shows the electric water chiller power consumption was measured at different permeate temperature. The maximum power consumed by the water chiller was 0.92 KW for the parallel flow arrangement and 1.07 KW for the series flow arrangement at permeate temperature 15°C.

Under steady state operation, the power consumed by the electric heater increase with the increase in feed temperature due to the increase in heat losses to the surroundings and vice versa, the power consumed by the water chiller increase with the decrease in the permeate temperature because of losses increase from the chiller to the surroundings.

Furthermore, it is obvious that the power consumed by the MS-DCMD system in the series flow arrangement is much higher than the system in the parallel flow arrangement because the series flow arrangement has a higher (than the parallel) temperature difference between the inlet and the outlet of the same stream cycle.
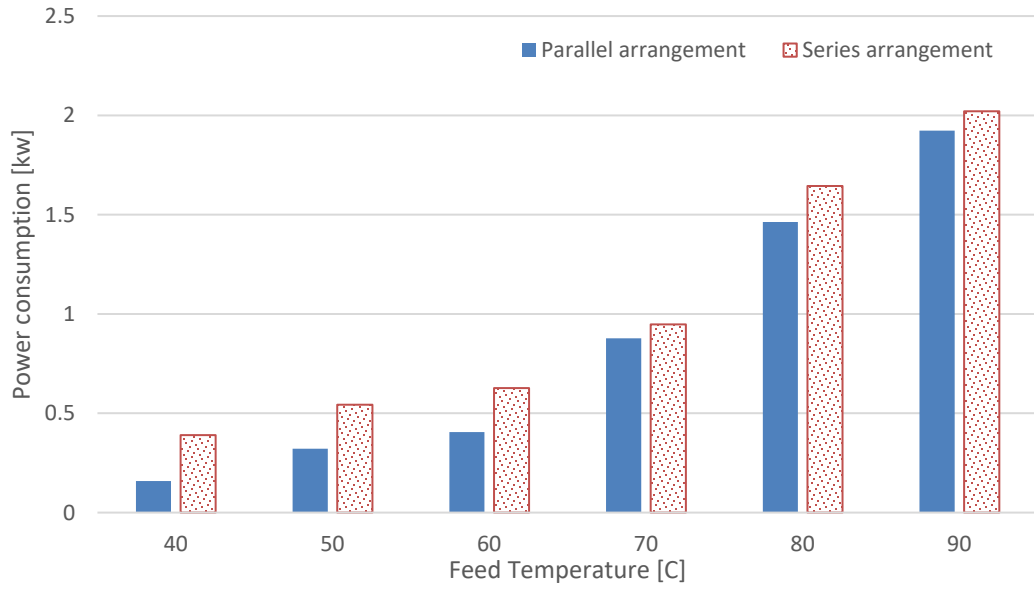
Figure 3.16: The power consumption of the electric heater for different flow arrangements at the same operating

conditions

Conditions: membrane PTFE 0.22 μm, permeate temperature 25ºC, feed and permeate flow rates of 2 L/min
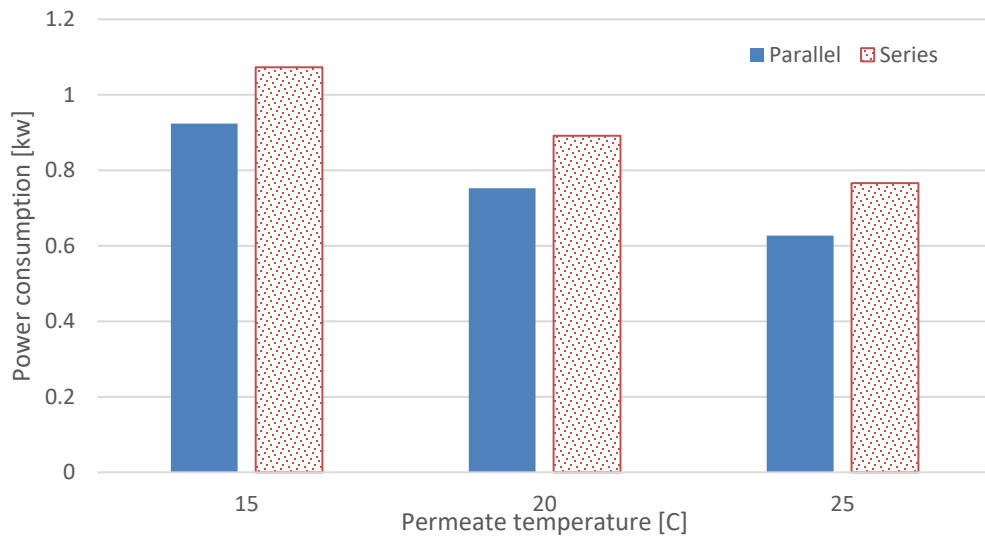
for each module.

Figure 3.17: The power consumption of the electric chiller for different flow arrangements at the same operating

conditions

Conditions: membrane PTFE 0.22 μm, feed temperature 50ºC, feed and permeate flow rates of 2 L/min for

each module.

3.7.2 Effect of flow rate on the power consumption

The electric heater power consumption was measured at different feed flow rates which are 5, 6, and 7 L/min for the parallel flow arrangement and 1.67, 2, and 2.3 L/min for the series flow arrangement. Figure 3.18 shows the electric heater power consumption at different feed flow rates for the two flow arrangements. It's clearly seen that; the electric heater power consumption increases with the increase in feed flow rate due to the increase in circulation rate in the feed cycle which lead to a lower heating rate. Furthermore, the power consumed by the MS-DCMD system in the series flow arrangement is much higher than system power in the parallel flow arrangement due to the high temperature difference along the same hot stream in the series case compared to the parallel one.
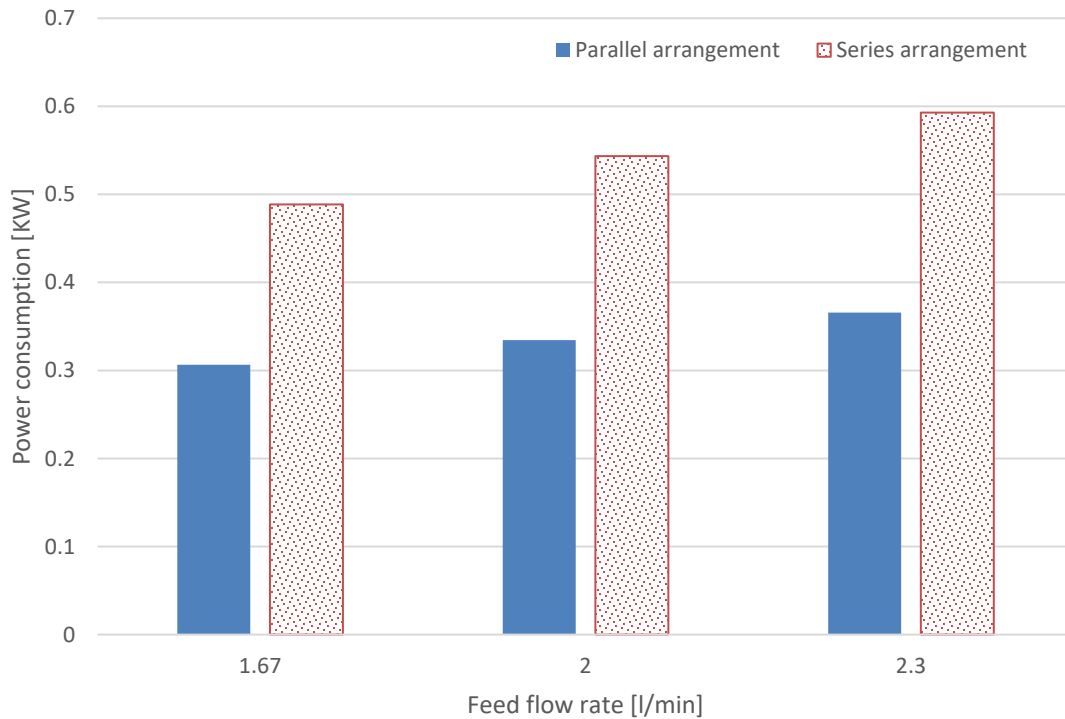
Figure 3.18: The effect of feed flow rate on the electric heater power consumption

Conditions: membrane PTFE 0.22 μm, feed temperature 50°C, permeate temperature 25°C, permeate flow rate of 2 L/min for each module.

Figure 3.19 presents the effect of permeate flow rate on the chiller power consumption. It's clearly seen that; the chiller power consumption increases with the increase in the permeate flow rate due to the increase in the recirculation rate which decrease the water cooling rate in the permeate cycle. Moreover, the chiller power consumption in the series flow arrangement case is higher than the parallel flow arrangement case due to the high temperature difference along the same permeate stream in the series case compared to the parallel flow arrangement.
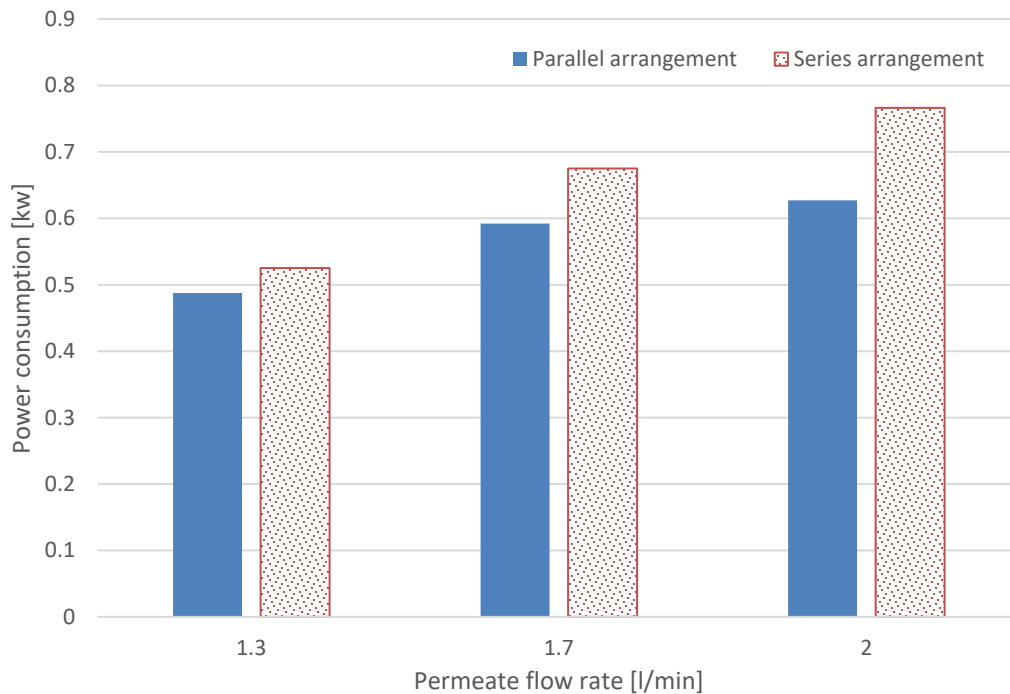
Figure 3.19: The effect of permeate flow rate on the electric chiller power consumption

Conditions: membrane PTFE 0.22 μm, feed temperature 50°C, permeate temperature 25°C, feed flow rate of 2 L/min for each module.

3.7.3 Temperature difference across feed and permeate cycles

The temperature difference between inlet of the first module and outlet of the last module in the feed cycle was measured. Feed temperature was changed from 40 to 90°C with 10°C increment where feed and permeate flow rates are 2 L/min passing each module in parallel and series flow arrangements. Figure 3.20 shows the variation of temperature differences with feed temperature for parallel and series flow arrangements. It is clearly seen that the temperature difference increases with increasing feed temperature. Also, the temperature difference for the series flow arrangement is higher compared to parallel flow arrangement at the same feed temperature.
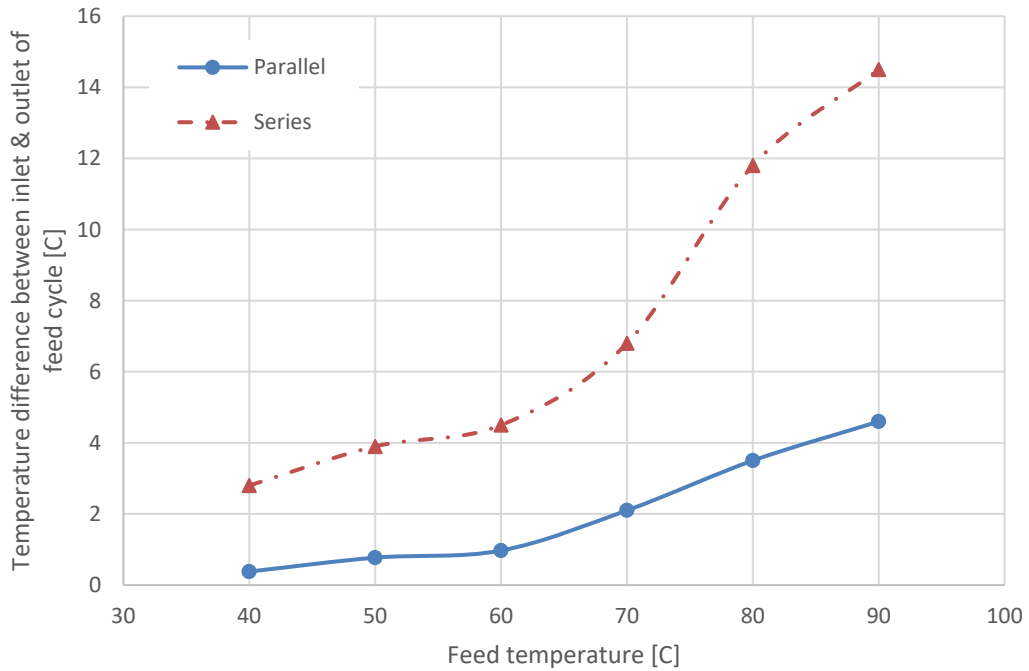
Figure 3.20: The variation of temperature differences with feed temperature for parallel and series connections

Conditions: membrane PTFE 0.22 μm, permeate temperature 25°C, feed and permeate flow rates of 2 L/min for each module.

Figure 3.21 shows the variation of temperature differences with permeate temperature for parallel and series flow arrangements. Permeate temperature changed between 15 to 25°C where feed and permeate flow rates are 2 L/min passing each module in parallel and series flow arrangements. It is noticed that the temperature difference increases with decreasing the permeate temperature for parallel and series flow arrangements. Also, the temperature difference for the series flow arrangement is higher compared to parallel flow arrangement at the same permeate temperature.
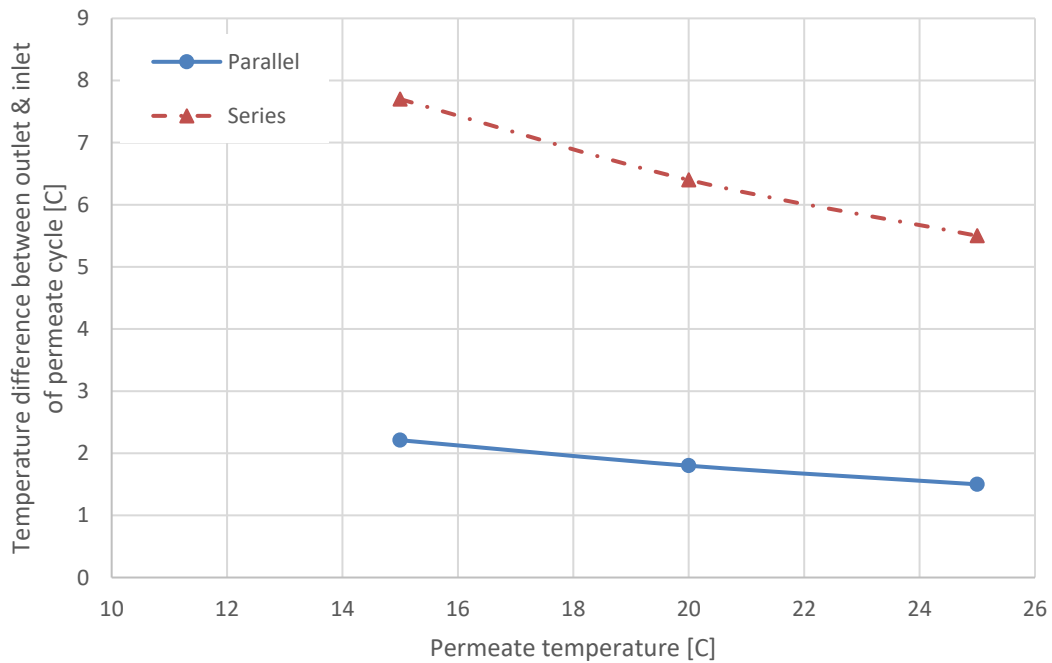
Figure 3.21: The variation of temperature differences with permeate temperature for parallel and series connections

CHAPTER 4

SOLAR MULTISTAGE DCMD SYSTEM

Solar energy is a sustainable, environmental friendly and cost-efficient way for heating the water. The evacuated tube solar collector (ETSC) is a solar heating device that can provide a great solution for many desalination technologies. Membrane Distillation technology is one of these water desalination techniques that can utilize the solar energy to reach the desired feed water temperature, which is between 60 to 90ºC.

In this chapter, a mathematical model was developed to predict the daily performance of the solar collector based on the energy balance equations. The model predicts the ETSC water tank temperature with the change in the solar irradiance over the day. Moreover, experimental investigations were conducted on the solar MS-DCMD system with different flow arrangements.

4.1   Initial testing of the solar system

We placed a thermocouple inside the solar collector tank to record the water temperature inside the tank. The ambient temperature was measured using a thermometer and the solar radiation was measured using a pyranometer (Frederiksen 4890.2). The water solar tank temperature compared to a mathematical model for validation. Figure 4.1 & Figure 4.2 show the variation of the solar radiation and the ambient temperature with the measurement time, on April 23rd, 2016. It can be clearly seen that; the ambient temperature and the solar radiation reach a higher value starting from 10 am to 2 pm and then it starts to decrease.
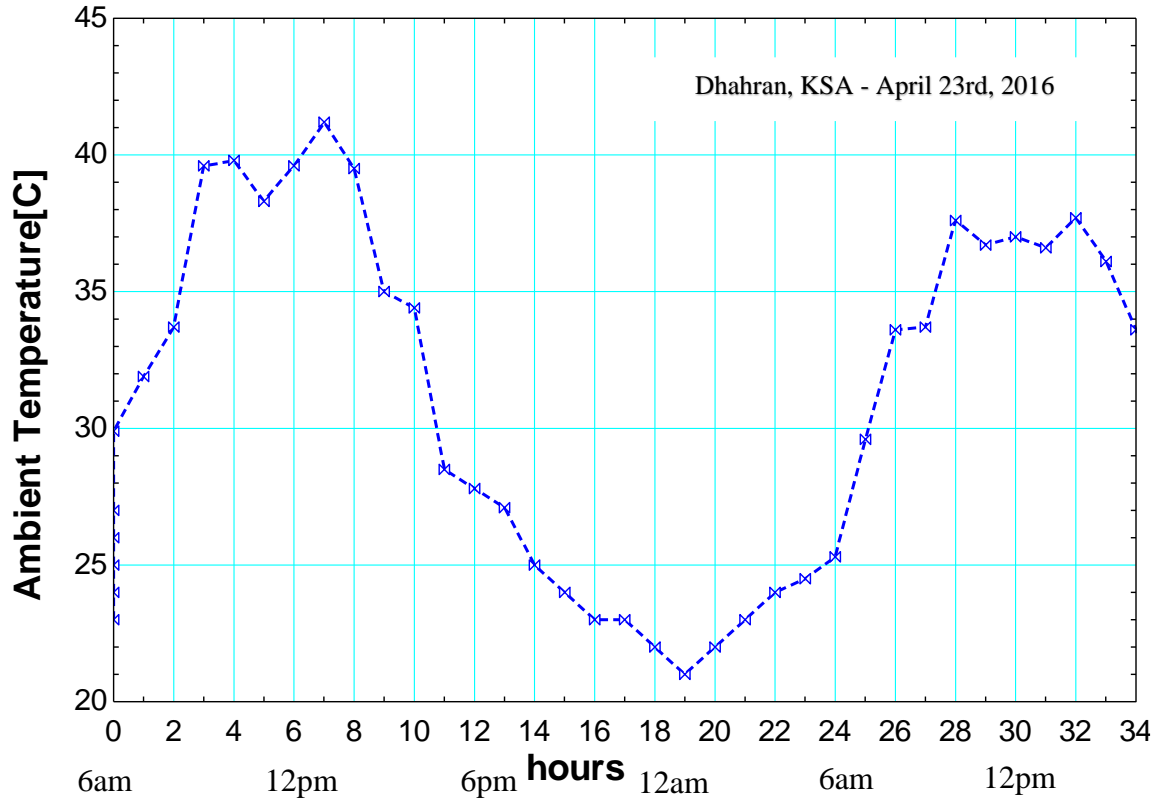
Figure 4.1: Ambient temperature variation with time
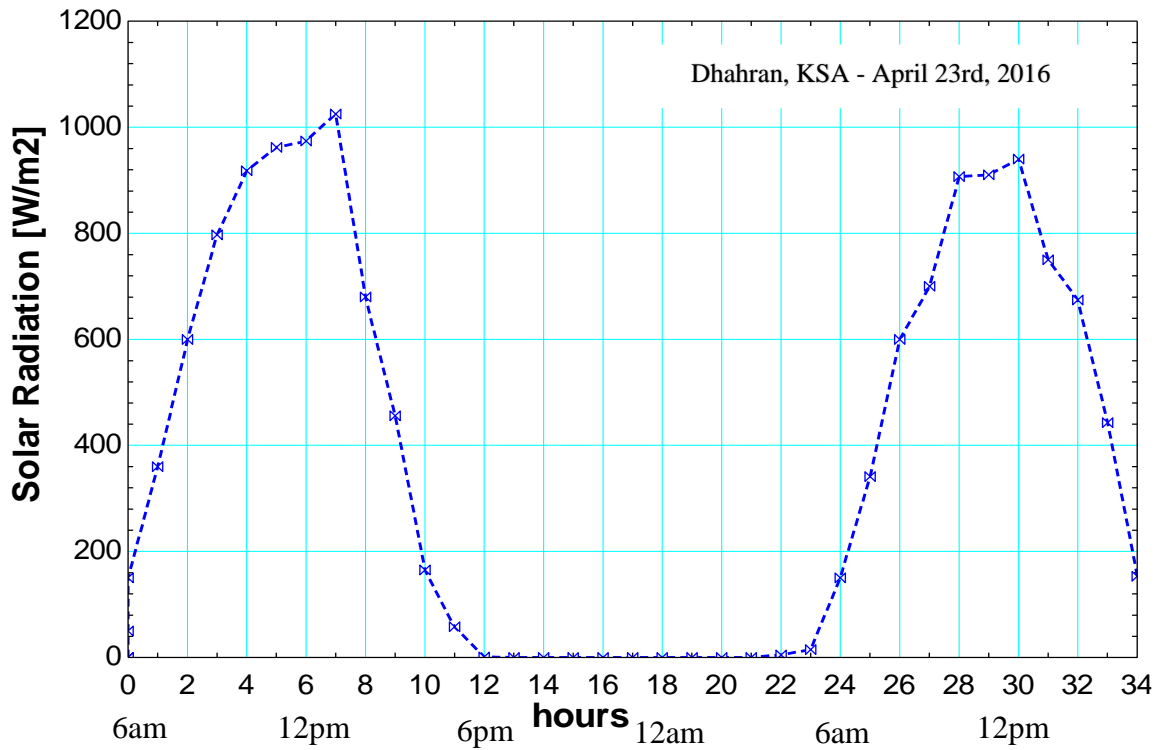
Figure 4.2: Solar irradiance variation with time

67

Figure 4.3 shows the variation of water temperature inside the solar tank. The water temperature reached 90°C after 34 hours from filling up the solar tank with raw water at 25°C.
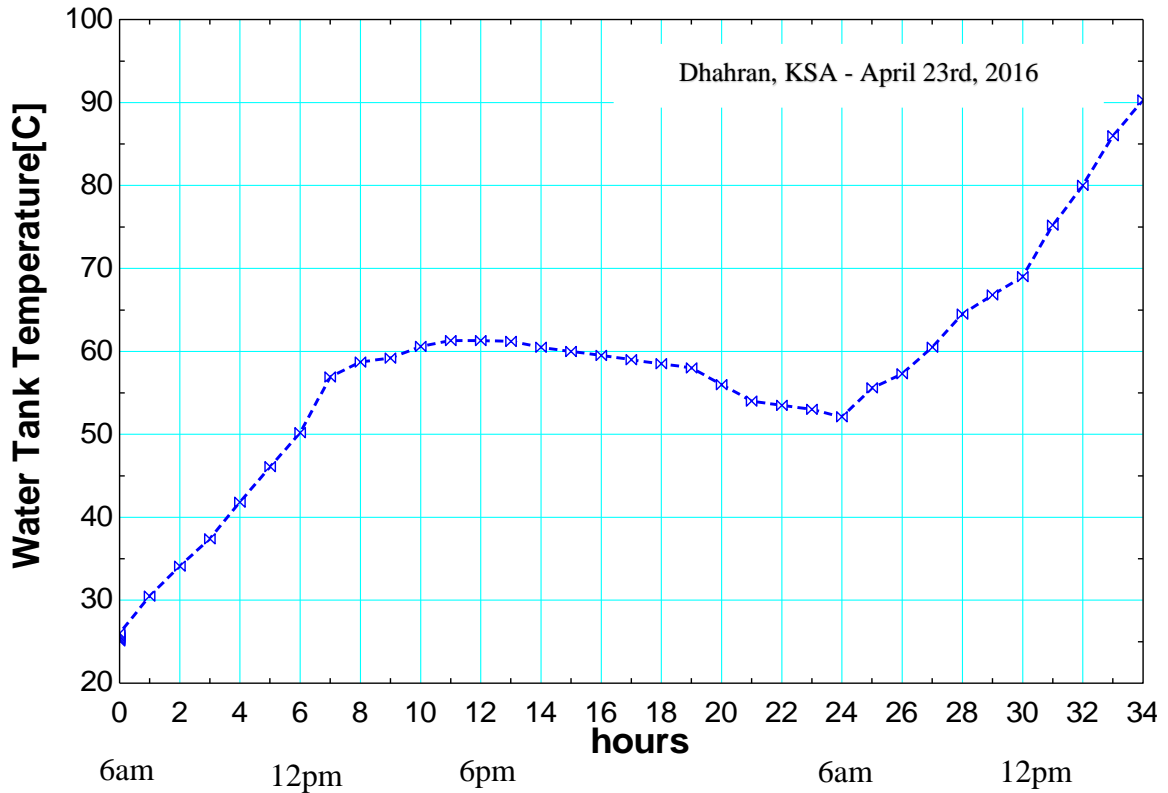
Figure 4.3: Experimental results for the water temperature variation in the solar tank

4.2 Energy analysis & modeling of the evacuated tube solar collector

In this section, a mathematical model is presented to predict the ETSC water tank temperature with variable solar irradiance over the day. First, we model the simple case of single glass evacuated tube solar collector and then the mathematical model is modified to consider the double glass evacuated tube solar collector, as shown in Figure 4.4. Experimental data of the ambient temperature and solar radiation in April 23rd, 2016 are

used as input to the mathematical models to predict the water tank temperature. Model

results are then compared to the measured water tank temperature for validation.

Figure 4.4:The Evacuated Tube Solar Collector

Glass evacuated tubes are the key component of the evacuated tube heat pipe solar

collectors. Each evacuated tube consists of two glass tubes. The outer tube is made of

extremely strong transparent borosilicate glass that can resist impact from hail up to 25mm

in diameter. The inner tube is also made of borosilicate glass, but coated with a special

selective coating, which features excellent solar heat absorption and minimal heat

reflection properties.
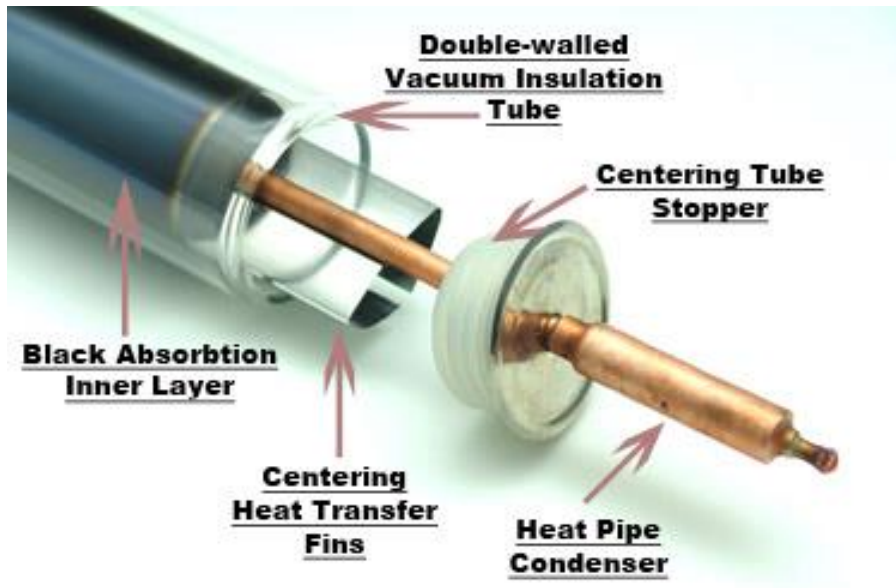
Figure 4.5: The detailed components of the ETSC tube

4.2.1 Mathematical model of the single glass evacuated tube solar collector

An energy balance that indicates the distribution of incident solar energy into useful energy gain, thermal losses, and optical losses is being developed to describe the performance of the solar system. The solar radiation absorbed by the tube per unit time is equal to the multiply of direct incident solar radiation, aperture area of the absorber and the absorptivity of the glass.

Assumptions made for this model are:

1- The convection and radiation losses between the copper pipe (heat pipe) and the glass is estimated as 5%.

2- The copper pipe thickness is very thin such that conduction resistance in the pipe wall is neglected.

3- The convective heat reaches the working fluid inside the copper pipe is the same amount of heat that reaches the water inside the solar collector tank without any losses (heat pipe efficiency is 100%).

4- The fin effect is neglected.
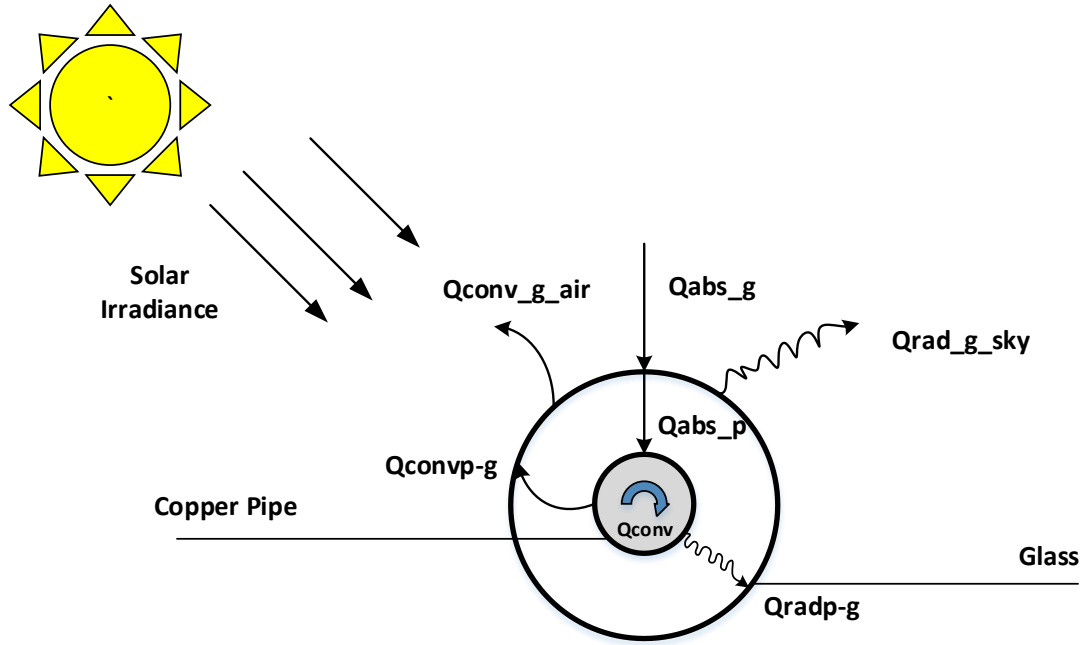
Figure 4.6: Energy Analysis for a cross-sectional cut in the single glass ETSC

As shown in Figure 4.6, the glass receives the radiation from the sun; part of it is lost due to radiation and convection effects from the glass to air and the other part is transmitted to the heat pipe through the vacuum layer. The energy balance for the glass:

$$A_{\text{s-g}} \, \alpha_{\text{g}} \, G = m_{\text{g}} C_{\text{pg}} \frac{dTg}{dt} + A_{\text{s-g}} \, q_{\text{g-air}} \tag{4.1}$$

Where the heat transfer losses between the glass and air due to radiation and convection are calculated as

$$q_{\text{g-air}} = \varepsilon \, \sigma \, (T_{\text{g}}^4 - T_{\text{sky}}^4) + h_{\text{g}} \, (T_{\text{g}} - T_{\text{a}}) \tag{4.2}$$

71

where the sky temperature is an average of the temperature between the ground and the upper troposphere ($T_{sky=}T_a-7$)

The convective heat transfer coefficient between the glass and air depends on the wind speed [73], and is given by

$$h_g = 5.7 + 3.8V \qquad (4.3)$$

The energy balance for the heat pipe is given by

$$A_{s-p}\ \alpha_p\tau_g\ G*0.95 = Q_{conv,fluid} \qquad (4.4)$$

where the radiation loss from the copper pipe to the outer glass is assumed to be 5%

Thermal heat gained by the water inside the tank can be calculated as

$$Q_{tank}=\text{Number of tubes} * Q_{conv,fluid} \qquad (4.5)$$

$$Q_{tank}=m_w\ Cp_w\ (T_{final}-T_{initial}) \qquad (4.6)$$

Figure 4.7 shows the variation of water temperature in the solar tank with time for the single glass ETSC mathematical model. This case is considered as a simplified case of the double glass ETSC model. It predicted that the water temperature in the solar tank can reach 84.5°C after 34 hours.

During night, the solar radiation was set to zero and the temperature drop per hour was estimated as one degree per hour.
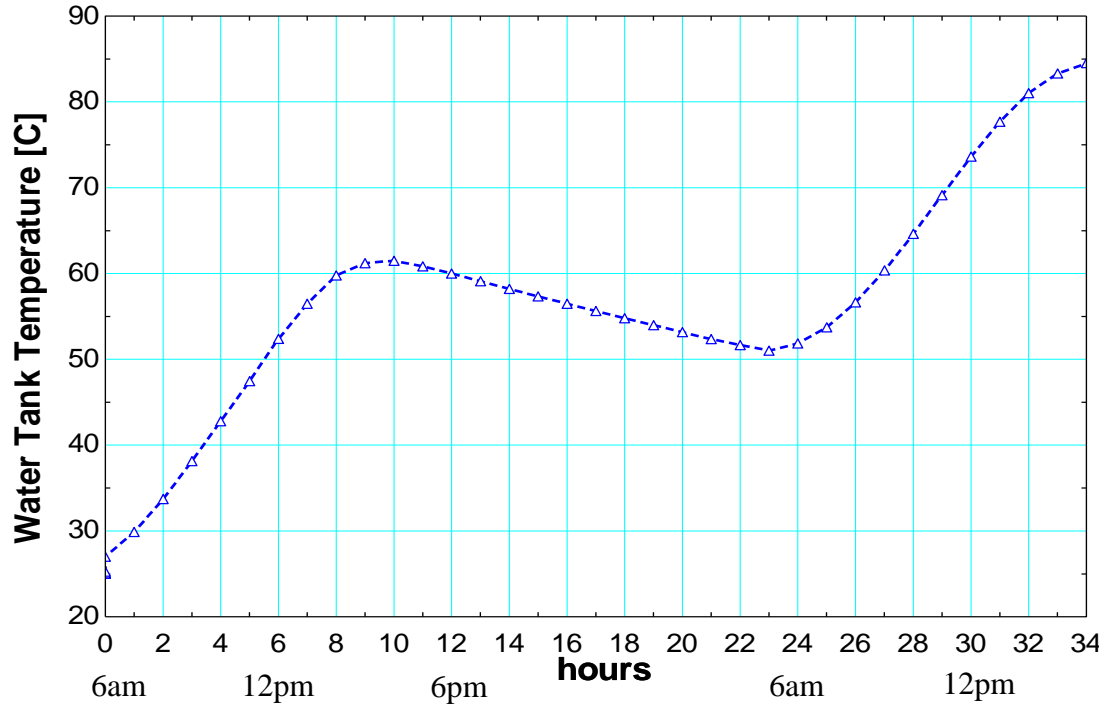
Figure 4.7: The variation of water tank temperature in the single glass ETSC model

4.2.2 Mathematical model for the double glass evacuated tube solar collector

The single glass model is modified by introducing an outer layer of glass to the single glass with a vacuum layer between the two glass layers. Then the results of the double glass model are validated with the experimental data of water tank temperature measured in April 23rd, 2016.

As shown in Figure 4.8, the main three components of the double glass ETSC are the outer glass, the inner glass and the copper pipe with a vacuum area between the outer and the inner glass. It is assumed that:

- There are no heat losses between the outer and the inner glass while the area between the inner glass and the copper pipe is filled with air.

73

- The copper pipe has a temperature that is approximately equal to the working fluid temperature inside it.

Figure 4.8 represents a schematic of the distribution of heat absorbed by the main three components, the convection and radiation heat loss from the outer glass, and the convection and radiation losses between the inner glass and the copper pipe.
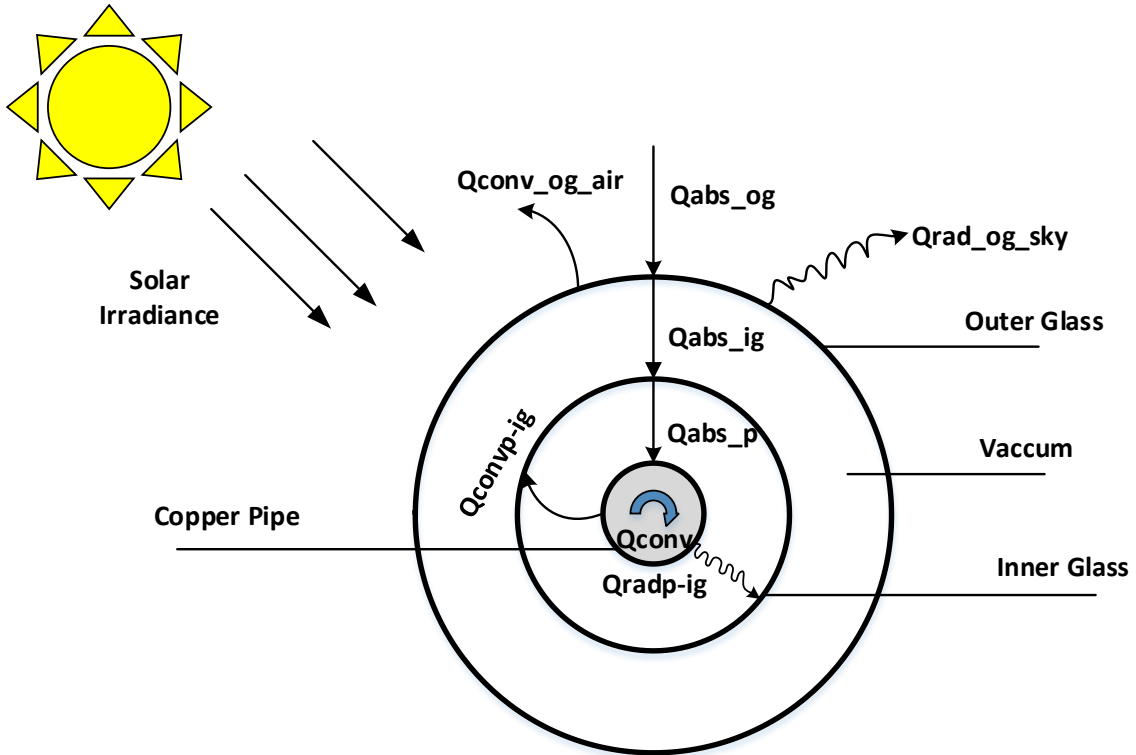
Figure 4.8: Energy analysis for a cross-sectional cut in the double glass ETSC

The outer glass receives the radiation from the sun; part of it is lost due to radiation and convection effect from the outer glass to air. The energy balance for the outer glass:

$$A_{\text{s-og}} \; \alpha_{\text{og}} \, G = m_{\text{og}} \, C_{\text{p og}} \frac{dTog}{dt} + A_{\text{s-og}} \; q_{\text{og-air}} \tag{4.7}$$

Where the heat losses between the outer glass and the air due to radiation and convection are calculated as,

$$q_{\text{og-air}} = \varepsilon \; \sigma \; (T_{\text{og}}{}^4 - T_{\text{sky}}{}^4) + h_{\text{og}} \; (T_{\text{og}} - T_{\text{a}}) \tag{4.8}$$

74

The convective heat transfer coefficient between the outer glass and the air depends on the wind speed [73], and is given by

$$h_{og} = 5.7 + 3.8V \qquad (4.9)$$

The inner glass receives the transmitted solar irradiance and also heat losses (radiation and convection) from the copper pipe. The energy balance for the inner glass is given by

$$A_{s\text{-}ig}\, \alpha_g\, \tau_{og}\, G = m_{ig}C_{pig}\frac{dTig}{dt} + A_{s\text{-}ig}\, q_{rad\ p\text{-}ig} + A_{s\text{-}ig}\, q_{conv\ p\text{-}ig} \qquad (4.10)$$

The energy balance for the copper pipe is given by

$$A_{s\text{-}p}\, \alpha_p\, \tau_{og}\, \tau_{ig}\, G = A_{s\text{-}p}\, q_{conv,fluid} + A_{s\text{-}p}\, q_{rad\ p\text{-}ig} + A_{s\text{-}p}\, q_{conv\ p\text{-}ig} + m_p\, C_{p\text{-}p}\frac{dTp}{dt} \qquad (4.11)$$

Thermal heat gained by the water inside the tank can be calculated as

$$Q_{tank} = \text{Number of tubes} * Q_{conv,fluid} \qquad (4.12)$$

$$Q_{tank} = m_w\, C_{pw}\, (T_{final} - T_{initial}) \qquad (4.13)$$

The measurement of the water temperature inside the solar tank started at 6 am and continued for 34 hours with one sample measurement every one hour. Figure 4.9(a) shows a comparison between the predicted water temperature inside the solar tank using the single glass model and the double glass model of the evacuated solar collector. Figure 4.9(b) shows the measured hourly variation of water temperature inside the solar tank and the variation of the predicted water temperature inside the tank with the double glass ETSC model. It is clearly seen that this model estimates that the water temperature inside the solar tank can reach 87°C (higher than the water temperature of the single glass model 84.5°C) after 34 hours and it is close to the experimental result (90°C) at the same measuring hour.
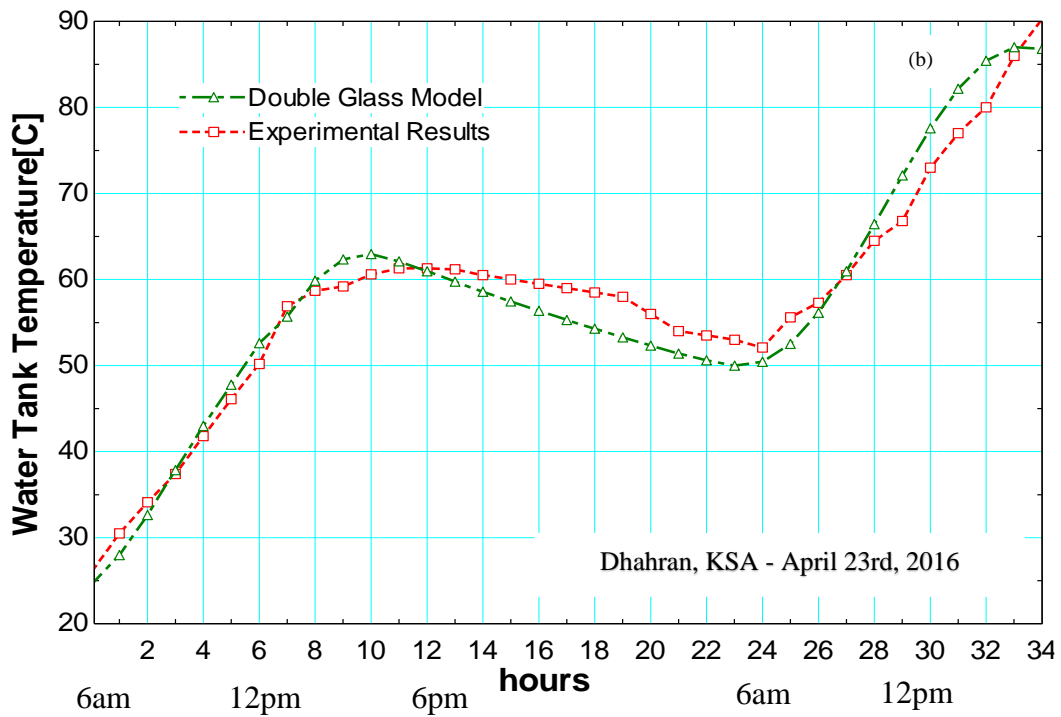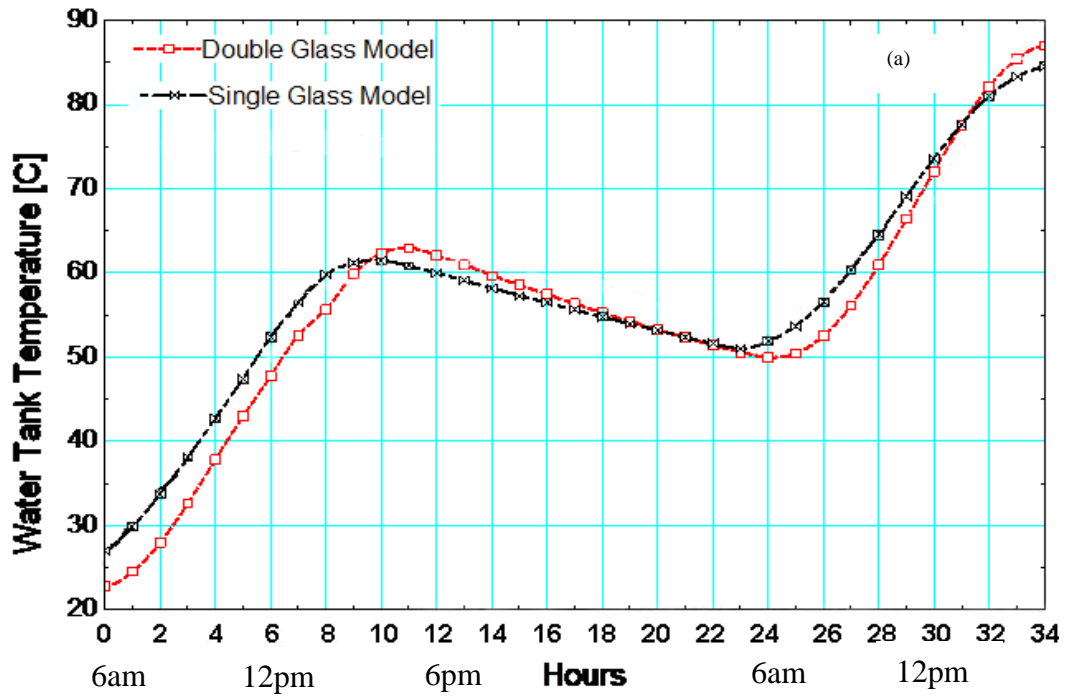
Figure 4.9: (a) Water temperature variation in single and double glass models

(b) Experimental results of hourly water temperature variation inside the solar tank with the results of the double glass model

76

Also, the modeling of the evacuated tube glass temperature shows an agreement with the experimental results as shown in Figure 4.10.
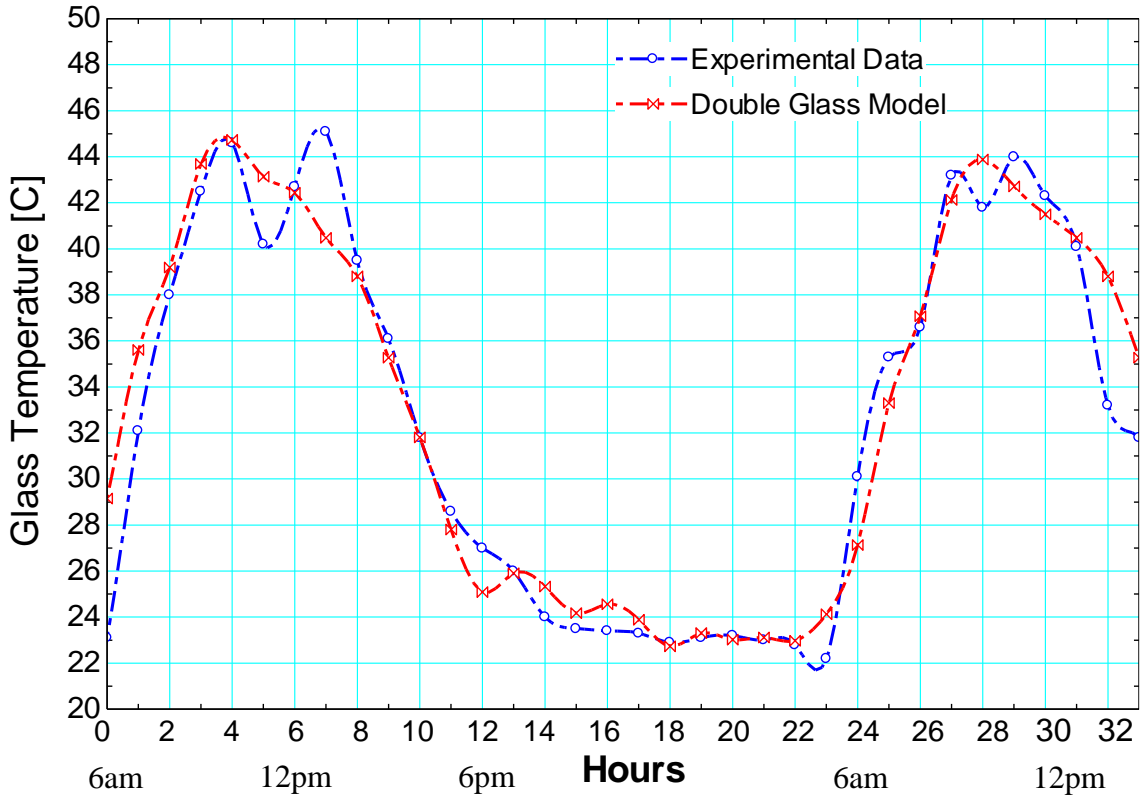
Figure 4.10: The variation of the glass temperature in the double glass model with the experimental results

From the mathematical model of double glass evacuated tube solar collector and the experimental results of the solar collector, Figure 4.9 shows that the feed water temperature can reach around 90ºC which is perfect condition for the multi-stage direct contact membrane distillation system and accordingly ETSCs can be used as pre-heaters for the feed water in the MD systems. The maximum deviation error is 8% and was after 19 hours from starting the experiment.

4.3 Performance of solar powered parallel flow MS-DCMD system

In April 28th, 2017, the solar MS-DCMD system have been tested with parallel flow arrangement. The controlled input parameters for the MS-DCMD system are total feed and permeate flow rates= 6 L/min (the total flow rate for the three modules) and 3500 mg/L feed salinity. Two chillers where used to control the permeate water temperature in the cold cycle due to high heat transfer between hot and cold sides through the membrane. The permeate water was collected from an opening in one of these two chillers.

Figure 4.11 presents the ETSC outer glass temperature variation along with the change in ambient temperature from 9 am to 3:30 pm which is the experiment working hours.
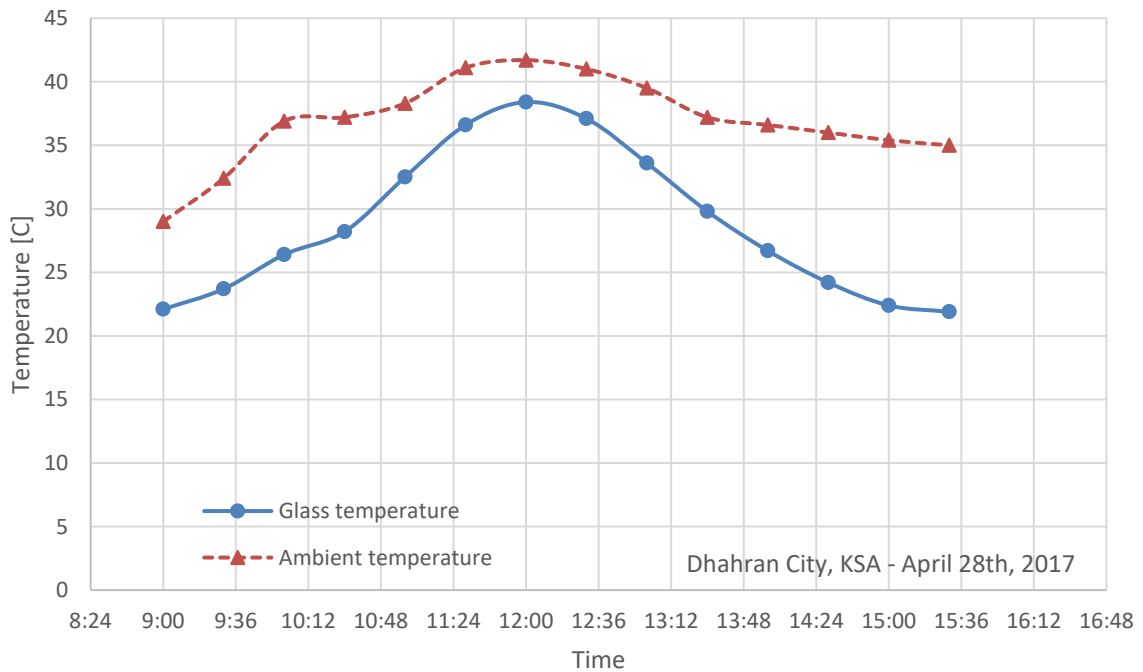
Figure 4.11: The variation of the ETSC outer glass temperature and the ambient temperature along the experiment

Figure 4.12 shows the variation of the solar radiation along the experiment working hours. It reaches a maximum value of 940 W/m^2 at 12 pm.
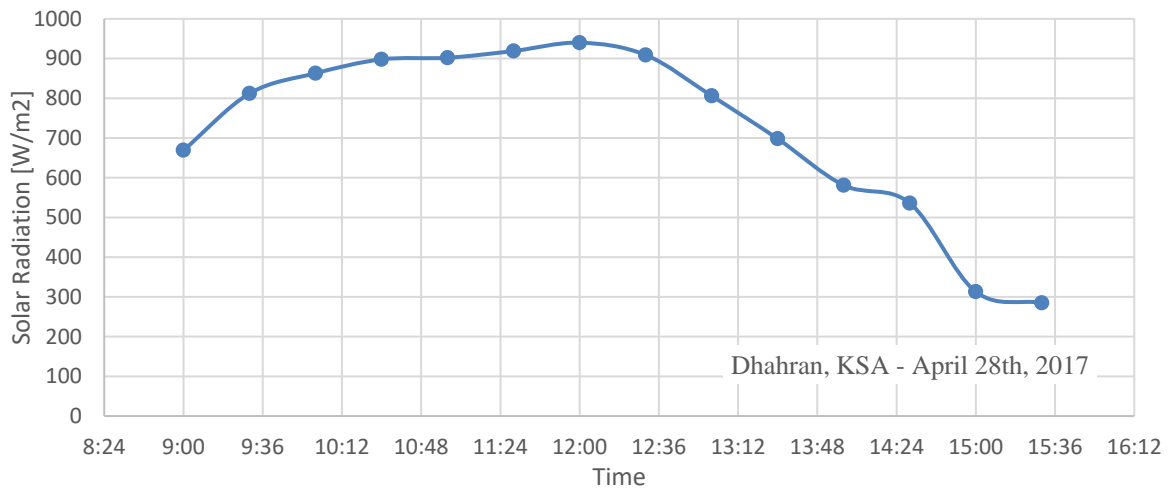
Figure 4.12: Solar radiation variation along the experiment

Figure 4.13 presents the water temperature variation in the ETSC tank (feed cycle tank) and the water temperature variation in the chiller (permeate cycle tank). It was noted that the main chiller could not control the permeate temperature in the desired temperature range. A heat exchanger connected to an auxiliary chiller was placed inside the main chiller tank to increase the cooling power supply in the permeate cycle. The set temperature of the two chillers was 5°C. However, the two chillers were not able to reach the set value. The water temperature inside the chiller tank was 25°C at the beginning of the experiment and then there was an increase in it until 10:30 am and after that it starts to decrease with the sharp decrease in the water solar tank temperature. It's clearly seen that the water temperature in both feed and permeate hard to control in the desired temperature range due to high conduction heat transfer rate between feed and permeate sides across the membrane in the three MD modules.
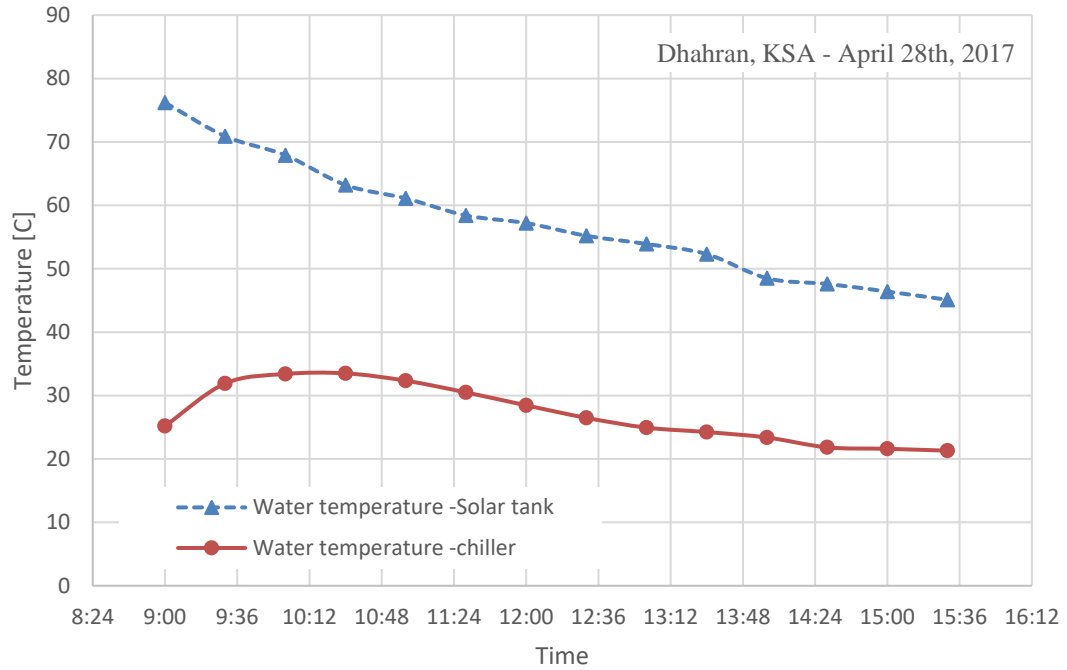
Figure 4.13: The water temperature variation in the solar tank with change in the chiller water temperature for the parallel MS-DCMD solar system

Figure 4.14 presents the permeate flux variation with time. The permeate flux started with the maximum value 68.36 kg/m^2.hr due to the high temperature difference between the feed and permeate sides. Then it starts to sharply decrease as the time goes on because of the high heat transfer between the feed and permeate sides across the membrane in the three MD modules which decreases the feed water temperature and increases the permeate temperature with continuous cooling from the two chillers. After that the permeate flux starts to decrease will a lower rate because the temperature difference between the feed and permeate sides becomes almost constant which is shown in Figure 4.13 from 11 pm to 3:30 pm. The total productivity of the system after operating it from 9 am to 3:30 pm was 5.61 Liter.

80
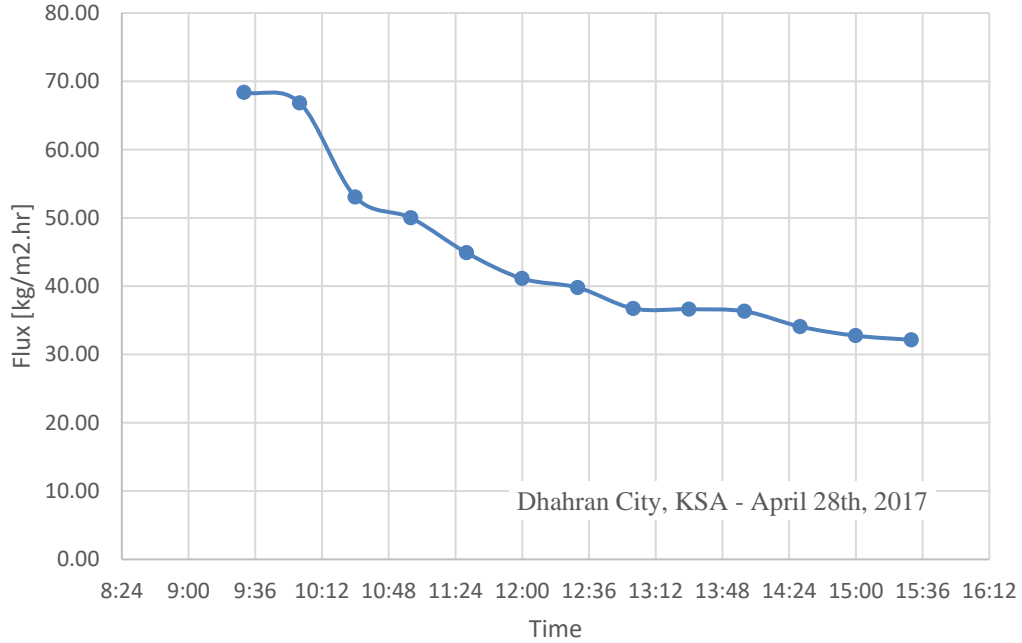
Figure 4.14: The permeate flux variation with time for parallel MS-DCMD solar system

Conditions: membrane PTFE 0.22 μm, feed salinity 3500 mg/L, feed and permeate flow rates of 2 L/min for each module

4.4 Performance of solar powered series flow MS-DCMD system

In May 7th, 2017, the solar MS-DCMD system have been tested with series flow arrangement. The controlled input parameters for the MS-DCMD system are feed and permeate flow rates passing the three modules= 2 L/min and 3500 mg/L feed salinity. Figure 4.15 presents the ETSC outer glass temperature variation along with the change in ambient temperature from 9 am to 3:30 pm which is the experiment working hours.
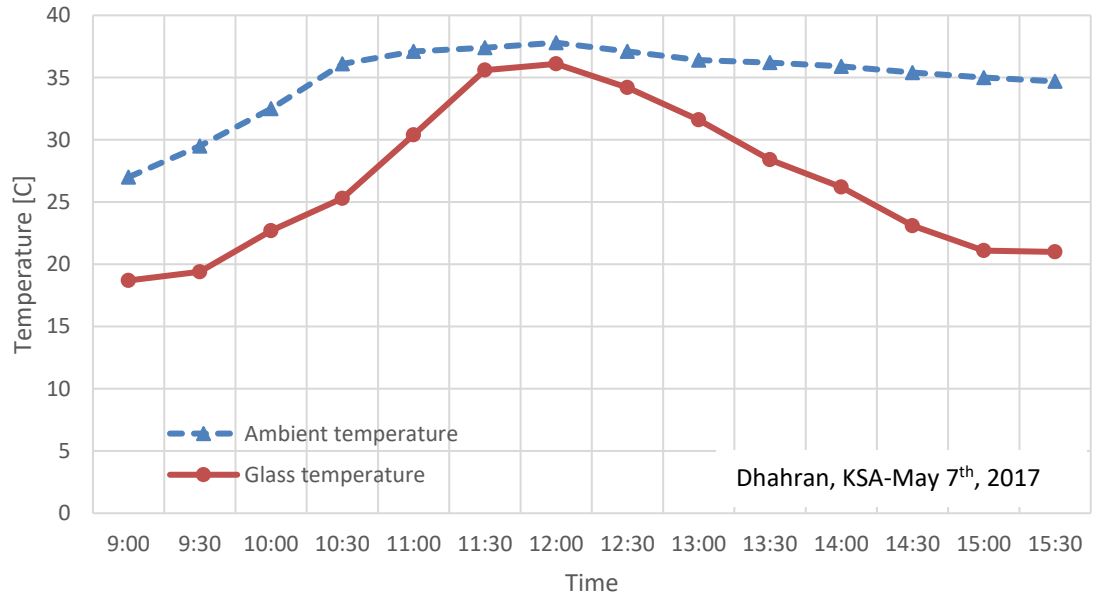
Figure 4.15: The variation of the ETSC outer glass temperature and the ambient temperature along the experiment

Figure 4.16 shows the variation of the solar radiation along the experiment working hours.

It reaches a maximum value of 847 W/m^2 at 12 pm.
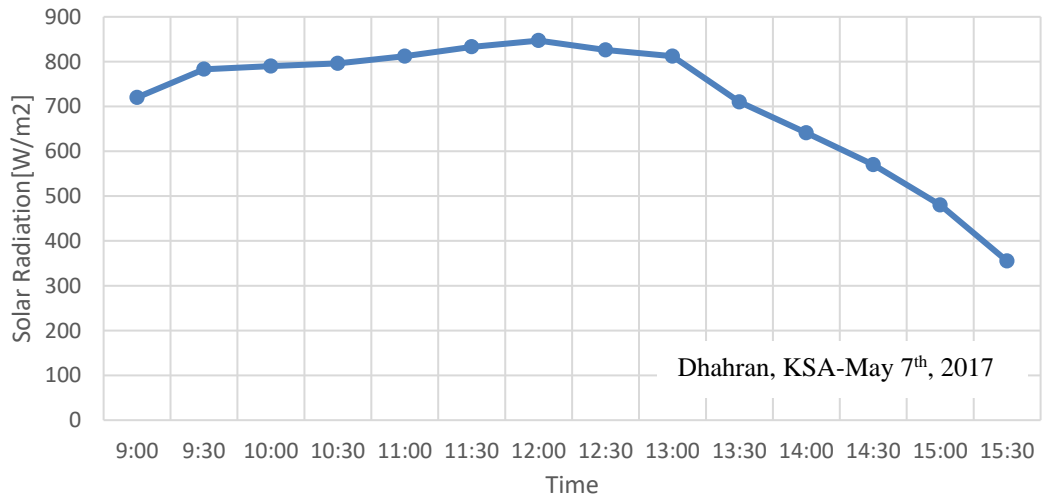
Figure 4.16: Solar radiation variation along the experiment

82

Figure 4.17 presents the water temperature variation in the ETSC tank (feed cycle tank) and the water temperature variation in the chiller (permeate cycle tank). The same problem of the solar powered parallel flow MS-DCMD system experiment repeated itself. The main chiller could not control the permeate temperature in the desired temperature range. A heat exchanger connected to an auxiliary chiller was placed inside the main chiller tank to increase the cooling rate in the permeate cycle. The water temperature inside the chiller tank was 27°C at the beginning of the experiment and then there was an increase in it until its value 10:30 am and after that it starts to decrease with the sharp decrease in the water temperature in the solar tank and becomes constant from 2 to 3:30 pm. It's clearly seen that the water temperature in both feed and permeate hard to control in the desired temperature range due to high conduction heat transfer rate between feed and permeate sides across the membrane in the three MD modules.
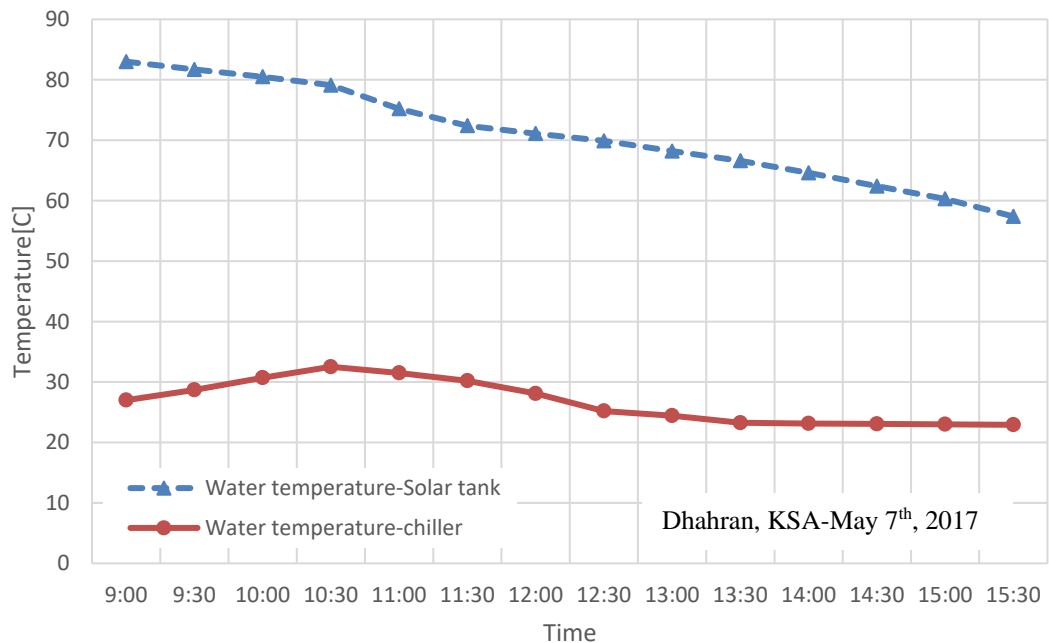
Figure 4.17: The water temperature variation in the solar tank with change in the chiller water temperature

Figure 4.18 presents the permeate flux variation with time. The permeate flux started with the maximum value 57.4 kg/m^2.hr due to the high temperature difference between the feed and permeate sides. Then it starts to sharply decrease as the time goes on because of the high heat transfer between the feed and permeate sides across the membrane in the three MD modules which decreases the feed water temperature and increases the permeate temperature with continuous cooling from the two chillers. After that the permeate flux starts to decrease with a lower rate. The total productivity of the system after operating it from 9 am to 3:30 pm was 4.5 Liter.

Dhahran, KSA-May 7th, 2017
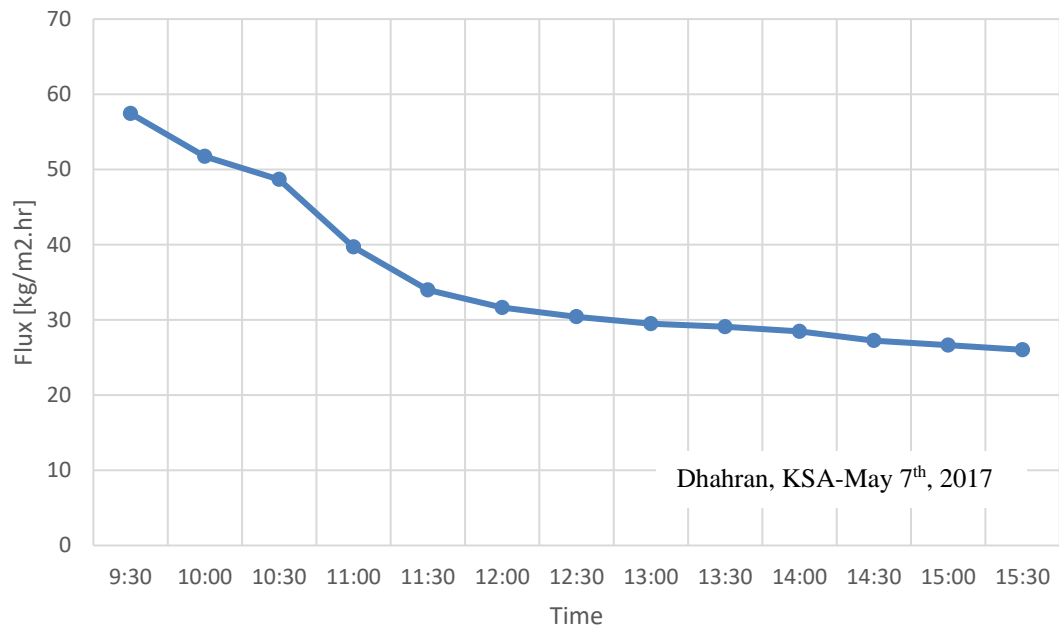
Figure 4.18: The permeate flux variation with time for the solar powered MS-DCMD series connected system

Conditions: membrane PTFE 0.22 μm, feed salinity 3500 mg/L, feed and permeate flow rates of 2 L/min passing the three modules.

84

4.5 Comparison between parallel and series flow arrangements

The solar MS-DCMD system has been tested with series and parallel flow arrangements on two different days from 9 am to 6 pm.

In the series flow arrangement, the feed flow rate has been changed for two different days; August 3rd, 2017 and August 7th, 2017. The controlled input parameters for the MS-DCMD system are feed flow rates =1.167, 2.334 l/min, permeate flow rate 1.167 l/min passing the three modules and 3500 mg/L feed salinity.

Figure 4.19 shows the variation of the solar radiation with time for two different days. We can notice that the curve exhibits a concave down words, peaking at noon.
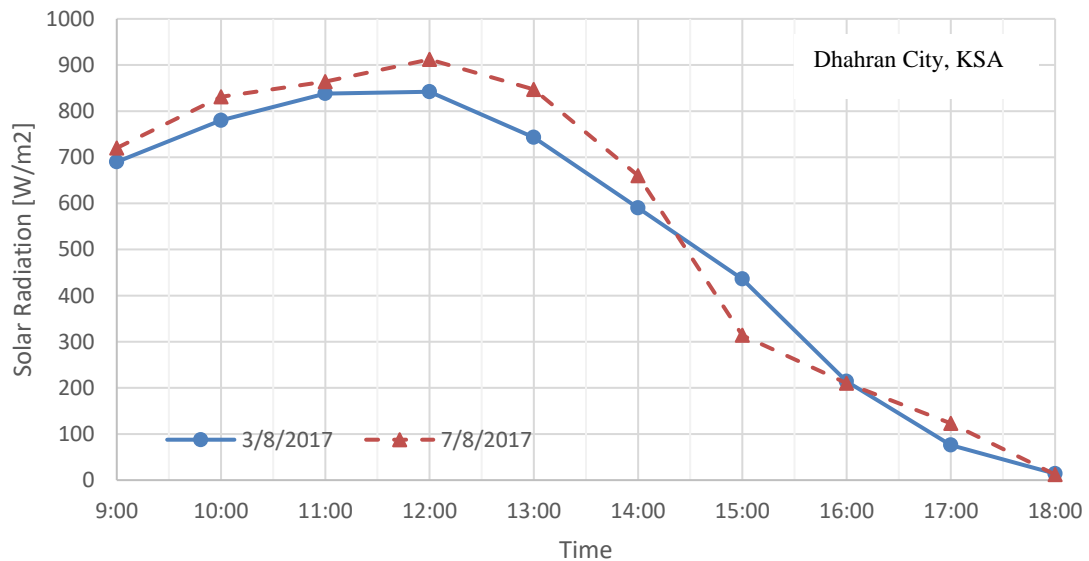
Figure 4.19: Solar radiation variation with time

Figure 4.20 shows the variation of water temperature inside the solar tank and the electric chiller with time for two different days (different feed flow rates). The feed water temperature decreases with time because of high heat transfer between hot and cold sides across the membrane. The permeate water temperature in the electric chiller starts to

85

increase due heat transfer between the two sides and after that starts to decrease with time in parallel with the feed water temperature.

Figure 4.20: The variation of water temperature inside the solar tank and the electric chiller (feed and permeate sides) with time for the series arrangement

In the parallel flow arrangement, the feed flow rate has been changed for two different days; August 12th, 2017 and August 17th, 2017. The controlled input parameters for the MS-DCMD system are feed flow rates =1.167, 2.334 l/min, permeate flow rate 1.167 l/min passing each of the three modules and 3500 mg/L feed salinity.

Figure 4.21 shows the variation of the solar radiation with time for two different days. We can notice that the curve exhibits a concave down words, peaking at noon.

Figure 4.21: Solar radiation variation with time

Figure 4.22 shows the variation of water temperature inside the solar tank and the electric chiller with time for two different days (different feed flow rates). The feed water temperature decreases with time because of high heat transfer between hot and cold sides across the membrane. The cold-water temperature in the electric chiller starts to increase due heat transfer between the two sides and after that starts to decrease with time in parallel with the feed water temperature.

Figure 4.22: The variation of water temperature inside the solar tank and the electric chiller (feed and permeate sides) with time for the parallel flow arrangement

Figure 4.23 shows the variation of the flux at different feed flow rates from 10 am to 6 pm with different flow arrangements. We observed that the flux decreases with time for different flow arrangements due to the decrease in feed water temperature with time. Also, the system at parallel flow arrangement yields more output flux compared to the system in the series case. This is attributed to high temperature difference across the membrane in the parallel case. Furthermore, the output flux increases with increasing the feed flow rates in the two arrangements due to the increase in the turbulence levels in feed side which increase the heat and mass transfer coefficients and also the rate of condensation of the vapor.
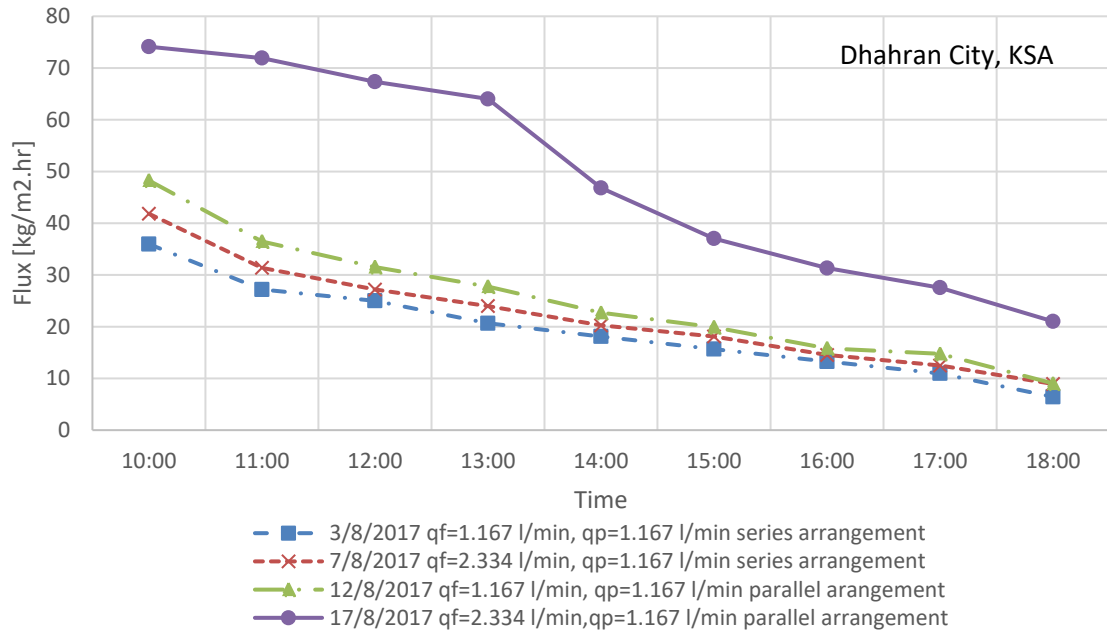
Figure 4.23: Flux variation at different feed flow rates with time for different flow arrangements

4.6   Effect of feed and permeate flow rates on the MS-DCMD solar

system with parallel flow arrangement

The solar MS-DCMD system has been tested with parallel flow arrangement on four different days from 9 am to 6 pm.

The feed salinity was 3500 mg/L and feed and permeate flow rates have been changed for four different days as follows:

- August 12th, 2017, feed flow rate=1.167 l/min and permeate flow rate=1.167 l/min passing each module.

- August 17th, 2017, feed flow rate=2.334 l/min and permeate flow rate=1.167 l/min passing each module.

- August 21st, 2017, feed flow rate=2.334 l/min and permeate flow rate=2.334 l/min passing each module.

- August 25th, 2017, feed flow rate=1.75 l/min and permeate flow rate=2.334 l/min passing each module.

Figure 4.24 shows the solar radiation variation with time for the four different days. We can notice that the curve exhibits a concave down words, peaking at noon.
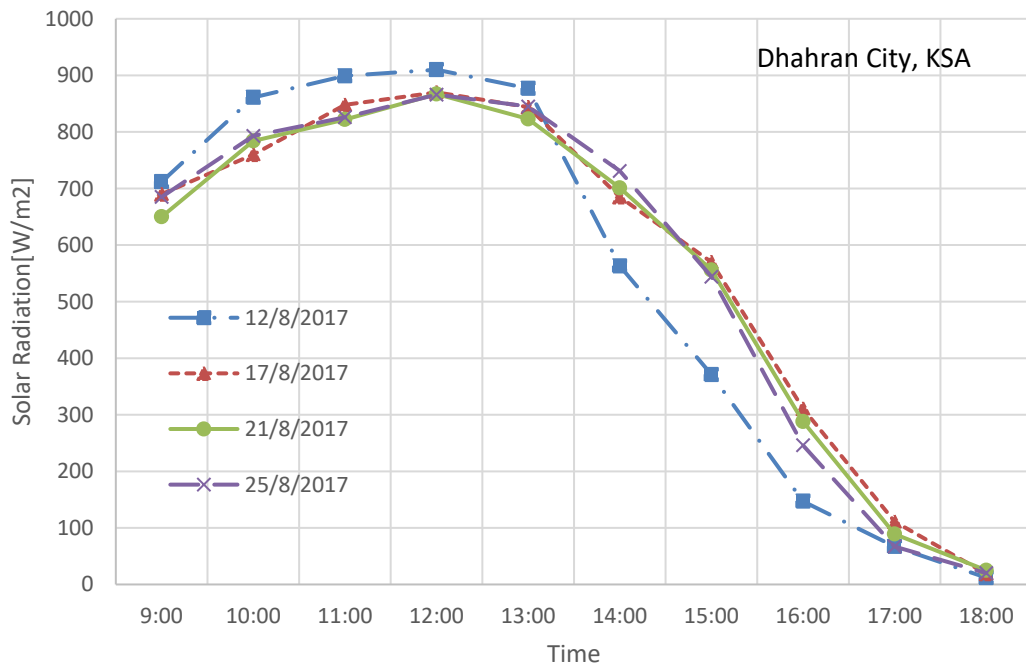
Figure 4.24: Solar radiation variation with time for four different days

Figure 4.25 & Figure 4.26 show the variation of water temperature inside the solar tank and the electric chiller with time for the four different days (different feed and permeate flow rates). The feed water temperature decreases with time because of high heat transfer between hot and cold sides across the membrane. The permeate water temperature in the electric chiller starts to increase due heat transfer between the two sides and after that starts to decrease with time with the decrease in feed water temperature.
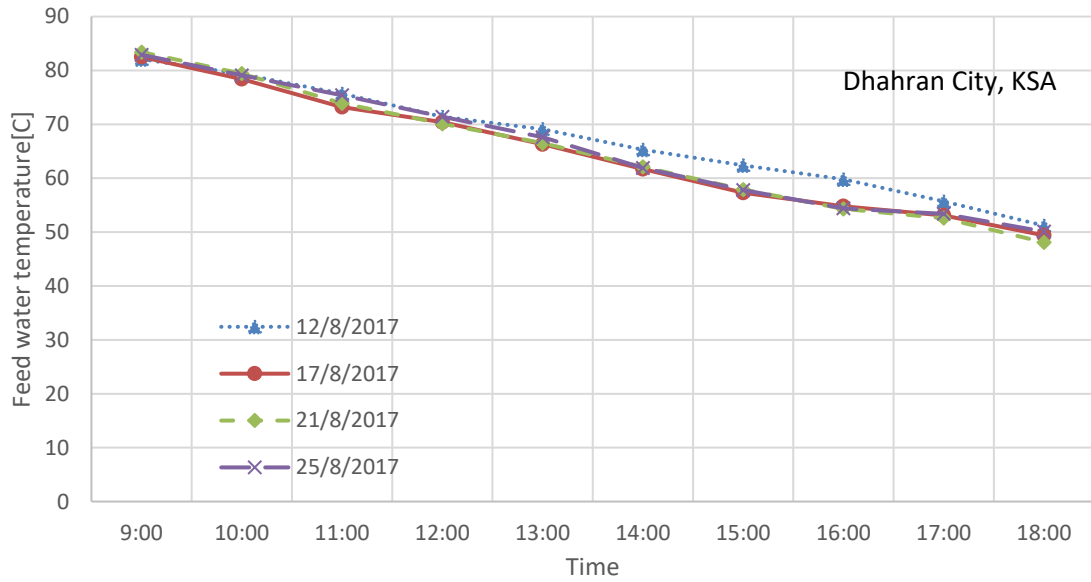
Figure 4.25: feed water temperature variation with time for four different days
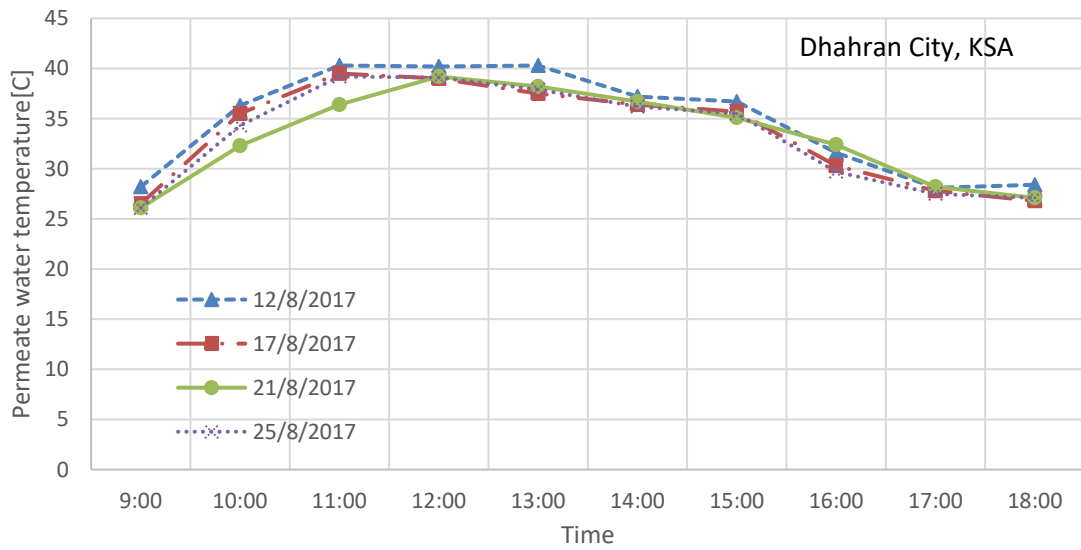
Figure 4.26: Permeate water temperature variation with time for four different days

Figure 4.27 shows the variation of the flux at different feed and permeate flow rates from 10 am to 6 pm with different flow arrangements. We observed that the flux decreases with time for the parallel flow arrangement due to the decrease in feed water temperature with time. Also, the output flux increases with increasing the feed and permeate flow rates due

to the increase in the turbulence levels in both the feed and permeate sides which increase the heat and mas transfer coefficients and also the rate of condensation of the vapor.
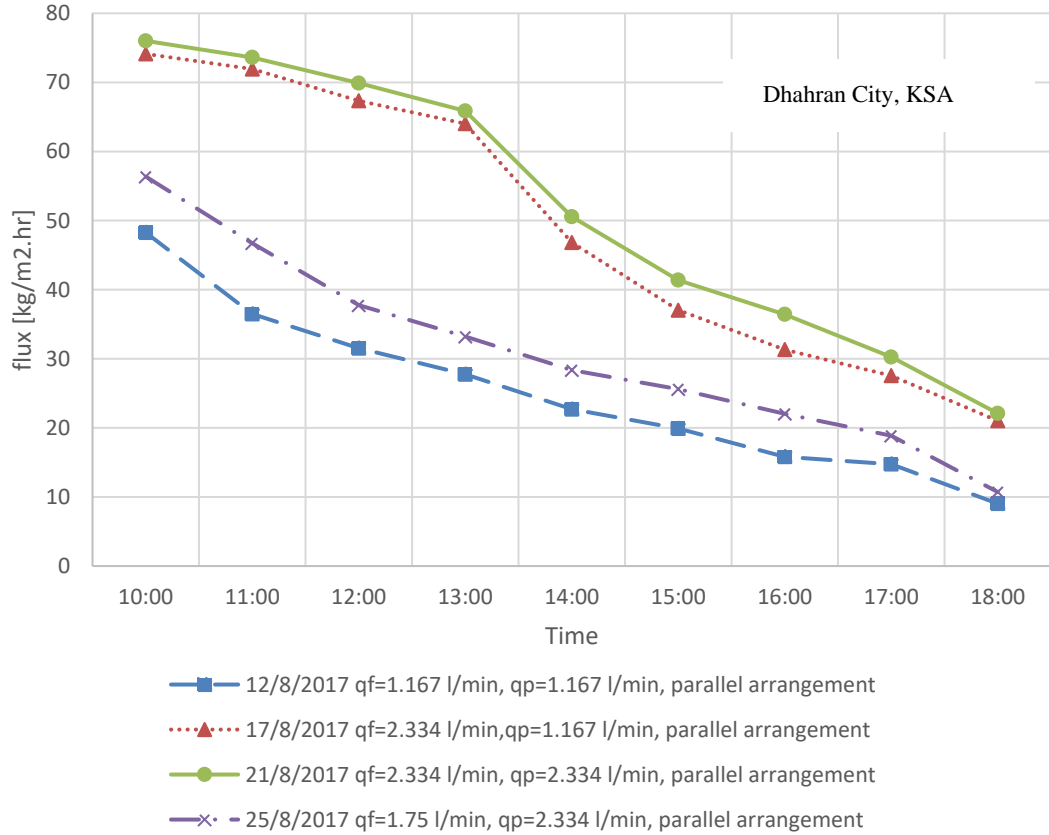
Figure 4.27: Flux variation at different feed and permeate flow rates with time for the parallel flow arrangement

The total productivity of the system after operating it from 9 am to 6 pm was as follows:

- August 12th, 2017, feed flow rate=1.167 l/min and permeate flow rate=1.167 l/min passing each module. The total productivity of the system was 4.4 L.

- August 17th, 2017, feed flow rate=2.334 l/min and permeate flow rate=1.167 l/min passing each module. The total productivity of the system was 8.6 L.

- August 21st, 2017, feed flow rate=2.334 l/min and permeate flow rate=2.334 l/min passing each module. The total productivity of the system was 9.1 L.

92

- August 25th, 2017, feed flow rate=1.75 l/min and permeate flow rate=2.334 l/min passing each module. The total productivity of the system was 5.48 L.

4.7 Performance of the MS-DCMD solar system without cooling with parallel flow arrangement

In August 29th, 2017, the solar MS-DCMD system has been tested with parallel flow arrangement without cooling the permeate cycle from 9 am to 6 pm. The controlled input parameters for the MS-DCMD system are feed flow rate=1.167 l/min, permeate flow rate 1.167 l/min passing each module and 3500 mg/L feed salinity.

Figure 4.28 shows the variation of the solar radiation with time for the parallel flow arrangement. We can notice that the curve exhibits a concave down words, peaking at noon.
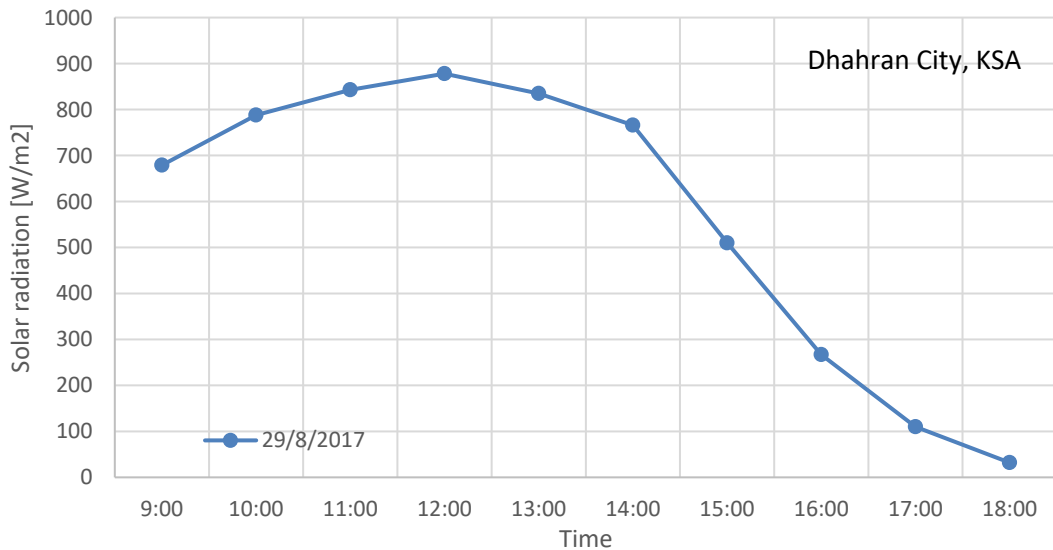
Figure 4.28: Solar radiation variation with time for the parallel flow arrangement

Figure 4.29 shows the variation of water temperature inside the solar tank and the permeate water tank with time for the parallel flow arrangement. The feed water temperature decreases with time because of high heat transfer between hot and cold sides across the membrane. The cold-water temperature in the permeate water tank starts to sharply increase due high heat transfer between the two sides and after that starts to decrease with time in parallel with the feed water temperature.
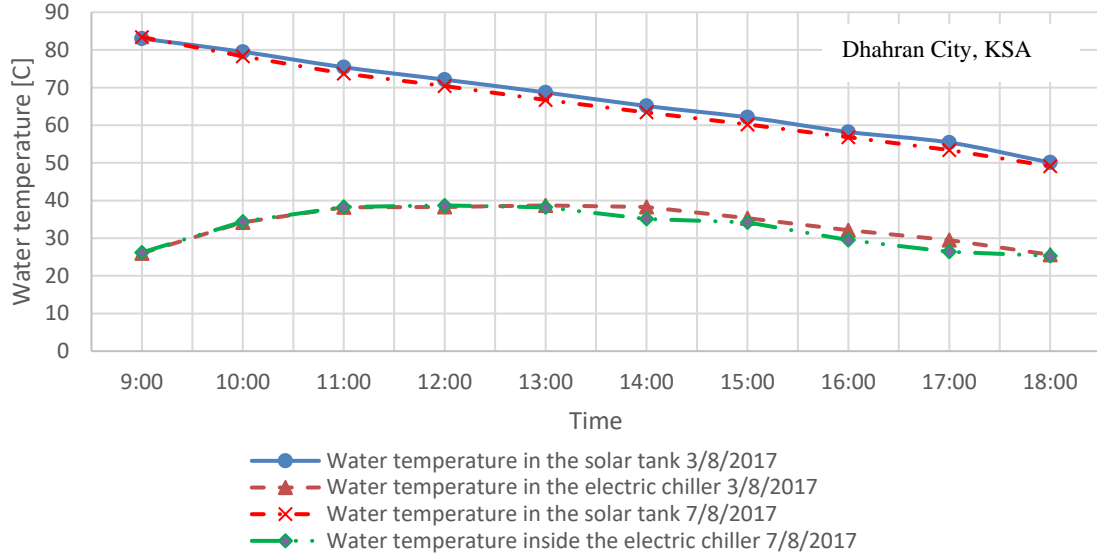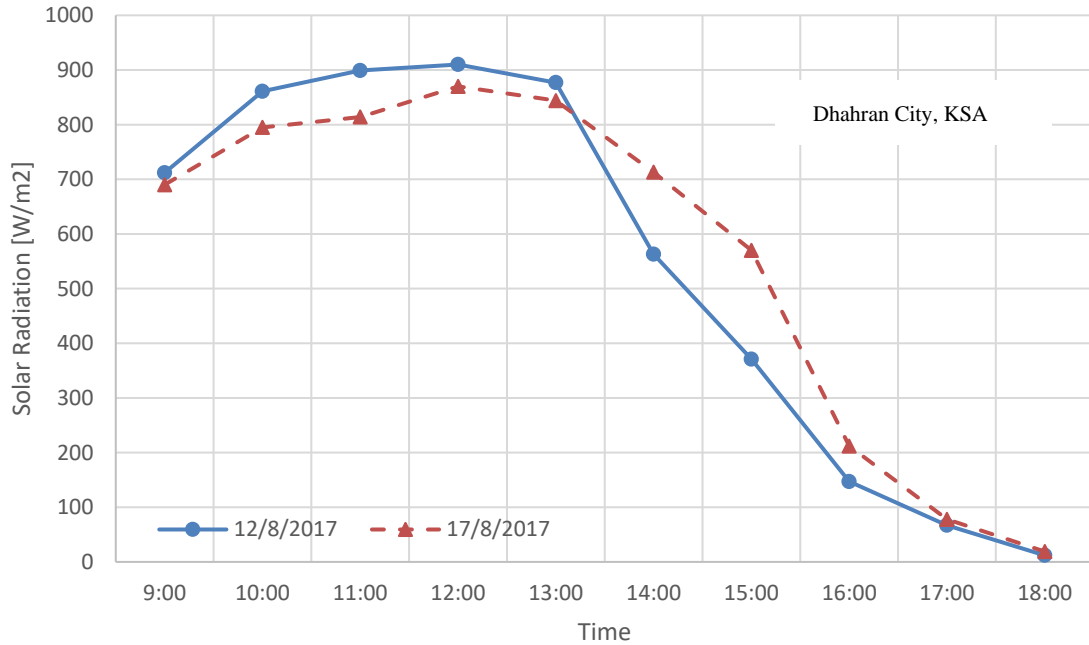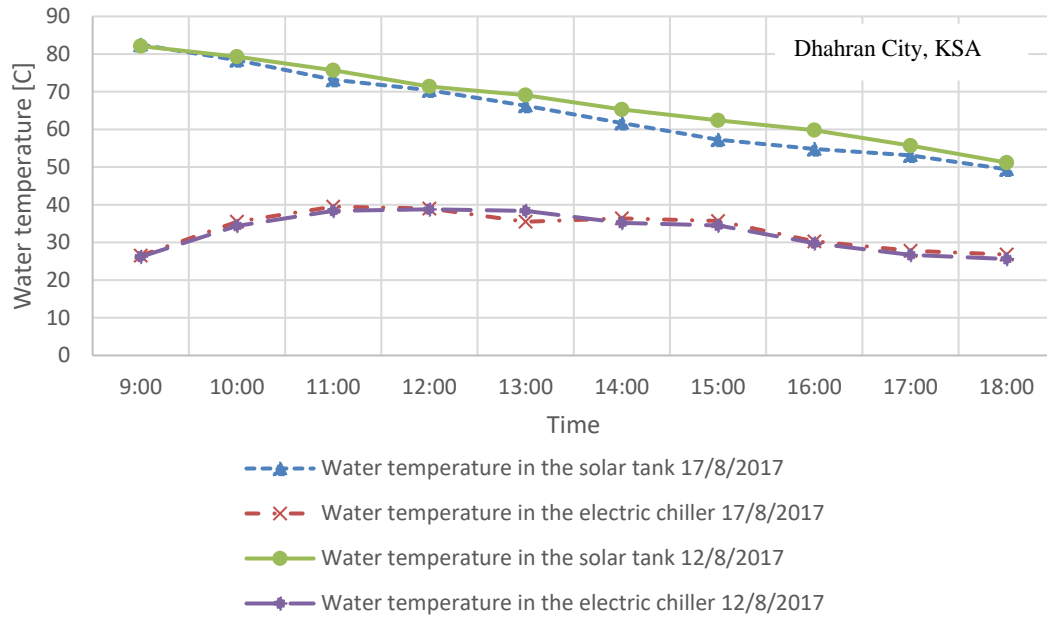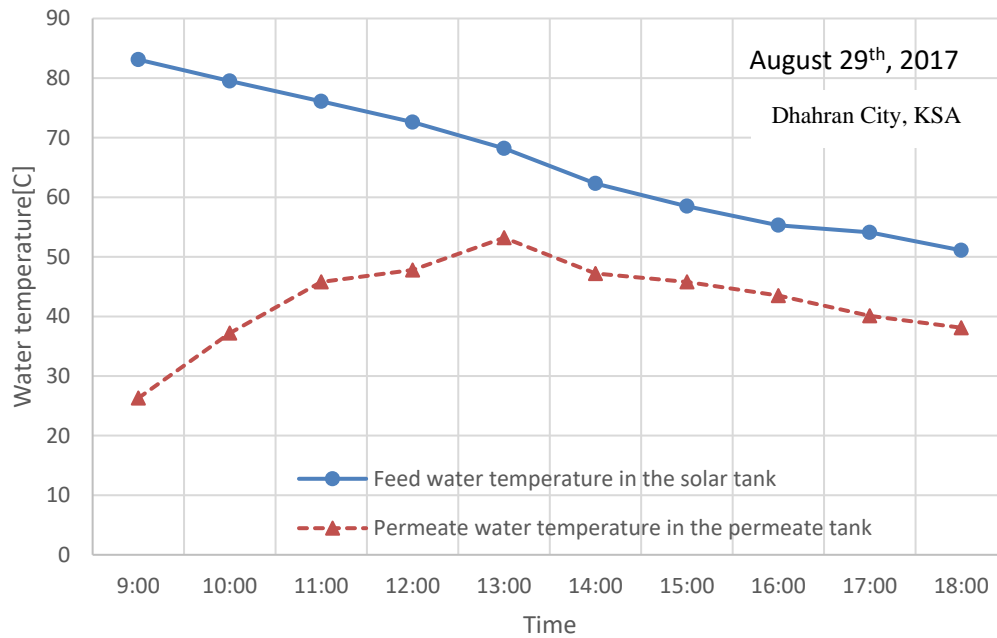

Figure 4.29: The variation of feed water temperature and permeate water temperature with time for the parallel flow arrangement

Figure 4.30 presents the permeate flux variation with time. The permeate flux started with the maximum value 49.2 kg/m^2.hr due to the high temperature difference between the feed and permeate sides. Then it starts to sharply decrease as the time goes on because of the high heat transfer between the feed and permeate sides across the membrane in the three MD modules which decreases the feed water temperature and increases the permeate

temperature. At 3 pm, the permeate flux is becoming almost zero, due to the small difference in the temperature between feed and permeate sides (about 15°C). The total productivity of the system was 1.9 Liter/day.
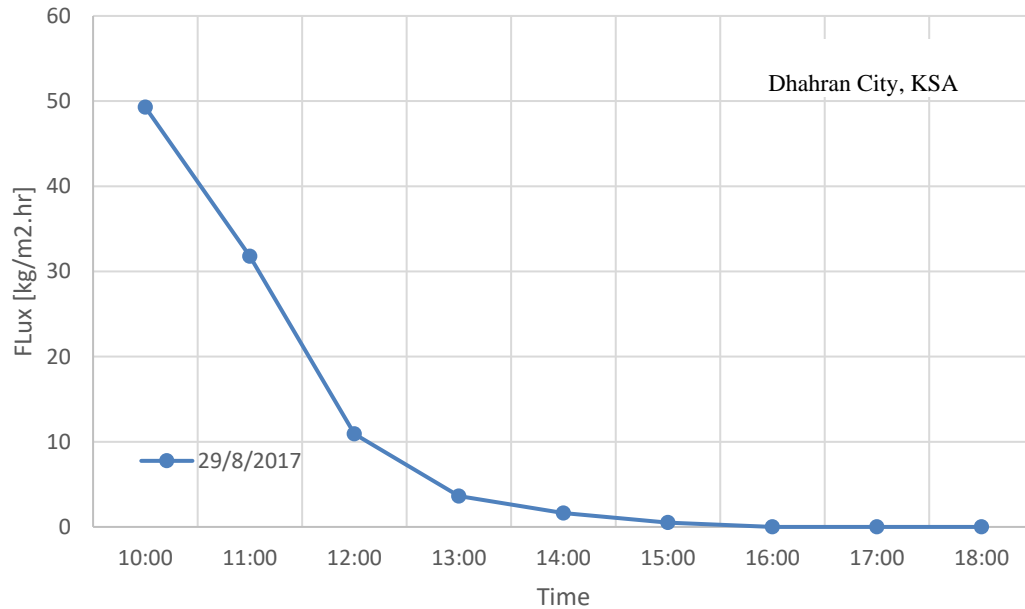
Figure 4.30: Permeate flux variation with time for the MS-DCMD system in the parallel flow arrangement without cooling

Figure 4.31 shows the variation of the permeate flux for two different days. The MS-DCMD solar system performance has been tested with and without cooling the permeate cycle at the same feed and permeate flow rates=1.167 L/min. It is clearly seen that, the permeate flux from the system with cooling the permeate cycle is higher than the system without cooling the permeate side. In both cases, the permeate flux of the system starts at 10 am at almost the same value and it decreases with time.
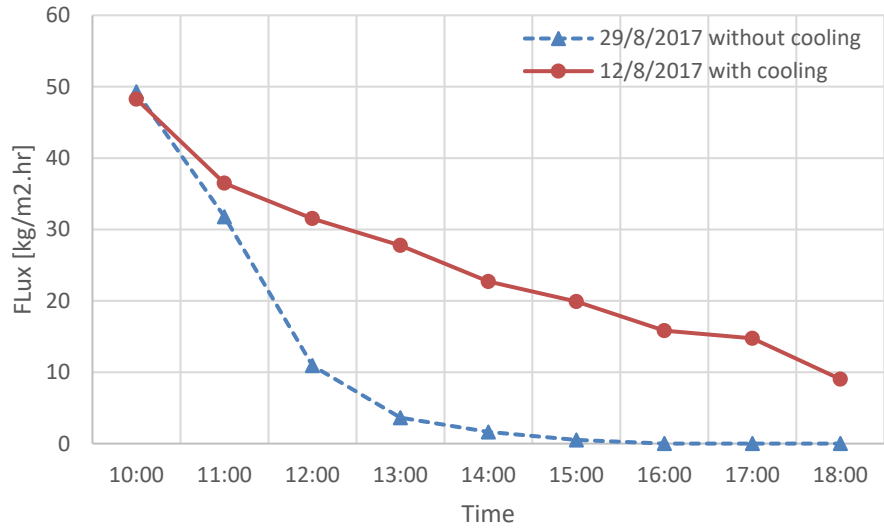
Figure 4.31: The permeate flux variation with time for two different days with and without cooling the permeate cycle

Table 4.1 represents the estimated productivity of the MS-DCMD solar system in parallel and series flow arrangements with different feed and permeate flow rates.

Table 4.1: The total productivity of the MS-DCMD solar system from 9 am to 6 pm at different feed and parallel flow rates

Flow arrangement	Feed flow rate[L/min]	Permeate flow rate[L/min]	Productivity from 9am to 6pm [L]
Series	1.167	1.167	3.396
Series	2.334	1.167	3.895
Parallel	1.167	1.167	4.434
Parallel	2.334	1.167	8.648
Parallel	2.334	2.334	9.136
Parallel	1.75	2.334	5.482
Parallel (without cooling)	1.167	1.167	1.916

CHAPTER 5

CONCLUSIONS

Experimental investigations had been carried out on multistage direct contact membrane distillation systems. These investigations included lab test and solar driven test for the MS-DCMD system. Additionally, a mathematical model had been studied and developed and validated to predict the performance of the evacuated tube solar collector as the heating source of feed water in the MD systems.

The permeate flux had been studied at different operating parameters including feed temperature, permeate temperature, feed flow rate, permeate flow rate, and feed salinity concentration. Additionally, the power consumption for the MS-DCMD system had been measured.

The following conclusions can be made from the experimental study:

1- Lab test of the MS-DCMD system

- The increase in the feed temperature, feed flow rate, and permeate flow rate increases the permeate flux for the MS-DCMD system. While the permeate flux decreases with the increase in the permeate temperature and feed salinity.

- The output flux from the MS-DCMD system in the parallel flow arrangement is higher than flux output from the series and mixed flow arrangements

- The percentage increase in flux due to the change of connection from series to mixed flow arrangement is around 20% and from series to parallel flow arrangement is 32.4% at feed temperature 90°C.

- A very high salt rejection factor (SRF) had been achieved around 99.9%.

- The electric heater power consumption is higher than the power consumed by the chiller for the MS-DCMD in both parallel and series flow arrangements due to the high temperature difference across the feed flow stream.

- The power consumed by the chiller increases with the decrease in the permeate temperature and also with the increase in permeate flow rate. Similarly, the power consumed by the electric heater increases with the increase in feed temperature and feed flow rate due to the increase in heat transfer rate and also heat losses.

- The MS-DCMD system power consumption in the series flow arrangement is much higher than the system power consumption in the parallel flow arrangement due to high temperature drop in both feed and permeate cycles.

2- Mathematical modeling of ETSC

- The mathematical model showed a close agreement with the experimental results. It can predict the water temperature inside the solar tank.

3- Solar powered MS-DCMD system

- For the MS-DCMD system, it's hard to control feed and permeate temperatures because of the high heat transfer across the membranes in the three MD modules. To maintain the feed and permeate water temperature, one needs a huge amount of energy to be supplied to the system for heating and cooling.

- The temperature difference between feed and permeate streams is the most influential parameter on the permeate flux in the solar MS-DCMD system.

- The MS-DCMD system with parallel flow arrangement produces higher permeate flux compared to the system in series flow arrangement.

- It's not recommended to operate the MS-DCMD system without cooling the water in permeate cycle due to high heat transfer between feed and permeate sides.

- Running the solar MS-DCMD system from 9 am to 6 pm in summer months, the system productivity was between 4 to 8 Liters

Recommendations

- To use solar cooling subsystems integrated to the MS-DCMD system.

- To use more solar collectors for heating feed water to the MS-DCMD system.

REFERENCES

[1]   W. A. Jury and H. Vaux, "The role of science in solving the world's emerging water problems.," *Proc. Natl. Acad. Sci. U. S. A.*, vol. 102, no. 44, pp. 15715–20, Nov. 2005.

[2]   E. DeNicola, O. S. Aburizaiza, A. Siddique, H. Khwaja, and D. O. Carpenter, "Climate Change and Water Scarcity: The Case of Saudi Arabia," *Ann. Glob. Heal.*, vol. 81, no. 3, pp. 342–353, 2015.

[3]   M. A. Shannon, P. W. Bohn, M. Elimelech, J. G. Georgiadis, B. J. Mariñas, and A. M. Mayes, "Science and technology for water purification in the coming decades," *Nature*, vol. 452, no. 7185, pp. 301–310, Mar. 2008.

[4]   M. Shatat and S. B. Riffat, "Water desalination technologies utilizing conventional and renewable energy sources," *Int. J. Low-Carbon Technol.*, vol. 9, no. 1, pp. 1–19, Mar. 2014.

[5]   M. A. Dawoud, "The role of desalination in augmentation of water supply in GCC countries," *Desalination*, vol. 186, no. 1–3, pp. 187–198, Dec. 2005.

[6]   N. Ghaffour, T. M. Missimer, and G. L. Amy, "Technical review and evaluation of the economics of water desalination: Current and future challenges for better water supply sustainability," *Desalination*, vol. 309, pp. 197–207, 2013.

[7]   G. Meerganz von Medeazza, "Water desalination as a long-term sustainable solution to alleviate global freshwater scarcity? A North-South approach," *Desalination*, vol. 169, no. 3, pp. 287–301, Oct. 2004.

[8]   P. H. Gleick and P. I. for S. in D., *Environment, and Security, and S. E. Institute, Water in Crisis: A Guide to the World's Fresh Water Resources*. Oxford University Press, 1993.

[9]   F. Gassert, P. Reig, tianyi luo, and andrew maddocks, "A Weighted Aggregation of Spatially Distinct Hydrological Indicators," 2013.

[10]   S. O. Al-Saadi, "Analytical Study of Water Requirements in KSA for Next Twenty Years," *Sr. Proj. C.E. Dept., King Saud Univ.*, 2006.

[11]   S. Lattemann and T. Höpner, "Environmental impact and impact assessment of seawater desalination," *Desalination*, vol. 220, no. 1, pp. 1–15, 2008.

[12]   N. Voutchkov, "Desalination – Past, Present and Future - International Water Association," *International Water Association*, 2016. [Online]. Available: http://www.iwa-network.org/desalination-past-present-future/.

[13]   A. Bushnak, H. Khordagui, S. Damianidis, and V. Konstantianos, "Sustainable Water Integrated Management -Support Mechanism (SWIM-SM) ASSESSMENT OF BEST AVAILABLE TECHNOLOGIES FOR DESALINATION IN RURAL/LOCAL AREAS."

[14]   G. Micale, A. Cipollina, and L. Rizzuti, "Seawater Desalination for Freshwater Production," 2009, pp. 1–15.

[15]   H. El-Dessouky, I. Alatiqi, and H. Ettouney, "Process synthesis: The multi-stage flash desalination system," *Desalination*, vol. 115, no. 2, pp. 155–179, Jul. 1998.

[16]   A. Kogan, "Direct contact condensation multistage flash distillation," *Desalination*, vol. 19, no. 1–3, pp. 299–307, Dec. 1976.

[17] M. A. Darwish, M. M. El-Refaee, and M. Abdel-Jawad, "Developments in the multi-stage flash desalting system," *Desalination*, vol. 100, no. 1–3, pp. 35–64, Jan. 1995.

[18] A. Chorak, P. Palenzuela, D.-C. Alarcón-Padilla, and A. Ben Abdellah, "Experimental characterization of a multi-effect distillation system coupled to a flat plate solar collector field: Empirical correlations," *Appl. Therm. Eng.*, vol. 120, pp. 298–313, 2017.

[19] C. Qi, X. Wang, H. Feng, and Q. Lv, "Performance analysis of low-temperature multi-effect distillation system under different feeding modes," *Appl. Therm. Eng.*, vol. 112, pp. 1452–1459, 2017.

[20] L. Chen, Q. Xu, J. L. Gossage, and H. H. Lou, "Simulation and economic evaluation of a coupled thermal vapor compression desalination process for produced water management," *J. Nat. Gas Sci. Eng.*, vol. 36, pp. 442–453, 2016.

[21] D. Han, W. F. He, C. Yue, and W. H. Pu, "Study on desalination of zero-emission system based on mechanical vapor compression," *Appl. Energy*, vol. 185, pp. 1490–1496, 2017.

[22] D. Zejli, A. Ouammi, R. Sacile, H. Dagdougui, and A. Elmidaoui, "An optimization model for a mechanical vapor compression desalination plant driven by a wind/PV hybrid system," *Appl. Energy*, vol. 88, no. 11, pp. 4042–4054, 2011.

[23] N. Lukic, L. L. Diezel, A. P. Fröba, and A. Leipertz, "Economical aspects of the improvement of a mechanical vapour compression desalination plant by dropwise condensation," *Desalination*, vol. 264, no. 1, pp. 173–178, 2010.

[24] J. M. Ochando-Pulido and A. Martinez-Ferez, "Experimental design optimization of reverse osmosis purification of pretreatedolive mill wastewater," *Sci. Total Environ.*, vol. 587, pp. 414–422, 2017.

[25] A. M. Blanco-Marigorta, A. Lozano-Medina, and J. D. Marcos, "The exergetic efficiency as a performance evaluation tool in reverse osmosis desalination plants in operation," *Desalination*, vol. 413, pp. 19–28, 2017.

[26] S. M. Shalaby, "Reverse osmosis desalination powered by photovoltaic and solar Rankine cycle power systems: A review," *Renew. Sustain. Energy Rev.*, vol. 73, pp. 789–797, 2017.

[27] F.-M. Allioux, L. He, F. She, P. D. Hodgson, L. Kong, and L. F. Dumée, "Investigation of hybrid ion-exchange membranes reinforced with non-woven metal meshes for electro-dialysis applications," *Sep. Purif. Technol.*, vol. 147, pp. 353–363, 2015.

[28] Q. Wang, X. Gao, Y. Zhang, Z. He, Z. Ji, X. Wang, and C. Gao, "Hybrid RED/ED system: Simultaneous osmotic energy recovery and desalination of high-salinity wastewater," *Desalination*, vol. 405, pp. 59–67, 2017.

[29] O. S. Burheim, F. Seland, J. G. Pharoah, and S. Kjelstrup, "Improved electrode systems for reverse electro-dialysis and electro-dialysis," *Desalination*, vol. 285, pp. 147–152, 2012.

[30] A. Khalifa, D. Lawal, M. Antar, and M. Khayet, "Experimental and theoretical investigation on water desalination using air gap membrane distillation," *Desalination*, vol. 376, pp. 94–108, 2015.

[31] A. E. Khalifa, "Water and air gap membrane distillation for water desalination – An experimental comparative study," *Sep. Purif. Technol.*, vol. 141, pp. 276–284, 2015.

[32] A. E. Khalifa and D. U. Lawal, "Performance and Optimization of Air Gap

Membrane Distillation System for Water Desalination," *Arab. J. Sci. Eng.*, vol. 40, no. 12, pp. 3627–3639, Dec. 2015.

[33] L. M. Camacho, J. A. Fox, and J. O. Ajedegba, "Optimization of electrodialysis metathesis (EDM) desalination using factorial design methodology," *Desalination*, vol. 403, pp. 136–143, 2017.

[34] H. Jaroszek, A. Lis, and P. Dydo, "Transport of impurities and water during potassium nitrate synthesis by electrodialysis metathesis," *Sep. Purif. Technol.*, vol. 158, pp. 87–93, 2016.

[35] M. Taherian and S. M. Mousavi, "Modeling and simulation of forward osmosis process using agent-based model system," *Comput. Chem. Eng.*, vol. 100, pp. 104–118, 2017.

[36] A. A. Monjezi, H. B. Mahood, and A. N. Campbell, "Regeneration of dimethyl ether as a draw solute in forward osmosis by utilising thermal energy from a solar pond," *Desalination*, vol. 415, pp. 104–114, 2017.

[37] H.-Q. Liang, W.-S. Hung, H.-H. Yu, C.-C. Hu, K.-R. Lee, J.-Y. Lai, and Z.-K. Xu, "Forward osmosis membranes with unprecedented water flux," *J. Memb. Sci.*, vol. 529, pp. 47–54, 2017.

[38] P. Patel and R. Kumar, "Comparative Performance Evaluation of Modified Passive Solar Still Using Sensible Heat Storage Material and Increased Frontal Height," *Procedia Technol.*, vol. 23, pp. 431–438, 2016.

[39] E. Mathioulakis, V. Belessiotis, and E. Delyannis, "Desalination by using alternative energy: Review and state-of-the-art," *Desalination*, vol. 203, pp. 346–365, 2007.

[40] O. K. Siddiqui, M. H. Sharqawy, M. A. Antar, and S. M. Zubair, "Performance evaluation of variable pressure humidification-dehumidification systems," *Desalination*, vol. 409, pp. 171–182, 2017.

[41] M. I. Zubair, F. A. Al-Sulaiman, M. A. Antar, S. A. Al-Dini, and N. I. Ibrahim, "Performance and cost assessment of solar driven humidification dehumidification desalination system," *Energy Convers. Manag.*, vol. 132, pp. 28–39, 2017.

[42] F. A. Al-Sulaiman, M. I. Zubair, M. Atif, P. Gandhidasan, S. A. Al-Dini, and M. A. Antar, "Humidification dehumidification desalination system using parabolic trough solar air collector," *Appl. Therm. Eng.*, vol. 75, pp. 809–816, 2015.

[43] A. M. Karam, A. S. Alsaadi, N. Ghaffour, and T. M. Laleg-Kirati, "Analysis of direct contact membrane distillation based on a lumped-parameter dynamic predictive model," *Desalination*, vol. 402, pp. 50–61, 2017.

[44] S. G. Talbert, "PB-201 029 MANUAL ON SOLAR DISTILLATION OF SALINE WATER," 1970.

[45] A. Delyannis and E. Delyannis, "RECENT SOLAR D I STI LLATI ON DEVELOPMENTS," *Desalin. Elsevier Sci. Publ. B.V*, vol. 45, pp. 361–369, 1983.

[46] M. T. Ali, H. E. S. Fath, and P. R. Armstrong, "A comprehensive techno-economical review of indirect solar desalination," *Renew. Sustain. Energy Rev.*, vol. 15, pp. 4187–4199, 2011.

[47] M. E. Findley, V. V. Tanna, Y. B. Rao, and C. L. Yeh, "Mass and heat transfer relations in evaporation through porous membranes," *AIChE J.*, vol. 15, no. 4, pp. 483–489, Jul. 1969.

[48] K. K. Sirkar, "Other New Membrane Processes," in *Membrane Handbook*, Boston, MA: Springer US, 1992, pp. 885–912.

[49]   K. W. Lawson and D. R. Lloyd, "Membrane distillation," *J. Memb. Sci.*, vol. 124, no. 1, pp. 1–25, 1997.

[50]   A. BURGOYNE and M. M. VAHDATI, "Direct Contact Membrane Distillation," *Sep. Sci. Technol.*, vol. 35, no. 8, pp. 1257–1284, Jan. 2000.

[51]   L. Martinez and F. J. Florido-Diaz, "Theoretical and experimental studies on desalination using membrane distillation."

[52]   J.-M. Li, Z.-K. Xu, Z.-M. Liu, W.-F. Yuan, H. Xiang, S.-Y. Wang, and Y.-Y. Xu, "DESALINATION Microporous polypropylene and polyethylene hollow fiber membranes. Part 3. Experimental studies on membrane distillation for desalination," *Desalination*, vol. 155, pp. 153–156, 2003.

[53]   D. U. Lawal and A. E. Khalifa, "Flux Prediction in Direct Contact Membrane Distillation," *Int. J. Mater. Mech. Manuf.*, vol. 2, no. 4, pp. 302–308, 2014.

[54]   D. U. Lawal and A. E. Khalifa, "Theoretical and Statistical Models for Predicting Flux in Direct Contact Membrane Distillation," *J. Eng. Res. Appl.*, vol. 4, no. 8, pp. 124–135, 2014.

[55]   A. Khalifa, H. Ahmad, M. Antar, T. Laoui, and M. Khayet, "Experimental and theoretical investigations on water desalination using direct contact membrane distillation," *Desalination*, vol. 404, pp. 22–34, 2017.

[56]   H. M. Ahmad, A. E. Khalifa, and M. A. Antar, "Water Desalination Using Direct Contact Membrane Distillation System," in *Volume 6A: Energy*, 2015, p. V06AT07A024.

[57]   T. Y. Cath, V. D. Adams, and A. E. Childress, "Experimental study of desalination using direct contact membrane distillation: a new approach to flux enhancement," *J. Memb. Sci.*, vol. 228, pp. 5–16, 2004.

[58]   E. K. Summers, H. A. Arafat, and J. H. Lienhard, "Energy efficiency comparison of single-stage membrane distillation (MD) desalination cycles in different configurations," *Desalination*, vol. 290, pp. 54–66, 2012.

[59]   J.-G. Lee, Y.-D. Kim, S.-M. Shim, B.-G. Im, and W.-S. Kim, "Numerical study of a hybrid multi-stage vacuum membrane distillation and pressure-retarded osmosis system," *DES*, vol. 363, pp. 82–91, 2015.

[60]   B. L. Pangarkar, S. K. Deshmukh, and P. V Thorat, "Energy efficiency analysis of multi-effect membrane distillation (MEMD) water treatment."

[61]   J. Gilron, L. Song, and K. K. Sirkar, "Design for Cascade of Crossflow Direct Contact Membrane Distillation," *Ind. Eng. Chem. Res.*, vol. 46, no. 8, pp. 2324–2334, Apr. 2007.

[62]   F. He, J. Gilron, K. K. Sirkar, and K. K. Sirkar, "High water recovery in direct contact membrane distillation using a series of cascades," *DES*, vol. 323, pp. 48–54, 2013.

[63]   J. G. Lee and W. S. Kim, "Numerical study on multi-stage vacuum membrane distillation with economic evaluation," *Desalination*, vol. 339, no. 1, pp. 54–67, 2014.

[64]   H. Geng, J. Wang, C. Zhang, P. Li, and H. Chang, "High water recovery of RO brine using multi-stage air gap membrane distillation," *Desalination*, vol. 355, pp. 178–185, 2015.

[65]   D. Priya, P. Sivakumar, and M. Sutha, "A Review on Desalination using Membrane Distillation : Status and Potential," vol. 6, no. 9, pp. 4259–4263, 2014.

[66] A. Chafidz, S. Al-Zahrani, M. N. Al-Otaibi, C. F. Hoong, T. F. Lai, and M. Prabu, "Portable and integrated solar-driven desalination system using membrane distillation for arid remote areas in Saudi Arabia," *Desalination*, vol. 345, pp. 36–49, 2014.

[67] K. Zhao, W. Heinzl, M. Wenzel, S. Büttner, F. Bollen, G. Lange, S. Heinzl, and N. Sarda, "Experimental study of the memsys vacuum-multi-effect- membrane-distillation (V-MEMD) module," *Des*, vol. 323, pp. 150–160, 2013.

[68] P. A. Hogan, Sudjito, A. G. Fane, and G. L. Morrison, "Desalination by solar heated membrane distillation," *Desalination*, vol. 81, no. 1, pp. 81–90, 1991.

[69] F. Suárez, J. A. Ruskowitz, S. W. Tyler, and A. E. Childress, "Renewable water: Direct contact membrane distillation coupled with solar ponds," *Appl. Energy*, vol. 158, pp. 532–539, 2015.

[70] H. J. Zwijnenberg, G. H. Koops, and M. Wessling, "Solar driven membrane pervaporation for desalination processes," *J. Memb. Sci.*, vol. 250, no. 1, pp. 235–246, 2005.

[71] J.-P. Mericq, S. Laborie, and C. Cabassud, "Evaluation of systems coupling vacuum membrane distillation and solar energy for seawater desalination," *Chem. Eng. J.*, vol. 166, no. 2, pp. 596–606, 2011.

[72] E. Guillén-Burrieza, G. Zaragoza, S. Miralles-Cuevas, and J. Blanco, "Experimental evaluation of two pilot-scale membrane distillation modules used for solar desalination," *J. Memb. Sci.*, vol. 409, pp. 264–275, 2012.

[73] I. Tal-Tarlo and Y. Zvirin, "The Effects of Radiation Properties of Surfaces and Coatings on the Performance of Solar Collectors," *J. Sol. Energy Eng.*, vol. 110, no. 3, p. 217, 1988.

[74] A. E. Khalifa, S. M. Alawad, and M. A. Antar, "Parallel and series multistage air gap membrane distillation," *Desalination*, vol. 417, pp. 69–76, Sep. 2017.

Appendix I

```
"This code is used to make an analysis for a single evacuated tube
solar collector. Assumption made evacuated tube cosists of a single
glass layer and a copper pipe which transfers the heat to the water
inside the tank"

As_g=0.4                              " surface area of glass m2"
As_p=0.053                           " surface area of copper pipe (m2)"
D_p=508E-4                            "Diameter of the pipe m"
ag=0.15                               "absorptivity of the glass"
ap=0.95                               "absorptivity of the copper
pipe"
touh_g=1-ag                          "transmittivity of the glass"
e=0.1                                 "Emissivity of the glass"
s=5.6697E-08                         "Stephan Boltzman constant W/m2 K4"
V=2                                   "Wind Speed m/s"

hg=5.7+(3.8*V)                                "Convection heat tranfer
coeff (W/m2 k)"
Tin=25                                "intial temperaure of the tank K"
N_t=20                                "number of tubes"
mw=150                                "mass of water stored in the tank
kg"
mg=1.5                                "mass of the glass kg"
Tgo=25                                "initial temperature for the glass
K"
mp=0.5                                " mass of the copper pipe kg"
Tpo=25                                "intial temperaure for the copper
pipe in K"
Pa=100                                "atmospheric pressure kpa"
Nu_D=4.364
losses = 0.02


 " -------------Solar Irradiance - Experimental Data------------------"


G[1..48]=[0,0,0,0,13.1,42,360,600,797,918,962,974,1025,845.1,690.3,480.
4,250.4,58.9,13.1,0,0,0,0,0,0,0,0,0,13.1,31.4,174.4,387,602.3,774.6,883
.6,935.8,938.8,845.1,690.3,480.4,250.4,58.9,13.1,0,0,0,0,0]

"-------------Outer Glass Temperature- Experimental Data----------"

Tgexp[1..48]=[22.9,23,23.1,23.2,23,22.8,23.1,32.1,38,42.5,44.6,40.2,42.
7,45.1,39.5,36.1,31.8,28.6,27,26,24,23.5,23.4,23.3,22.9,23.1,23.2,23,22
.8,22.2,30.1,35.3,36.6,43.2,41.8,44,42.3,40.1,33.2,31.8,28.6,27,26,24,2
3.5,23.4,23.3,22.9]

"------------Air Ambient Temperature - Experimental Data----------"

Ta[1..48]=[22.9,23.5,23.2,23.3,23,24,25.5,29.5,31,34.3,34.9,33.1,31.8,3
1.8,31.8,30.5,29.5,27.5,25.2,26.2,25.6,24.4,24.8,24.1,22.9,23.5,23.2,23
.3,23,24,25.5,29.5,31,34.3,34.9,33.1,31.8,31.8,31.8,30.5,29.5,27.5,25.2
,26.2,25.6,24.4,24.8,24.1]
```

```
Tf[1]=25                 "Initial guess for the water temperature in C"
cpg=753                  "specific heat transfer coefficient for the
glass pipe j/kg k"
cpw[1]=4183              "specific heat transfer coefficient for the
water pipe j/kgk"

H[1]=0
Duplicate i=1,48

H[i+1]=H[i]+1

End

Duplicate i=1,47


cpw[i+1]=cp(Water,T=Tf[i],P=Pa) "specific heat transfer coefficient for
the water pipe j/kg k"



End

Duplicate i=1,15

qrad_g_a[i]=e*s*(Tg[i]^4-(Ta[i]-7)^4)    "radiation losses from the
glass to the air W/m2"

qconv_g_a[i]=hg*(Tg[i]-(Ta[i]))"convection losses from the glass to the
air W/m2"

Qrad_ga[i]=qrad_g_a[i]*As_g "radiation losses from the glass to the air
in W"

Qconv_ga[i]=qconv_g_a[i]*As_g  "convection losses from the glass to the
air W"


".................{Energy balance for the glass} ...............″

(As_g*ag*G[i])=Qrad_ga[i]+Qconv_ga[i]+mg*cpg*(Tg[i]-Tgo)/3600


".............{""Energy balance for the copper pipe""}.........″


(As_p*ap*touh_g*G[i])*(1-losses) =Qconv[i]


".....{heat transfer equations from the pipe to the methanol}......."

mw*cpw[i] * (Tf[i+1] - Tf[i])=Qconv[i]*N_t*3600

End
```

```
Duplicate i=16,30

qrad_g_a[i]=e*s*(Tg[i]^4-(Ta[i]-7)^4)"radiation losses from the glass
to the air W/m2"
qconv_g_a[i]=hg*(Tg[i]-(Ta[i]))"convection losses from the glass to the
air W/m2"
Qrad_ga[i]=qrad_g_a[i]*As_g "radiation losses from the glass to the air
in W"
Qconv_ga[i]=qconv_g_a[i]*As_g "convection losses from the glass to the
air W"


".....................{Energy balance for the glass}............."

(As_g*ag*G[i])=Qrad_ga[i]+Qconv_ga[i]+mg*cpg*(Tg[i]-Tgo)/3600


"..............{""Energy balance for the copper pipe""}........."

(As_p*ap*touh_g*G[i]) *(1-losses)=Qconv[i]


"......{heat transfer equations from the pipe to the methanol}...."

mw*cpw[i] * (Tf[i+1] - (0.985*Tf[i]))=Qconv[i]*N_t*3600

End

Duplicate i=31,48

qrad_g_a[i]=e*s*(Tg[i]^4-(Ta[i]-7)^4) "radiation losses from the glass
to the air W/m2"
qconv_g_a[i]=hg*(Tg[i]-(Ta[i]))"convection losses from the glass to the
air W/m2"
Qrad_ga[i]=qrad_g_a[i]*As_g "radiation losses from the glass to the air
in W"
Qconv_ga[i]=qconv_g_a[i]*As_g "convection losses from the glass to the
air W"


".............{Energy balance for the glass}........................ "

(As_g*ag*G[i])=Qrad_ga[i]+Qconv_ga[i]+mg*cpg*(Tg[i]-Tgo)/3600


"...........{""Energy balance for the copper pipe""}..............."

(As_p*ap*touh_g*G[i])*(1-losses)=Qconv[i]


".......{heat transfer equations from the pipe to the methanol}.."

mw*cpw[i] * (Tf[i+1] - Tf[i])=Qconv[i]*N_t*3600

End
```

Appendix II

"This code is used to make an energy analysis for the double glass
evacuated tube solar collector"

```
As_g=0.6                           " surface area of outer glass m2"
As_p=0.06                          " surface area of copper pipe (m2)"
As_g_2=0.45                        "surface area of the inner
glass(m2)"
hg_2=10        "Convective heat transfer coefficient between the copper
pipe and the inner glass"
touh_g_2=1-ag_2                    "Transmittivity of the inner glass"

D_p=508E-4                    "Diameter of the pipe m"
ag=0.15                       "absorptivity of the outer glass"
ag_2=0.09                     "absorptivity of the inner glass"
ap=0.95                       "absorptivity of the copper pipe"
touh_g=1-ag                   "transmittivity of the glass"
e=0.1                         "Emissivity of the glass"
s=5.6697E-08                  "Stephan Boltzmann constant W/m2 K4"
V=2                           "Wind Speed m/s"

hg=5.7+(3.8*V)            "Convection heat transfer coeff (W/m2 k)"
Tin=25                   "initial temperature of the tank K"
N_t=18                   "number of tubes"
mw=150                   "mass of water stored in the tank kg"
mg=1.5                   "mass of the glass kg"
Tgo=18                   "initial temperature for the glass K"
mp=0.5                   " mass of the copper pipe kg"
Tpo=30                   "initial temperature for the copper pipe
in K"
Pa=100                   "atmospheric pressure kpa"
Nu_D=4.364               "Nusselt Number of the heat pipe at
constant heat flux -fully developed flow"
losses = 0.02            "Assumed value for the convection and
radiation heat between the heat pipe and the inner glass"
 mg_2=1                  "mass of the inner glass in Kg"
Tgo_2=20                 "Initial temperature of the inner glass"
Cp_p=1000                "Specific heat transfer coefficient of the
copper pipe"

 " --------------Solar Irradiance - Experimental Data---------------"


G[1..48]=[0,0,0,0,13.1,42,360,600,797,918,962,974,1025,845.1,690.3,480.
4,250.4,58.9,13.1,0,0,0,0,0,0,0,0,0,13.1,31.4,174.4,387,602.3,774.6,883
.6,935.8,938.8,845.1,690.3,480.4,250.4,58.9,13.1,0,0,0,0,0]




"-------------Outer Glass Temperature- Experimental Data-------------"

Tgexp[1..48]=[22.9,23,23.1,23.2,23,22.8,23.1,32.1,38,42.5,44.6,40.2,42.
7,45.1,39.5,36.1,31.8,28.6,27,26,24,23.5,23.4,23.3,22.9,23.1,23.2,23,22
```

```
.8,22.2,30.1,35.3,36.6,43.2,41.8,44,42.3,40.1,33.2,31.8,28.6,27,26,24,2
3.5,23.4,23.3,22.9]

"---------------Air Ambient Temperature - Experimental Data----------"

Ta[1..48]=[22.9,23.5,23.2,23.3,23,24,25.5,29.5,31,34.3,34.9,33.1,31.8,3
1.8,31.8,30.5,29.5,27.5,25.2,26.2,25.6,24.4,24.8,24.1,22.9,23.5,23.2,23
.3,23,24,25.5,29.5,31,34.3,34.9,33.1,31.8,31.8,31.8,30.5,29.5,27.5,25.2
,26.2,25.6,24.4,24.8,24.1]

Tf[1]=30      "Initial guess for water temperature inside the ETSC tank"
cpg[1]=753    "initial guess for the specific heat transfer coefficient
for the outer glass pipe j/kg k"
cpg_2[1]=753"initial guess for the specific heat transfer coefficient
for the inner glass pipe j/kg k"
cpw[1]=4183   "specific heat transfer coefficient for the water pipe
j/kg k"
H[1]=0        "Initial Hours Guess"
hp_2=100      "Convective Heat Transfer coefficient between the copper
pipe and water inside the tank"

Duplicate i=1,48

H[i+1]=H[i]+1

End

".............."{Thermal properties- Assumed values}".................."

Duplicate i=1,47

cpg[i+1]=cp(Silicon, T=Tg[i])"specific heat transfer coefficient for
the outer glass j/kg k"

cpw[i+1]=cp(Water,T=Tf[i],P=Pa)"specific heat transfer coefficient for
the water pipe j/kg k"

cpg_2[i+1]=cp(Silicon, T=Tg_2[i])"specific heat transfer coefficient
for the outer glass j/kg k"

End


Duplicate i=1,14
qrad_g_a[i]=e*s*(Tg[i]^4-(Ta[i]-7)^4)"radiation losses from the glass
to the air W/m2"

qconv_g_a[i]=hg*(Tg[i]-(Ta[i]))"convection losses from the glass to the
air W/m2"

Qrad_ga[i]=qrad_g_a[i]*As_g   "radiation losses from the glass to the
air in W"

Qconv_ga[i]=qconv_g_a[i]*As_g "convection losses from the glass to the
air W"

Qrad_pg[i]=As_g_2* e*s*(Tp[i]^4-(Tg_2[i])^4)
```

```
Qconv_pg[i]=As_g_2* hg * (Tp[i]-(Tg_2[i]))
```

"................{Energy balance for the outer glass}..............."

```
(As_g*ag*G[i])=Qrad_ga[i]+Qconv_ga[i]+mg*cpg[i]*(Tg[i]-Tgo)/3600
```

"............{ Energy balance for the inner glass}............ "

```
(As_g_2*touh_g*ag_2*G[i])+Qrad_pg[i]+Qconv_pg[i]=mg_2*cpg_2[i]*(Tg_2[i]
-Tgo_2)/3600
```

"...............{""Energy balance for the copper pipe""}........"

```
(As_p*ap*touh_g*touh_g_2*G[i]) =Qconv[i]     + Qrad_pg[i] +
Qconv_pg[i]+mp*cp_p*(Tp[i]-Tpo)/3600
```

```
Qconv[i]=hp_2*As_p*(Tp[i]-Tf[i])
```

 ".......{heat transfer equations from the pipe to the methanol}......"

```
mw*cpw[i] * (Tf[i+1] -0.955*Tf[i])=Qconv[i]*N_t*3600
```

End

 Duplicate i=15,30
```
qrad_g_a[i]=e*s*(Tg[i]^4-(Ta[i]-7)^4) "radiation losses from the glass
to the air W/m2"
```

```
qconv_g_a[i]=hg*(Tg[i]-(Ta[i]))        "convection losses from the glass
to the air W/m2"
```

```
Qrad_ga[i]=qrad_g_a[i]*As_g   "radiation losses from the glass to the
air in W"
```

```
Qconv_ga[i]=qconv_g_a[i]*As_g "convection losses from the glass to the
air W"
```

```
Qrad_pg[i]=As_g_2* e*s*(Tp[i]^4-(Tg_2[i])^4)
```

```
Qconv_pg[i]=As_g_2* hg * (Tp[i]-(Tg_2[i]))
```

"............. .{Energy balance for the outer glass}.............."

```
(As_g*ag*G[i])=Qrad_ga[i]+Qconv_ga[i]+mg*cpg[i]*(Tg[i]-Tgo)/3600
```

"..............{ Energy balance for the inner glass}..............."

```
(As_g_2*touh_g*ag_2*G[i])+Qrad_pg[i]+Qconv_pg[i]=mg_2*cpg_2[i]*(Tg_2[i]
-Tgo_2)/3600
```

```
"..............{""Energy balance for the copper pipe""}.........."


(As_p*ap*touh_g*touh_g_2*G[i]) =Qconv[i] + Qrad_pg[i] +
Qconv_pg[i]+mp*cp_p*(Tp[i]-Tpo)/3600


Qconv[i]=hp_2*As_p*(Tp[i]-Tf[i])


".......{heat transfer equations from the pipe to the methanol } .... "

mw*cpw[i] * (Tf[i+1] -Tf[i])=Qconv[i]*N_t*3600

End

  Duplicate i=31,48

qrad_g_a[i]=e*s*(Tg[i]^4-(Ta[i]-7)^4) "radiation losses from the glass
to the air W/m2"

qconv_g_a[i]=hg*(Tg[i]-(Ta[i]))         "convection losses from the glass
to the air W/m2"

Qrad_ga[i]=qrad_g_a[i]*As_g            "radiation losses from the glass
to the air in W"

Qconv_ga[i]=qconv_g_a[i]*As_g         "convection losses from the glass
to the air W"

Qrad_pg[i]=As_g_2* e*s*(Tp[i]^4-(Tg_2[i])^4)

Qconv_pg[i]=As_g_2* hg * (Tp[i]-(Tg_2[i]))

".................{Energy balance for the outer glass }..............."

(As_g*ag*G[i])=Qrad_ga[i]+Qconv_ga[i]+mg*cpg[i]*(Tg[i]-Tgo)/3600

"...............{ Energy balance for the inner glass} ............."

(As_g_2*touh_g*ag_2*G[i])+Qrad_pg[i]+Qconv_pg[i]=mg_2*cpg_2[i]*(Tg_2[i]
-Tgo_2)/3600

"..............{""Energy balance for the copper pipe" "}........"


(As_p*ap*touh_g*touh_g_2*G[i]) =Qconv[i] + Qrad_pg[i] +
Qconv_pg[i]+mp*cp_p*(Tp[i]-Tpo)/3600

Qconv[i]=hp_2*As_p*(Tp[i]-Tf[i])

"...........{heat transfer equations from the pipe to the methanol}..."

mw*cpw[i] * (Tf[i+1] - Tf[i])=Qconv[i]*N_t*3600

End
```

Vitae

Name	: Ahmed Abdalmonem Abdalghany Abdalmonem
Nationality	: Egyptian
Date of Birth	: 18-Feb-1990
Email	: mr.ahmedabdalmonem@gmail.com
Address	: Nasr City, Cairo, Egypt
Academic Background:	Master of Science (MSc.), May 2017,
	Mechanical Engineering Department,
	King Fahd University of Petroleum & Minerals,
	Dhahran, Saudi Arabia.
	Bachelor of Science (BSc.), July 2011,
	Aeronautical Engineering Department,
	Institute of Aviation Engineering & Technology,
	Giza, Egypt.